



Cite this: *Chem. Soc. Rev.*, 2018,  
47, 7659

## Quantum dot-sensitized solar cells

Zhenxiao Pan,<sup>a</sup> Huashang Rao,<sup>a</sup> Iván Mora-Seró,<sup>b</sup> Juan Bisquert<sup>\*b</sup> and Xinhua Zhong<sup>ID \*a</sup>

Quantum dot-sensitized solar cells (QDSCs) have emerged as a promising candidate for next-generation solar cells due to the distinct optoelectronic features of quantum dot (QD) light-harvesting materials, such as high light, thermal, and moisture stability, facilely tunable absorption range, high absorption coefficient, multiple exciton generation possibility, and solution processability as well as their facile fabrication and low-cost availability. In recent years, we have witnessed a dramatic boost in the power conversion efficiency (PCE) of QDSCs from 5% to nearly 13%, which is comparable to other kinds of emerging solar cells. Both the exploration of new QD light-harvesting materials and interface engineering have contributed to this fantastically fast improvement. The outstanding development trend of QDSCs indicates their great potential as a promising candidate for next-generation photovoltaic cells. In this review article, we present a comprehensive overview of the development of QDSCs, including: (1) the fundamental principles, (2) a history of the brief evolution of QDSCs, (3) the key materials in QDSCs, (4) recombination control, and (5) stability issues. Finally, some directions that can further promote the development of QDSCs in the future are proposed to help readers grasp the challenges and opportunities for obtaining high-efficiency QDSCs.

Received 14th June 2018

DOI: 10.1039/c8cs00431e

rsc.li/chem-soc-rev

### 1. Introduction

Energy is a vital issue concerning humanity in the present and particularly in the future.<sup>1</sup> The great consumption of fossil energy has led to a global energy crisis as well as issues of environmental pollution. Therefore, there is an urgent need to

explore renewable clean energy to help solve these problems. Among such energy sources, solar energy is believed by many to be the most promising renewable energy resource due to its fascinating characteristics, such as an inexhaustible supply and its environmentally friendly nature. For instance, in a single year, the earth's surface can receive 3850 zettajoules (ZJ) of energy from the sun, meaning that the solar energy absorbed by the earth's surface in one hour is larger than the energy used by the whole world in a single year.<sup>2,3</sup> There is no doubt that the rational utilization of solar energy is of great importance for humanity in the future. A solar cell is a device that provides the

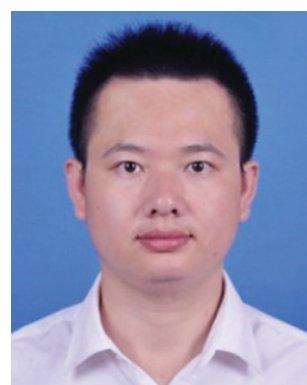
<sup>a</sup> College of Materials and Energy, South China Agricultural University, Guangzhou 510642, China. E-mail: zhongxh@scau.edu.cn

<sup>b</sup> Institute of Advanced Materials (INAM), Universitat Jaume I, 12006 Castelló, Spain. E-mail: sero@uji.es, bisquert@fca.uji.es



Zhenxiao Pan received his PhD degree in Applied Chemistry from East China University of Science and Technology in 2015. Currently he is a professor at the South China Agricultural University. His research interests are focused on the materials and interface design for high-efficiency quantum dot-sensitized solar cells.

Zhenxiao Pan



Huashang Rao

Huashang Rao is an associate professor at the South China Agricultural University, China. He received his BE and PhD degrees from Sun Yat-sen University in 2012 and 2017, respectively. His current research interest lies in the field of new energy materials and their applications in quantum dot-/perovskite-based solar cells.

important advantage of converting solar energy directly into electric energy on the basis of a photoelectric effect and can be used everywhere without the need for big facilities, and also it can be upscaled for massive energy production. Benefiting from the distinct characteristics of such a clean, low-cost, and abundant energy source, photovoltaic technology is considered to be the most promising of all the renewable energy technologies.<sup>4</sup>

Since the appearance of the first crystalline silicon solar cell invented by Bell Labs in 1954, solar cell technology has undergone a dramatically fast development.<sup>5</sup> A variety of solar cells have been developed and some have been followed through into industrial production. Typically, solar cells can be classified into three generations according to the materials and technology development.<sup>6,7</sup> The first generation of solar cells refers to silicon-based solar cells, including monocrystalline and polycrystalline silicon cells.<sup>8–10</sup> To date, silicon solar cells are the most mature photovoltaic technology and dominate with more than 90% of the photovoltaic market. The second generation of solar cells refers to thin film solar cells, including amorphous silicon-, copper indium gallium selenide (CIGS)-, GaAs-, and CdTe-based devices.<sup>11–15</sup> The direct band gap of these materials, in comparison with the indirect one from Si, allows harvesting the light in thin films with a very few micron thickness. Thin film solar cell take advantage of a cost reduction in



Iván Mora-Seró

*Iván Mora-Seró is an associate professor at the Institute of Advanced Materials (INAM) at the Universitat Jaume I de Castelló. His research involves quantum dots and halide perovskites for the development of optoelectronic devices and solar cells.*



Juan Bisquert

*Juan Bisquert is a professor of applied physics at the Universitat Jaume I de Castelló and the director of the Institute of Advanced Materials (INAM). His main topics of interest are perovskite solar cells and solar fuel production. He has developed applications for measurement techniques and physical modeling related to device operation for the elementary steps that take place at the nanoscale.*

the manufacturing process due to material saving and the use of a lower processing temperature. Even though second generation solar cells exhibit comparable photovoltaic performance to silicon solar cells, they only possess a small market share (<10%) due to the limitation of the module technology and their stability. The third-generation solar cells are usually defined as emerging solar cells, most of which are still in the scientific research phase.<sup>4,16–23</sup> The motivation for the exploration of third-generation solar cells is to achieve a higher efficiency solar cell with the use of novel physical phenomena, materials, and structures that can largely reduce the production cost. Currently, third-generation solar cells mainly include dye-sensitized solar cells (DSCs), organic/polymer solar cells (OSCs), perovskite solar cells (PSCs), and quantum dot (QD) based solar cells.<sup>4,16–23</sup> In the past two decades, third-generation solar cells have attracted tremendous research interest and undergone fast development.

In the study of third-generation solar cells, particular interest has been focused on QD-based solar cells,<sup>19,20,25–27</sup> motivated by the dramatic characteristics of semiconductor QDs as a light-harvesting material, such as their facilely tunable band gap through size or composition control, high molar extinction coefficient, large intrinsic dipole moments, and their higher light, thermal, and moisture stability in comparison with dye molecules and lead halide perovskites. Additionally, QDs have a number of non-conventional properties, as shown in Fig. 1, such as multiple exciton generation (MEG) possibility, which could enable QD-based solar cells to overcome the Shockley–Quessier efficiency limit of 32.9% for single absorber solar cells.<sup>20,28</sup>

Typically, QD-based solar cells can be classified into four kinds (Fig. 2): Schottky junction solar cells, p–n junction solar cells (both homojunction and heterojunction), hybrid QD–polymer solar cells, and quantum dot-sensitized solar cells (QDSCs).<sup>29–31</sup> Among these, QDSCs possess the advantages of a low-cost device fabrication process due to the simple device structure derived from their analogous DSC counterparts.<sup>24,26,30,32–42</sup> It is noted that, over the past 12 years, the power conversion efficiency (PCE) of QDSCs has shown a dramatic improvement from less than 1% to nearly 13%, as shown in Fig. 3. The spectacular



Xinhua Zhong

*Xinhua Zhong is a professor at the South China Agricultural University. Before his current position, he worked at the East China University of Science and Technology, China. His research mainly involves nanoscale materials and their applications in energy conversion and storage. His research group has created and developed efficiency records for quantum dot-sensitized solar cells since 2012.*

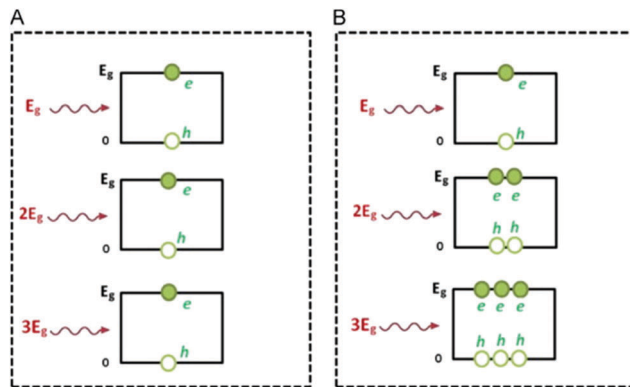


**Fig. 1** Schematic illustration of the generation of carriers under the excitation of photon energy: (A) traditional solar cell and (B) ideal multiple exciton generation in a QD-based solar cell. Reprinted with permission from ref. 24. Copyright (2014) Elsevier.

development trend of this kind of solar cell indicates its great potential as a promising candidate for the next-generation photovoltaic cells.

In recent years, many reviews about QDSCs have been published. Most of these review articles focused on a single component of the cell device, such as the photoanode, electrolyte, and counter electrodes.<sup>24,26,30,32–53</sup> While, a comprehensive overview about QDSCs, integrating their fundamental principles, recent material, and technical advances as well as the limitations of this kind of solar cell still lacking. Hence, this review article presents a comprehensive overview of the integrated development of QDSCs from their appearance to the current state of play. First, we review the fundamental working principle behind QDSCs together with the characterization techniques that are commonly used. Second, a brief overview of the landmark works on QDSCs is presented. Third, we summarize the recent advances in key materials used in QDSCs, including metal oxide electron-transporting materials (ETMs), light-harvesting material QD sensitizers, counter electrode (CE) catalytic materials, and electrolyte redox couple or hole-transporting materials (HTM). Then, we review the recent

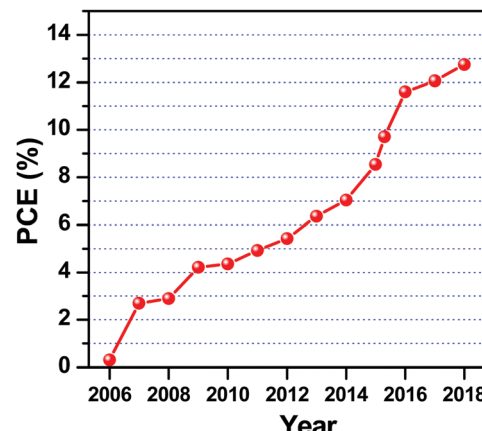


**Fig. 3** Evolution of the record PCE of QDSCs since 2006 (for cells based on a standard two-electrode configuration and tested under the irradiation of AM 1.5 G full one sun). The detailed data and the corresponding references are listed in Table 1.

advances in charge-recombination control in QDSCs, which is a critical factor limiting the performance of QDSCs. Afterward, we discuss the stability issue for QDSCs, which is usually neglected but is very crucial for the development of this kind of photovoltaic technology. Finally, we propose some possible research areas and issues that deserve to be addressed for promoting the development of QDSCs in the future.

## 2. Fundamental principles of QDSCs

### 2.1 Basic principles of QDSCs

The concept of a “sensitized semiconductor,” in which a wide-band-gap semiconductor is sensitized with a narrow band gap semiconductor to harvest sunlight and to generate charge carriers, can be dated back to the 1960s.<sup>54</sup> On the basis of this concept, devices based on DSCs were preliminarily studied and constructed as early as the 1980s.<sup>55</sup> Initially, smooth semiconductor electrodes were used for dye loading. The light-harvesting efficiency of this flat electrode, however, was very

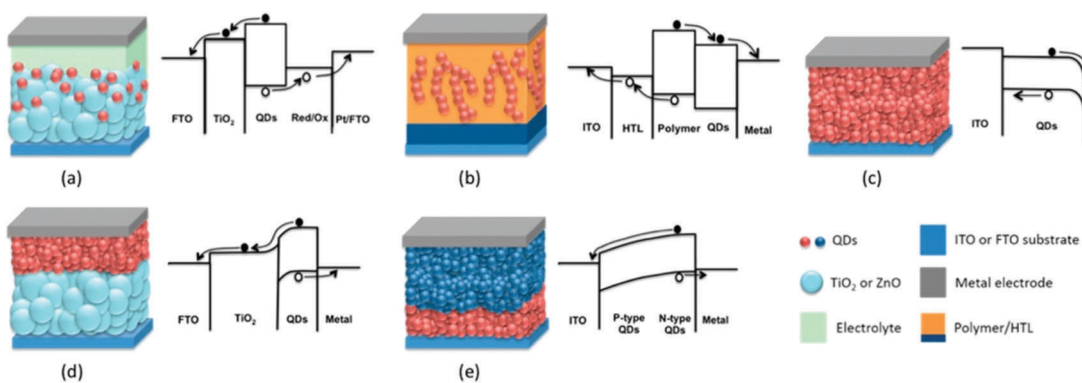


**Fig. 2** Schematic illustration of device configurations and energy band diagrams of QD-based solar cells: (a) QD-sensitized solar cell, (b) hybrid QD-polymer solar cell, (c) Schottky junction solar cell, (d) p–n heterojunction solar cell, and (e) p–n homojunction solar cell. Reprinted with permission from ref. 29. Copyright (2015) American Chemical Society.

low due to the small dye loading amount, and so the efficiency of the cell device was very low. In 1991, O'Regan and Grätzel produced the first breakthrough in this technology by replacing the flat semiconductor electrode by a  $\text{TiO}_2$  mesoporous film, allowing them to obtain a significant improvement in the loading amount of dye and boosting the PCE of the DSC to 7.1%.<sup>56</sup> From that time, DSCs started to draw lots of attention from researchers all over the world, such that the DSC is often also called a "Grätzel cell."<sup>16,57–62</sup> The pioneering work by Grätzel and coworkers is also regarded as a milestone marking the beginning of the investigation of third-generation PV technology.

The great contribution of these sensitized cells is that they decouple the charge generation and the charge transport. In silicon or in thin film solar cells, both processes occur in the same material and consequently the quality of materials has to be high in order to avoid defects promoting recombination. In sensitized devices, charge generation is produced in the dye while photogenerated charge is quickly injected into two different transport media. Thus, a medium only transports a certain type of carriers, consequently decreasing recombination and allowing the high standards for the quality of materials to be relaxed and therefore manufacturing costs to be reduced.<sup>63</sup>

The architecture of a QDSC is directly derived from DSCs, using QDs to replace organic dye molecules as the light-harvesting material.<sup>43</sup> The investigation of QDSCs was initially motivated by the attractive photoelectronic properties of QDs.<sup>20,26,64</sup> Typically, as shown in Fig. 4, a QDSC is composed of a QD-sensitized photoanode, an electrolyte, and a counter electrode.<sup>30,37,45</sup> Upon light irradiation, the QDs absorb solar energy and electrons in the valence band (VB) of the QDs are excited to the conduction band (CB), generating electron-hole pairs. Then, electrons in the CB of the QDs are quickly injected into the CB of a metal oxide (generally  $\text{TiO}_2$ ) electron acceptor under the driving force of the energetic difference in the CB between the QDs and metal oxide, thereby achieving a charge-separation process. The electrons transfer through the  $\text{TiO}_2$  mesoporous film to the transparent conductive oxide substrate and then to the counter electrode through an external circuit. Meanwhile, the oxidized QDs are regenerated by reduced species of the redox couple in the electrolyte, while the oxidized species of the redox couple are reduced by the electrons from the external circuit under the catalysis of CE. Apart from

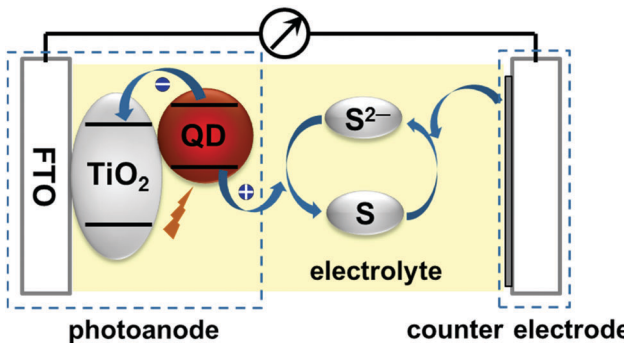


Fig. 4 Schematic illustration of the device structure of QDSCs.

these desired charge-transport processes, some other unwanted processes, also known as charge recombination, take place simultaneously and significantly deteriorate the solar cell performance.<sup>33,38</sup> This is discussed in detail in the following section.

## 2.2 Characterizations of QDSCs

In order to evaluate the photovoltaic performance of the cell device and get insights into the charge-transfer dynamics at the interfaces, such as the charge-separation and -recombination processes, a variety of characterization methods have been developed for QDSCs. Among them, current-voltage ( $J$ - $V$ ), incident photon conversion efficiency (IPCE), absorbed photon to current conversion efficiency (APCE), time-resolved photoluminescence (TRPL), transient absorption (TA), electrochemical impedance spectroscopy (IS), open-circuit voltage-decay (OCVD), and charge-extraction measurements are the most widely used characterization routes for QDSCs.

**2.2.1. Photovoltaic performance measurements.** Similar to all kinds of solar cells, the photovoltaic performance measurements of QDSCs consist of  $J$ - $V$  and IPCE tests. The  $J$ - $V$  curve is usually used to determine the PCE of the solar cell, showing the relationship between the output current and voltage of the solar cell under irradiation. From a  $J$ - $V$  curve (Fig. 5), we can directly obtain the short-circuit current density ( $J_{sc}$ ) and the open-circuit voltage ( $V_{oc}$ ) values on the basis of the intercepts of the  $J$ - $V$  curve with the lateral and vertical axes, respectively. The  $J_{sc}$  and  $V_{oc}$  values represent the maximum photocurrent and photovoltage output capability of the cell, respectively. In a  $J$ - $V$  curve, there exists a point that the product of the photocurrent ( $I_{mp}$ ) and photovoltage ( $V_{mp}$ ), namely the output power ( $P_{max}$ ), is at a maximum. The specific value of  $P_{max}$  to the product of  $V_{oc}$  and  $J_{sc}$  is defined as the fill factor (FF), which is in the range from 0 to 1. The PCE of the QDSCs can be calculated as follows:

$$\text{PCE} = \frac{I_{mp} \cdot V_{mp}}{P_{in}} = \frac{J_{sc} \cdot V_{oc} \cdot \text{FF}}{P_{in}} \quad (1)$$

where  $P_{in}$  is the power density of the incident light.

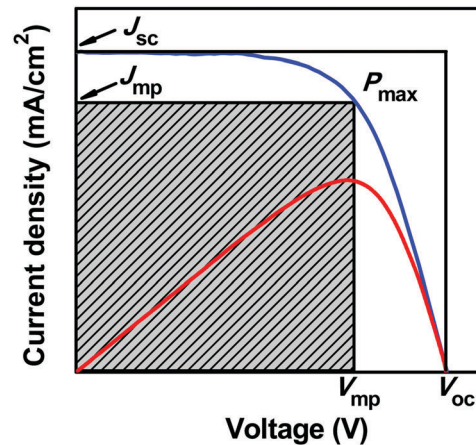


Fig. 5  $J$ - $V$  characteristic curves of QDSCs.

It should be noted that *J*-*V* measurement conditions should be strict and standard to get credible results.<sup>65</sup> This is very crucial to allow comparisons of the results from different labs. For example, a proper black mask should be used in the measurement to define the active area and to avoid excess light getting into the QDSCs. Furthermore, the spectrum of the light source should be exactly the same as the solar spectrum (AM 1.5 G), with a Si standard solar cell used to calibrate the intensity of the light (100 mW cm<sup>-2</sup>, one sun). To render the photovoltaic performances reported by different laboratories comparable, a certified PCE by a third party is therefore very important, especially for record devices defining a new state-of-the art performance. In addition, some other parameters, such as the scan rate, direction, and delay time, should also be carefully taken into account during the measurement.<sup>65</sup> It is noted that unlike the case for perovskite solar cells, the hysteresis in *J*-*V* measurements is barely observed in QDSCs.

A solar cell can be seen as an equivalent circuit that consists of a light-generated current source, diode, and series resistance.<sup>65</sup> Normally, there are two approaches resulting in power dissipation, which are the leakage current from shunt (parallel) resistance ( $R_{\text{shunt}}$ ) and the voltage loss from series resistance ( $R_{\text{series}}$ ). The  $R_{\text{shunt}}$  and  $R_{\text{series}}$  values of a device can be obtained from the slope of the *J*-*V* curve at the voltages of 0 V and  $V_{\text{oc}}$ , respectively. These two parameters have a great influence on the FF value of a solar cell, whereby a large  $R_{\text{shunt}}$  and a small  $R_{\text{series}}$  will promise a high FF. Generally, recombination reduction can decrease the leakage current, and then increase the value of  $R_{\text{shunt}}$ , but also has the beneficial effect of increasing the open-circuit potential. Besides, it is helpful to decrease the resistance of the contacts during charge transport, in order to reduce  $R_{\text{series}}$ .<sup>66</sup>

Another important photovoltaic performance measurement route in QDSCs is the IPCE, also known as external quantum efficiency (EQE), corresponding to the number of generated electrons ( $N_e$ ) divided by the number of incident monochromatic photons ( $N_p$ ).<sup>7,24,45</sup> The IPCE can be expressed as follows:

$$\text{IPCE}(\lambda) = \frac{N_e}{N_p} = \frac{1240 \cdot J_{\text{sc}}(\lambda)}{\lambda \cdot P_{\text{in}}} \quad (2)$$

where  $J_{\text{sc}}$  is the short-circuit current density under monochromatic light illumination (with the wavelength  $\lambda$ ) and  $P_{\text{in}}$  is the power density of incident light. IPCE measurements are usually used to confirm the photoresponse range of a device in addition to the  $J_{\text{sc}}$  value obtained from the *J*-*V* test. A  $J_{\text{sc}}$  value can also be obtained by integrating the product of the incident photon flux density ( $F$ ) and the measured IPCE values as follows:<sup>45</sup>

$$J_{\text{sc}} = \int qF(\lambda)\text{IPCE}(\lambda)d(\lambda) \quad (3)$$

where  $q$  is the electron elementary charge. The  $J_{\text{sc}}$  values obtained from the IPCE and *J*-*V* tests should be identical for an ideal solar cell, and this is an effective test of the correct measurement of the photocurrent. In addition, the IPCE value

is affected by the light-harvesting efficiency (LHE), electron-injection efficiency from the QD to TiO<sub>2</sub> ( $\varphi_{\text{inj}}$ ), and the charge-collection efficiency ( $\varphi_{\text{cc}}$ ). Therefore, the IPCE can also be described as follows:

$$\text{IPCE}(\lambda) = \text{LHE}(\lambda) \cdot \varphi_{\text{inj}} \cdot \varphi_{\text{cc}} \quad (4)$$

The absorbed photon to current conversion efficiency (APCE), also called the internal quantum efficiency (IQE), corresponds to the number of generated electrons ( $N_e$ ) divided by the number of absorbed photons ( $N_a$ ). The APCE results can reflect the efficiency of absorbed photons by a QD being converted into photocurrent, excluding the effect of the light-harvesting efficiency of the photoanode.<sup>24,65</sup> The APCE can be described by the following equation:

$$\text{APCE}(\lambda) = \frac{N_e}{N_a} = \frac{\text{IPCE}(\lambda)}{\text{LHE}(\lambda)} = \varphi_{\text{inj}} \cdot \varphi_{\text{cc}} \quad (5)$$

**2.2.2. Time-resolved photoluminescence (TRPL) and ultra-fast transient absorption (TA) measurements.** TRPL and ultra-fast TA spectroscopy are usually used to monitor the dynamics of charge-transfer processes in QDSCs, including the electron-injection rate from QDs to the metal oxide, the hole-transfer rate from oxidized QDs to the electrolyte, and the charge-recombination rate at the photoanode/electrolyte interface. Pullerits *et al.* carried out outstanding efforts in this regard and their works elaborated the related mechanism of the charge dynamics in QDSCs.<sup>67–72</sup>

In TRPL measurements, a pulsed laser with a high frequency is applied to excite samples. Typically, single photon counting is used to produce statistics of the decay time. After each laser pulse, the detector waits until the first emitted photon arrives, recording the delay between excitation and emission. The high frequency allows obtaining the PL decay behavior after the accumulation of enough detected events. Then, the corresponding excited state lifetime is obtained by fitting the decay curves of the photoluminescence.<sup>73,74</sup> For a sample of QDs in solution or attached to isolating semiconductor films, the photoexcited electrons directly decay back to the ground state through radiative or non-radiative recombination processes. As a result, this lifetime ( $\tau$ ), as determined from the decay curve, reveals the recombination dynamics of the QDs without charge-transfer processes. For a sample of QDs attached to electron-transporting metal oxide films, such as TiO<sub>2</sub> and ZnO, the electrons in the excited state can be extracted out *via* a charge-injection process. Herein, the lifetime ( $\tau'$ ) exhibits the dynamics of charge-transfer processes in QDSCs. The decay curve can be fitted with a multiple-exponential function by the following equation:

$$y = \sum_{i=1}^n A_n \exp(-t/\tau_n) \quad (6)$$

where  $\tau_n$  and  $A_n$  are the lifetimes and weighted coefficients for the multiple components, respectively. In QDSCs, the most common approach is a biexponential function ( $n = 2$ ). For the multiple-components process, an average lifetime ( $\tau_{\text{av}}$ ) of

photoexcited electrons can be calculated using the following equation:

$$\tau_{\text{av}} = \sum_{i=1}^n A\tau_i^2 / \sum_{i=1}^n A\tau_i \quad (7)$$

In principle, the charge-injection rate constant ( $K_{\text{et}}$ ) can be calculated according to the obtained average lifetimes ( $\tau_{\text{av}}$  and  $\tau_{\text{av}'}$ ) using the following equation:

$$K_{\text{et}} = \frac{1}{\tau_{\text{av}'}} - \frac{1}{\tau_{\text{av}}} \quad (8)$$

Moreover, ultrafast TA spectroscopy also plays a significant role in revealing the charge-transfer processes in most of the emerging solar cells.<sup>32,39,65,75-80</sup> A schematic diagram of the ultrafast TA equipment is shown in Fig. 6. In this measurement, pulses with a certain frequency are generated by a femtosecond Ti-sapphire laser and then split into pump and probe pulses. The wavelength of the pump pulses is modulated by an optical parametric amplifier (OPA), and a series of neutral-density filters is used to adjust the power of the pump beam. Meanwhile, the initial probe of monochromatic light is transformed into a white light after passing the crystal of sapphire or calcium fluoride. The pump and probe pulses are focus on the same point of the samples at a certain angle and at different delay times. The delay times ( $\Delta t$ ) between the pump and probe pulses can be adjusted through a motorized delay stage. A detector is used to record the absorption ( $A_t$ ) at different delay times ( $\Delta t$ ) after each pump pulse and the absorption ( $A_0$ ) without a pump pulse. The induced absorbance change ( $\Delta A$ ) can be calculated through  $A_t$  minus  $A_0$ . Since we can measure the TA spectra at different pump-probe delay times,  $\Delta A$  can be determined as a function of both the wavelength and time. Finally, the charge lifetimes are given by fitting with the decay curves of  $\Delta A$  versus time, similar to the TRPL measurement.

**2.2.3. Impedance spectroscopy (IS) measurements.** IS allows decoupling physical processes occurring at different time (frequency) scales. In this sense, it is very interesting for the study of a complete device under its working conditions, as information of the different parts can be extracted from a single measurement.<sup>33,65,66,81</sup> IS allows studying the kinetics of charge

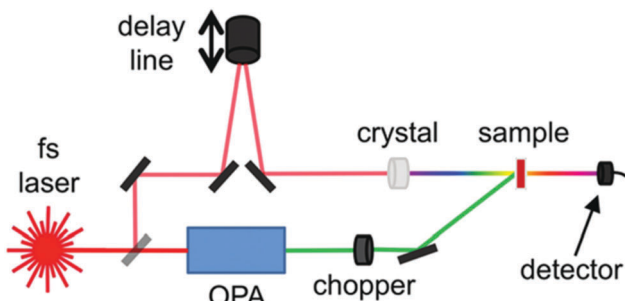


Fig. 6 Schematic diagram of the main components in ultrafast TA equipment. Reprinted with permission from ref. 65. Copyright (2017) Royal Society of Chemistry.

transport and recombination at  $\text{TiO}_2/\text{QD}/\text{electrolyte}$  interfaces. In addition, it also permits evaluating the catalytic activity of CEs in QDSCs. In this measurement, a DC voltage is applied to the system and a small AC signal is used to perturb the system simultaneously. Afterward, the sinusoidal current response is measured as a function of modulation frequency. According to the applied perturbation and the measured response, the impedance value can be obtained. On the basis of a well-developed equivalent circuit, the electrochemical parameters, such as series resistance ( $R_s$ ), charge-transfer resistance ( $R_{\text{ct}}$ ), recombination resistance ( $R_{\text{rec}}$ ), and diffusion resistance ( $Z_w$ ), can be obtained by fitting the data with software.<sup>66,81</sup> The IS results are often expressed in a complex plane plot (imaginary part of impedance vs. real part) or a Bode plot showing the parameter of interest vs. frequency. Typically, two semicircles can be found in a complex plane impedance plot for QDSCs. The  $R_s$  can be obtained from the starting point of the plot. The first semicircle at high frequency is assigned to the  $R_{\text{ct}}$  at the CE/electrolyte interface, while the second semicircle at middle and low frequency refers to the  $R_{\text{ct}}$  or  $R_{\text{rec}}$ , depending on the applied bias, at the  $\text{TiO}_2/\text{QD}/\text{electrolyte}$  interfaces. Finally, the electrochemical properties of the materials or the interfaces can be analyzed according to the obtained electrochemical parameters.

#### 2.2.4. Open-circuit voltage-decay (OCVD) measurements.

The OCVD measurement is an alternative tool that is commonly used to obtain the electron lifetime ( $\tau_n$ ) of excited electrons in DSCs or QDSCs.<sup>82,83</sup> Typically, in this measurement, the cell is first illuminated under open-circuit conditions for a certain period to get to a steady  $V_{\text{oc}}$ . Then, the light is turned off and the output  $V_{\text{oc}}$  is traced as a function of time. The  $V_{\text{oc}}$  decay rate is directly related to the electron lifetime of the cell since the variation of  $V_{\text{oc}}$  after turning off the light is determined by the lifetime of the photogenerated electrons. The corresponding  $\tau_n$  can be calculated according to the following equation:

$$\tau_n = -\frac{k_B T}{e} \left( \frac{dV_{\text{oc}}}{dt} \right)^{-1} \quad (9)$$

where  $k_B$  is the Boltzmann constant,  $T$  is the absolute temperature (298.15 K), and  $e$  is the elementary charge. The OCVD test can be used to estimate the whole degree of charge recombination in QDSCs. During the measurement, once the light is turned off, the decay of the  $V_{\text{oc}}$  is determined by the rate constant of charge recombination at  $\text{TiO}_2/\text{QD}/\text{electrolyte}$  interfaces. Therefore, we can evaluate the charge-recombination dynamics in solar cells according to the calculated electron lifetime from the decay curves.

**2.2.5. Charge-extraction measurements.** For DSCs and QDSCs, charge-extraction measurement is usually applied to indicate the shift of the Fermi level of an electron-transporting metal oxide, which is an important factor affecting the  $V_{\text{oc}}$  of devices.<sup>84-86</sup> At the beginning of the measurement, the device is illuminated and kept at open-circuit conditions. Afterward, the light is switched off and then the device is switched to short-circuit conditions with a delay time. Meanwhile, the current is

recorded and integrated *versus* time to obtain the amount of extracted charge ( $Q_{oc}$ ). The obtained  $Q_{oc}$  can reflect the density states of the metal oxide film electrode and therefore can be used to estimate the shift of its Fermi level.

### 3. Brief history of the evolution of QDSCs

Dating from the 1970s, researchers found that the efficiency of charge separation can be increased by contacting the semiconductor particle with another kind of semiconductor.<sup>87–94</sup> For example, in 1984, Grätzel *et al.* demonstrated that the combination of CdS and TiO<sub>2</sub> could increase the yield of H<sub>2</sub> generation from H<sub>2</sub>S, benefiting from electron transfer from the conduction band of CdS to that of TiO<sub>2</sub> particles.<sup>87</sup> Gerischer *et al.* introduced the concept of dye sensitization to semiconductor sensitization. They deposited CdS on TiO<sub>2</sub> and found that the photocurrent of the electrode was improved due to the extended light-absorption range.<sup>88</sup> These works established the initial concept of the present QDSCs. Since then, many kinds of light-harvesting semiconductors, such as CdSe, PbS, CdS, and Bi<sub>2</sub>S<sub>3</sub>, have been used to sensitize wide-band-gap semiconductors and their photoelectrochemical properties have been investigated.<sup>94</sup>

In 1990, Weller and coworkers sensitized a highly porous TiO<sub>2</sub> electrode by quantum-sized CdS particles through an *in situ* deposition approach.<sup>91</sup> They also fabricated a three-electrode-based photoelectrochemical cell and obtained a  $V_{oc}$  of 0.395 V, a  $J_{sc}$  of 175 mA m<sup>-2</sup>, and an FF of 0.75 under the illumination of monochromatic light with a wavelength of 460 nm. Then in 1998, Zaban and Nozik *et al.* deposited pre-synthesized InP QDs on a TiO<sub>2</sub> electrode and fabricated a sandwich-type QDSC device for the first time using I<sup>-</sup>/I<sub>3</sub><sup>-</sup> as the electrolyte and Pt as the counter electrode.<sup>95</sup> The photocurrent of the constructed cell device was monitored under the illumination of incident light. This was the first report of an integral QDSC device, even though the final PCE of the solar cell was not given. Afterward, InAs QDs with different sizes were also used as a sensitizer by Nozik's group and an efficiency of 0.3% was obtained.<sup>96</sup> Considering the limited stability of QDs in I<sup>-</sup>/I<sub>3</sub><sup>-</sup> electrolyte, Grätzel *et al.* constructed the first solid-state QDSC in 2002 employing 2,2',7,7'-tetrakis((N,N-di-*p*-methoxyphenylamine)-9,9'-spirobifluorene) (spiro-OMeTAD) as a hole-transport material (HTM) and obtained an efficiency of 0.49% under 0.1 sun illumination.<sup>97</sup> Up to 2006, QDSCs didn't draw much attention since their obtained efficiency was much lower in comparison with their analog DSCs.<sup>98</sup>

The first leap forward for QDSCs was achieved by Toyoda and coworkers in 2007,<sup>99</sup> who boosted the PCE of QDSCs to over 2%. In this work, they fabricated CdSe-sensitized TiO<sub>2</sub> inverse opal solar cells combined with a polysulfide electrolyte. Furthermore, the authors demonstrated that a ZnS thin layer overcoating on the photoanode could significantly improve the solar cell performance. It should be noted that this ZnS treatment has since evolved as an indispensable procedure in the

fabrication of high-efficiency QDSCs. After that, Lee *et al.* introduced a two-step QDs deposition approach, in which a pre-synthesized CdS seed layer was first self-assembled on a TiO<sub>2</sub> electrode surface using a bifunctional linker molecule, followed by a chemical bath deposition (CBD) process for the growth of the CdSe layer. This configuration achieved a PCE of 2.8%.<sup>100</sup> Then, Lee and coworkers put forward a classical CdS/CdSe co-sensitization structure through a successive ionic layer adsorption and reaction (SILAR) deposition approach, boosting the PCE of QDSCs to 4.22% in 2009.<sup>101</sup> Grätzel *et al.* developed a new procedure for preparing the selenide (Se<sup>2-</sup>) source by reducing the corresponding dioxide precursor in ethanol and then using this for depositing CdSe QDs on TiO<sub>2</sub> through a SILAR approach, exhibiting a PCE of 4.18% under 0.1 sun illumination using a cobalt redox couple.<sup>102</sup>

From 2009, QDSCs started to drew more and more attention due to their significantly improved photovoltaic performance. Fan *et al.* explored ordered multimodal porous carbon (OMPC) and mesoporous-carbon nanofibers (MCNFs) as counter electrode catalytic materials in QDSCs and achieved efficiencies of 4.36% and 4.81%, respectively.<sup>103,104</sup> Xu *et al.* designed a ZnO/Zn<sub>x</sub>Cd<sub>1-x</sub>Se core/shell nanocable array photoanode, delivering a PCE of 4.74%.<sup>105</sup> Meng *et al.* systematically optimized the structure of a TiO<sub>2</sub> film electrode based on a CdS/CdSe QDs system, giving a best efficiency of 4.92%.<sup>106</sup> Kamat *et al.* proposed a doping strategy in QD sensitizers to facilitate the charge-transfer and charge-separation processes. They employed Mn<sup>2+</sup> doping in a CdS layer and prepared Mn-doped-CdS/CdSe QD sensitizers, boosting the PCE of QDSCs to over 5% (5.4%) for the first time.<sup>107</sup>

Since 2012, we have been witnessing a rapid evolution of the record PCE of QDSCs arising from the development of both material and mechanisms following intense investigations. Until this year, the highest efficiencies were obtained with sensitized electrodes, where the QDs were directly grown on the mesoporous electrode by a CBD or SILAR method. However, the characterization of devices using QDs prepared in different ways pointed out a better potentiality for devices using colloidal QDs as sensitizers.<sup>108</sup> Nevertheless the efficiency of QDSCs using colloidal QDs was limited by their low QD loading, which limited the light harvesting. In 2012, Zhong's group focused on the utilization of high-quality pre-synthesized colloidal QDs as sensitizers, and deposited QDs on a TiO<sub>2</sub> electrode through a capping-ligand-induced self-assembly (CLIS) approach.<sup>109,110</sup> This novel deposition method was proven to be capable of realizing a fast, uniform, and high loading amount of colloidal QDs on a TiO<sub>2</sub> electrode.<sup>74</sup> Furthermore, the CLIS approach provided a way to introduce high-quality QDs as sensitizers in QDSCs, and since that moment, successively higher efficiency records were obtained with colloidal QDs as sensitizers.<sup>36,74,85,109–119</sup> Through the exploration of the superior colloidal QD sensitizers and interface modification engineering, the highest PCE of QDSCs has been improved from 5% to nearly 13% during the past 5 years, leading to a huge step forward and making them more competitive with other kinds of emerging solar cells. The evolution of the PCE



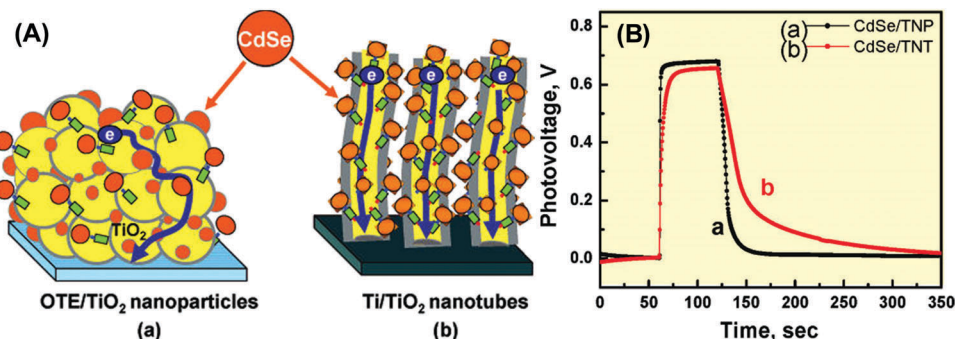


**Fig. 7** (A) Random versus directed electron transport through support architectures, (a) TiO<sub>2</sub>-particle and (b) TiO<sub>2</sub>-nanotube films modified with CdSe quantum dots. (B) Open-circuit photovoltage response of: (a) OTE/TiO<sub>2</sub>(particle)/CdSe and (b) Ti/TiO<sub>2</sub>(nanotube)/CdSe electrodes using 3.0 nm CdSe quantum dots as light absorbers. Reprinted with permission from ref. 73. Copyright (2008) American Chemical Society.

the effective area of the electrode decreases the QD-loading amount, thus decreasing the light-harvesting capability, see below.

As early as 2007, Kamat *et al.* showed that TiO<sub>2</sub>-NT is superior to TiO<sub>2</sub>-NP as an ETM in constructing QDSCs due to the better electron-transport capacity, since the large grain boundaries in a TiO<sub>2</sub>-NP-based film will increase the electron loss during the transport process (Fig. 7).<sup>73,146</sup> Shen *et al.* proposed a CdSe-sensitized TiO<sub>2</sub>-NT working electrode and constructed a complete QDSC device, achieving a PCE of 1.8%.<sup>122</sup> Meng *et al.* fabricated a CdS/CdSe-sensitized TiO<sub>2</sub>-NT photoanode and obtained a PCE of 3.18% with optimization of the CdSe deposition time and the length of the nanotube.<sup>128</sup> Zhang *et al.* applied a short-length and high-density rutile TiO<sub>2</sub>-NR array as an electrode and sensitized it with PbS QDs to fabricate all-solid-state QDSCs, delivering a PCE of 4.10%.<sup>147</sup> Kuang *et al.* employed vertically aligned anatase TiO<sub>2</sub>-NW with a branched architecture as the ETM in CdS/CdSe QDSCs (Fig. 8). The branched hierarchical structure was found to favor

an improvement of the  $J_{sc}$  value due to the increased light-scattering ability, and a final PCE of 4.2% was achieved.<sup>144</sup> Furthermore, they designed a three-dimensional (3D) hierarchically branched TiO<sub>2</sub>-NW-coated hollow-sphere photoanode with a high specific surface area, while maintaining roomy space, further boosting the PCE to 6.01%.<sup>145</sup>

Although a lot of effort has been devoted to exploring 1D-structured TiO<sub>2</sub>-based photoanodes in QDSCs, the obtained PCEs are still poor compared to that of TiO<sub>2</sub>-NP-based ones. Therefore, the potential of 1D-structured TiO<sub>2</sub>-based photoanodes has not been fully explored. This may be mainly derived from the low QD-loading amount on the 1D-structured TiO<sub>2</sub> film, resulting in a low light-harvesting efficiency and severe charge recombination. Therefore, further improvement of the performance of 1D-structured TiO<sub>2</sub>-based QDSCs should focus on the enhancement of the specific surface area of the photoanode film to therefore increase the QD-loading amount on the TiO<sub>2</sub> film.

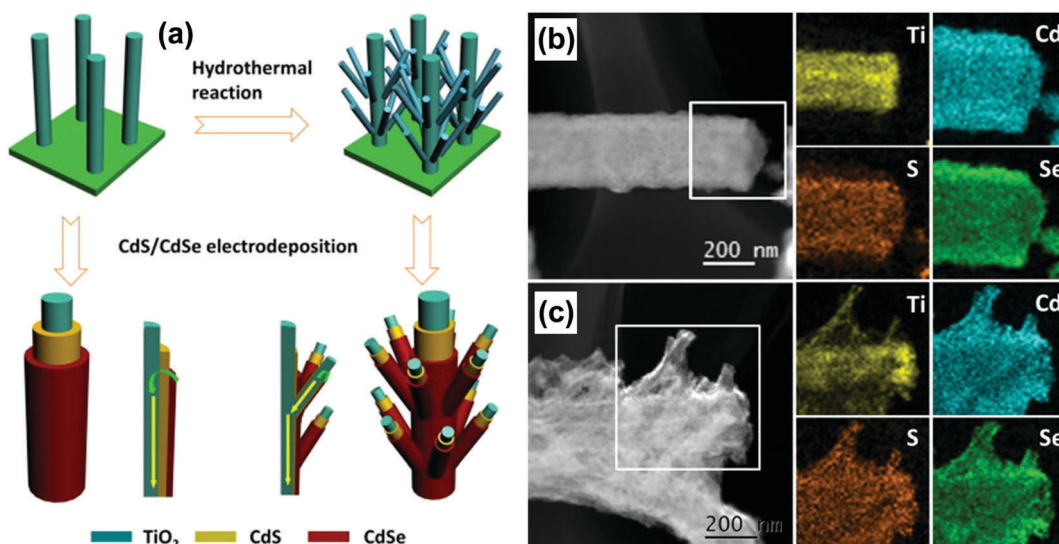


**Fig. 8** (a) Schematic diagram showing the preparation process and structure of CdS/CdSe-co-sensitized smooth and hierarchical TiO<sub>2</sub> nanowires as well as the path of electron injection (green arrow) and electron transport (yellow arrow). High-angle annular dark-field scanning transmission electron microscopy (HAADF-STEM) and energy dispersive X-ray spectroscopy (EDX) mappings of a TiO<sub>2</sub>/CdS/CdSe photoanode based on: smooth (b) and hierarchical (c) nanowires. Reprinted with permission from ref. 144. Copyright (2014) Elsevier.

**4.1.2. ZnO-Based photoanodes.** From the aspect of the electronic features, ZnO seems to be more suitable to serve as an ETM due to its higher electron mobility (130–200 vs. 0.1–4 cm<sup>2</sup> V<sup>-1</sup> s<sup>-1</sup>) and conduction band edge. These unique properties are beneficial for obtaining higher  $V_{oc}$  values.<sup>42,47</sup> Hence, much work on ZnO-based photoanode has been reported. However, from the aspect of chemical stability, the ZnO electrode is limited with a lower stability than TiO<sub>2</sub>. Its amphoteric nature leads to ZnO dissolving in both acidic and basic media, thereby limiting its application in QDSCs. This chemical instability would limit the long-term lifetime of cell devices. Another restriction is that its pre-functionalization would not be possible given the dissolution of ZnO by the acidic carboxylic anchoring groups of the capping ligands on QD sensitizers.

Similar to TiO<sub>2</sub>, ZnO nanoparticle (ZnO-NP)-based photoanodes were also investigated in QDSCs.<sup>149,155–162</sup> For example, Stathatos *et al.* prepared a ZnO-NP (10–30 nm)-based film prepared in a facile method with the use of an amino double-edged polypropylene oligomer and zinc precursor.<sup>160</sup> The film was then used to fabricate quasi-solid-state CdS/CdSe-sensitized QDSCs, delivering a PCE of 4.5%. Meng *et al.* prepared ZnO-NPs with a diameter of 20 nm on a film and then sensitized this with CdS/CdSe QDs to construct a photoanode, demonstrating a PCE of 4.46%.<sup>149</sup> Cao and Tian *et al.* applied a passivation strategy on the surface of ZnO nanoparticles using TiO<sub>2</sub> nanoparticles to reduce the charge recombination at the photoanode/electrolyte interface.<sup>161</sup> The results demonstrated that TiO<sub>2</sub> passivation could not only suppress the charge-recombination process, but also increased the specific surface area for loading more QDs, thus improving the PCE of CdS/CdSe-based QDSCs from 2.38% to 4.68%. They also reported a bilayer-structured photoanode with a ZnO-NP film as a transparent layer and ZnO microspheres (MSs) as a scattering layer for CdS/CdSe-based QDSCs.<sup>162</sup> The MS layer could effectively increase the light diffuse reflection so as to enhance the light-harvesting efficiency, and enabling the device to exhibit a PCE of 5.08%. Nevertheless, unlike the case of TiO<sub>2</sub>,

the solar cell performance of ZnO-NP-based QDSCs was inferior to that of the multi-dimensional ZnO-based ones, partially due to the severe charge-recombination losses at the ZnO/electrolyte interface.

Another unique property of ZnO is that it is relatively easy to crystallize and its growth is anisotropic, such that ZnO nanostructures can be easily prepared in various morphologies.<sup>47</sup> Accordingly, ZnO nanowires (ZnO-NWs),<sup>105,150,163–175</sup> nanorods (ZnO-NRs),<sup>176–186</sup> and nanotetrapods (ZnO-TPs)<sup>187,188</sup> have been employed as ETMs to construct photoanodes in QDSCs. For example, in 2007, Norris and Aydin and coworkers grew ZnO-NWs on an FTO substrate and sensitized this with CdSe QDs.<sup>163</sup> They fabricated QDSCs using I<sup>-</sup>/I<sub>3</sub><sup>-</sup> as the electrolyte and Pt as the CE, with the device delivering a PCE of 0.4%. After that, Yong *et al.* sensitized ZnO-NWs with CdS/CdSe QDs through a SILAR approach, improving the PCE of ZnO-NW-based QDSCs to 4.15%.<sup>175</sup> Due to the much larger  $K_{sp}$  value of Zn(OH)<sub>2</sub>, ZnO can be easily converted to ZnS or ZnSe. This property can be used to form QD sensitizers around ZnO through a facile ion-exchange approach. For example, Lee *et al.* prepared ZnO-NW arrays on an FTO substrate, and then formed a ZnO/ZnSe/CdSe nanocable-structured photoanode through an ion-exchange approach.<sup>150</sup> The QDSCs based on this nanocable photoanode exhibited a PCE of 4.54% and a  $V_{oc}$  as high as 0.836 V. The ZnSe layer was found to be crucial for achieving high efficiency since it could reduce charge recombination by passivating the surface of the ZnO-NW and upshift the CB of ZnO. Furthermore, employing the same deposition method, they fabricated a ZnO/Zn<sub>x</sub>Cd<sub>1-x</sub>Se core/shell-structured nanocable photoanode (Fig. 9).<sup>105</sup> The band gap of the nanocables could be tuned by the Zn content in the Zn<sub>x</sub>Cd<sub>1-x</sub>Se shell layer. Finally, a PCE of 4.74% was obtained with the use of this nanocable as a photoanode. It is well known that a key problem for ZnO ETMs is that the charge recombination at the interface of ZnO/electrolyte is more serious than that in TiO<sub>2</sub>-based systems, leading to a poor cell efficiency. However, it was found that treatment of the ZnO

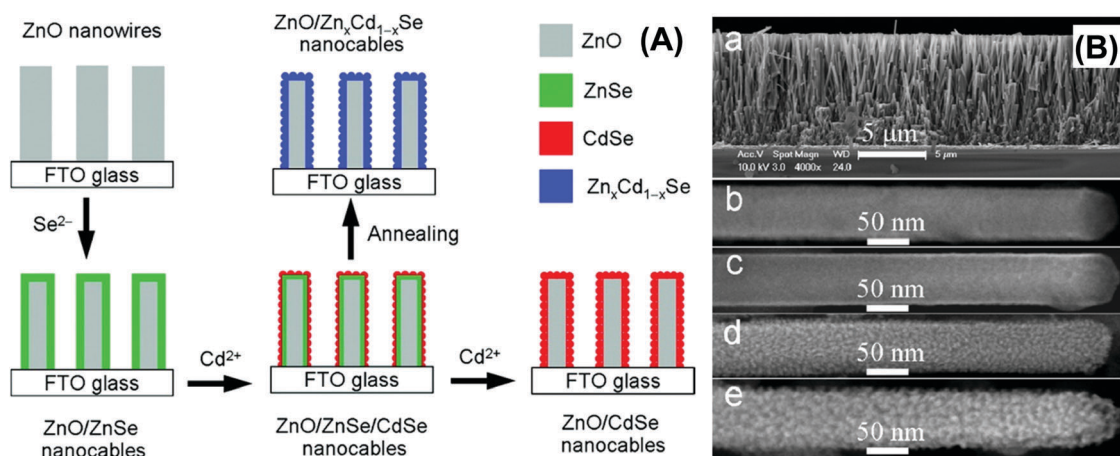
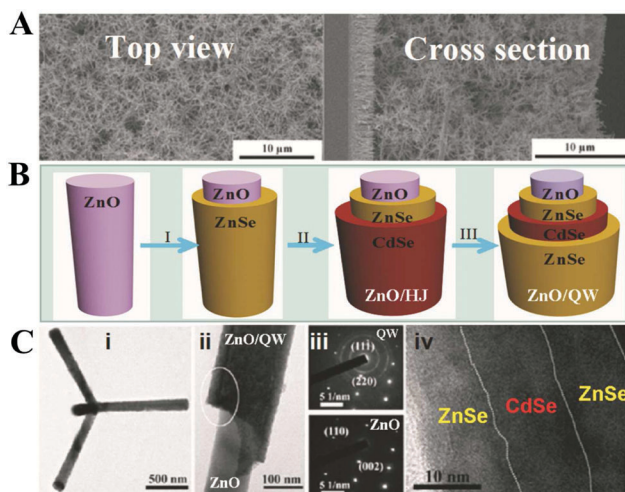


Fig. 9 (A) Schematic illustration of the formation processes of ZnO/Zn<sub>x</sub>Cd<sub>1-x</sub>Se core/shell nanocables. (B) SEM images of: (a) a ZnO nanowire array, (b) a ZnO/ZnSe nanocable, (c) a Zn<sub>0.7</sub>Cd<sub>0.3</sub>Se nanocable prepared by reacting a ZnO/ZnSe nanocable with Cd<sup>2+</sup> at 50 °C, (d) a ZnO/Zn<sub>0.33</sub>Cd<sub>0.67</sub>Se nanocable prepared by reacting a ZnO/ZnSe nanocable with Cd<sup>2+</sup> at 90 °C, and (e) a ZnO/CdSe nanocable prepared by reacting a ZnO/ZnSe nanocable with Cd<sup>2+</sup> at 140 °C. Reprinted with permission from ref. 105. Copyright (2011) American Chemical Society.

surface using  $\text{TiO}_2$  is an efficient way to inhibit interface charge recombination. For example, Cao and Tian and coworkers found that after the modification of  $\text{ZnO}$ -NR arrays with  $\text{TiO}_2$  nanoparticles, the PCE of the cell could be improved from 1.54% to 3.14%.<sup>181</sup> The  $\text{TiO}_2$  nanoparticles not only acted as a barrier layer to prevent electron back transfer from  $\text{ZnO}$  to the electrolyte, but also altered the surface characteristics of the  $\text{ZnO}$ -NRs so as to improve the QD-loading amount.

A key limitation for the  $\text{ZnO}$ -NW- and  $\text{ZnO}$ -NR-based photoanodes is their low specific surface area, leading to a low QD-loading amount and therefore resulting in a low  $J_{\text{sc}}$  value. Thus, a hierarchical architecture comprising long nanowire trunks and short nanorod branches is a suitable choice to offer more sites for loading QDs. Yang *et al.* reported a  $\text{ZnO}$  double-layer-architecture-based photoanode for QDSCs, consisting of a  $\text{ZnO}$ -NR underlayer and a  $\text{ZnO}$ -TP top layer.<sup>187</sup> It was shown that the double-layer strategy could reduce charge recombination at the interface between the FTO substrate and  $\text{ZnO}$ , leading to it yielding a higher  $V_{\text{oc}}$  of 0.703 V and a PCE of 5.24%. Furthermore, Yang and coworkers prepared  $\text{ZnO}$ -TP with diameters of 50–200 nm and lengths of 400–1000 nm, followed by sensitization with  $\text{ZnSe}/\text{CdSe}/\text{ZnSe}$  quantum wells (QWs) (Fig. 10).<sup>188</sup> The QW-sensitizer-based QDSCs delivered a record PCE of 6.20% and an impressive high  $V_{\text{oc}}$  of 0.761 V, which was higher than that for device based on  $\text{ZnSe}/\text{CdSe}$  heterojunction QDs (4.02%). A core/shell two-channel transport mechanism was proposed and demonstrated for the QW-based solar cells, indicating that the electron could travel through both the  $\text{ZnO}$  and sensitizer channel. Up to now, this is the highest reported PCE for  $\text{ZnO}$  ETM-based QDSCs.



**Fig. 10** Layer-by-layer formation of a  $\text{ZnSe}/\text{CdSe}/\text{ZnSe}$  quantum well (QW) sensitizer. (A) Top and cross-sectional view SEM images of a  $\text{ZnO}$  nanotetrapods photoanode for SSSCs. (B) Schematic diagram of the formation process: (i) first, the photoanode is placed in freshly prepared  $\text{NaHS}$ ; (ii) then it is dipped in  $\text{Cd}^{2+}$  and  $\text{NaHS}$  solution successively for four cycles; (iii) and finally dipped in  $\text{Zn}^{2+}$  and  $\text{NaHS}$  solution successively for two cycles. (C) TEM images of a QW-sensitized tetrapod, the arm part from the tetrapod and the electron diffractions corresponding to different sections with and without the QW shell and structure. Reprinted with permission from ref. 188. Copyright (2013) American Chemical Society.

On the whole, the PCEs of  $\text{ZnO}$  ETM-based QDSCs still lag far behind those of  $\text{TiO}_2$  ETM-based ones. Nevertheless,  $\text{ZnO}$  ETMs possess great potential to realize high-efficiency QDSCs due to their unique properties, especially high electron mobility. It should be noted that the obtained  $V_{\text{oc}}$  of  $\text{ZnO}$ -based QDSCs is obviously higher than that of the  $\text{TiO}_2$ -based one. So far, the highest  $V_{\text{oc}}$  for  $\text{ZnO}$ -based QDSCs is as high as 0.836 V, which is about 0.2 V higher than that of the  $\text{TiO}_2$ -based one.<sup>150</sup> Thus, it is necessary and meaningful to further improve the PCE of  $\text{ZnO}$ -based QDSCs through optimizing the QD sensitizers and interface characteristics.

**4.1.3. Other kinds of ETMs.** Apart from  $\text{TiO}_2$  and  $\text{ZnO}$ , other kinds of metal oxides, such as  $\text{SnO}_2$ ,<sup>153,189</sup>  $\text{ZrO}_2$ ,<sup>190</sup> and  $\text{Zn}_2\text{SnO}_4$ ,<sup>191</sup> have also been explored as ETMs in QDSCs. However, the cell performance based on these ETMs is usually poor, partially due to the unsatisfactory band edge position or the low electron mobility of the corresponding ETM. Among these, Meng *et al.* prepared highly ordered  $\text{SnO}_2$  inverse opal films with different thicknesses as a photoanode in  $\text{CdS}/\text{CdSe}$ -based QDSCs, delivering a PCE of 4.37%.<sup>153</sup> Zaban *et al.* demonstrated that the electron-injection process could also take place in  $\text{ZrO}_2$ -based QDSCs.

**4.1.4. p-Type metal oxide semiconductors and p-type QDSCs.** The above-mentioned wide-band-gap semiconductors (such as  $\text{TiO}_2$  and  $\text{ZnO}$ ), are of n-type, which are responsible for extracting photogenerated electrons from QD sensitizers in a QDSC. Another type of metal oxide semiconductors are p-type, which take the role of extracting photogenerated holes from QD sensitizers in a QDSC. A classic example of a p-type semiconductor is  $\text{NiO}$ , which is widely used in photoelectronic devices. Copper(I) thiocyanate,  $\text{CuSCN}$ , is a promising alternative to  $\text{NiO}$  as an inorganic p-type semiconductor material. Correspondingly, QDSCs based on the sensitization of a n-type semiconductor oxide, like  $\text{TiO}_2$  or  $\text{ZnO}$ , are known as standard (Grätzel) cells, while the cells based on the sensitization of wide-band-gap p-type semiconductor oxides, such as  $\text{NiO}$ , are referred to p-type (inverted) QDSCs. Usually, unless specially specified, QDSCs refer to standard ones. The extraction rate of a hole from a QD to a redox couple will be inherently slower than that of an electron to an n-type semiconductor matrix.<sup>39,70,192</sup> This leads to unbalanced charge transport in the standard QDSCs, whereas p-type QDSCs have the potential to solve this problem. Photophysical charge-transfer measurement results indicated that the hole-extraction rates in p-type QDSCs are in the same range as the electron-injection rates in conventional n-type QDSCs.<sup>193–195</sup> Moreover, the most promising application of p-type sensitized solar cells is the construction of a tandem configuration, with the combination of a p-type and an n-type, to overcome the Shockley–Queisser limit.<sup>196</sup>

Even though the concept of p-type QDSCs is very appealing, the efficiencies of most of them are very low or not reported,<sup>197–199</sup> with one exception being a value of 1.25% reported by Aldakov and coworkers in 2016.<sup>193</sup> To date, almost all p-type QDSCs have been based on  $\text{NiO}$  photocathodes due to the scarcity of transparent p-type nanostructured semiconductors. Recently,  $\text{CuSCN}$  has been proven to be a promising alternative to  $\text{NiO}$  as

a p-type material scaffold in liquid-junction QDSCs.<sup>194</sup> In this report, CuSCN nanowires were used as a photocathode in the construction of p-QDSSCs, and efficient sensitization by CuInS<sub>x</sub>Se<sub>2-x</sub> QDs was observed.

## 4.2 QD sensitizers

QDs are the core components in QDSCs that perform the function of harvesting sunlight and then generating electron-hole pairs.<sup>24,26,30</sup> Ideal QD sensitizers should possess the following characteristics: (1) a higher conduction band edge relative to that of the ETM for effective electron injection; (2) a narrow band gap to absorb sunlight over a wide range of the solar spectrum and a high absorption coefficient for high light-harvesting efficiency; (3) good stability toward light, heat, and electrolyte; (4) simple preparation and low toxicity. Apart from the design of the QDs' structure, the QD deposition route on the metal oxide substrate can also determine the final photovoltaic performance of the solar cells. Herein, we discuss the different methods to deposit QDs on metal oxide substrates and the various QD sensitizers that have been explored in QDSCs. The representative photovoltaic performances for QDSCs based on different QDs are summarized in Table 3.

**4.2.1. QD deposition routes.** Unlike molecular dyes, QDs are larger sized inorganic nanoparticles. It is difficult to tether a QD onto a metal oxide to form a fully covered monolayer due to the lack of anchoring sites on inorganic particles. Therefore, it is challenging to obtain a QD-sensitized photoanode with a high QD-loading amount.<sup>36,44,200</sup> Typically, the QD deposition techniques can be divided into two kinds: *in situ* and *ex situ* approaches. As shown in Fig. 11, for the *in situ* deposition,

QDs are grown directly on the metal oxide substrate from an ionic precursor solution, including by chemical bath deposition (CBD) and by successive ionic layer adsorption and reaction (SILAR) approaches. For the *ex situ* approach, colloidal QDs are pre-synthesized and then deposited onto the metal oxide substrate through direct adsorption, electrophoretic deposition, or linker-assisted deposition methods.

Due to the distinct advantages of easy processability, good reproducibility, and high QD-loading amount, until now, the *in situ* deposition method has been the most widely adopted to assemble QDSCs. In the CBD growth route, a bath solution containing cationic and anionic precursors is prepared.<sup>97,201–203</sup> By immersing the metal oxide film in the bath solution, QDs can grow directly on the surface of the metal oxide. The growth of the QDs can be controlled by varying the immersion time of the film in the solution as well as the reaction temperature. For the SILAR deposition, cationic and anionic precursors are separated and the metal oxide film is dipped into the two solutions alternatively.<sup>101</sup> The growth of the QDs is mainly controlled by the immersion cycles. Although a high QD-loading amount can be achieved by the *in situ* deposition method, it is difficult to control the QDs' size and size distribution as well as the density of trap state defects. As a result, QDs obtained through this route usually have a high density of trap states, resulting in severe charge recombination. Therefore, the highest PCE of QDSCs derived from the *in situ* QD deposition method is only about 7%.<sup>192,203</sup>

Benefiting from the well-developed QD synthesis technique, high-quality QDs can be facilely prepared through organometallic high-temperature synthetic methods.<sup>225–227</sup> There is no

**Table 3** Summary of the representative photovoltaic performance for QDSCs based on different QD sensitizers

QDs	CE	Electrolyte	$J_{sc}$ (mA cm <sup>-2</sup> )	$V_{oc}$ (V)	FF	PCE (%)	Ref.
CdS	C-Fabric/WO <sub>3-x</sub>	Polysulfide	10.38	0.891	0.64	5.91	204
CdSe	Cu <sub>2</sub> S/brass	Polysulfide	16.01	0.693	0.68	7.54	205
CdTe	Cu <sub>2</sub> S/brass	Polysulfide	16.58	0.629	0.694	7.24	206
PbS	Cu <sub>2</sub> S/brass	Polysulfide	29.98	0.398	0.468	5.58	207
Sb <sub>2</sub> S <sub>3</sub>	Au	PEDOT/PCPDTBT	16.1	0.711	0.65	7.5	208
InP	Cu <sub>2</sub> S/brass	Polysulfide	10.58	0.59	0.567	3.54	209
Ag <sub>2</sub> S	Pt	Polysulfide	9.28	0.509	0.52	2.41	210
Au <sub>x</sub>	Pt	[Co(bpy) <sub>3</sub> ] <sup>2+/3+</sup>	3.96	0.832	0.716	2.36	211
Carbon dot	Cu <sub>2</sub> S/brass	Polysulfide	6.47	0.43	0.31	0.87	212
PbS/Cds	Cu <sub>2</sub> S/FTO	Polysulfide	18.81	0.595	0.642	7.19	213
Cds/CdSe	Cu <sub>2</sub> S/brass	Polysulfide	21.49	0.61	0.55	7.24	214
CdTe/CdSe	Cu <sub>2</sub> S/brass	Polysulfide	19.59	0.606	0.569	6.76	74
ZnTe/CdSe	Cu <sub>2</sub> S/brass	Polysulfide	19.35	0.646	0.55	6.89	85
CdTe/CdS	Au	Polysulfide	13.60	0.682	0.41	3.80	215
CdTe/CdS/Cds	Cu <sub>2</sub> S/brass	Polysulfide	20.19	0.61	0.51	6.32	216
ZnSe/CdS	Pt	Polysulfide	2.29	0.44	0.27	0.27	217
ZnSe/CdSe	Cu <sub>2</sub> S/brass	Polysulfide	11.96	0.836	0.45	4.54	150
ZnSe/CdSe/ZnSe	Cu <sub>2</sub> S-RGO	Polysulfide	17.3	0.761	0.471	6.2	152
CdSe <sub>x</sub> Si <sub>1-x</sub>	Cu <sub>2</sub> S-RGO	Polysulfide	11.2	0.557	0.51	3.20	218
CdSe <sub>x</sub> Te <sub>1-x</sub>	MC/Ti	Polysulfide	20.69	0.807	0.689	11.51	118
Zn <sub>x</sub> Cd <sub>1-x</sub> Se	Cu <sub>2</sub> S/brass	Polysulfide	18.05	0.65	0.40	4.74	105
CuInS <sub>2</sub>	Cu <sub>2</sub> S/FTO	Polysulfide	22.82	0.601	0.62	8.54	219
Zn–Cu–In–S	Cu <sub>2</sub> S/brass	Polysulfide	22.70	0.612	0.615	8.55	220
CuInSe <sub>2</sub>	Cu <sub>2</sub> S/brass	Polysulfide	26.93	0.528	0.57	8.10	221
Zn–Cu–In–Se	MC/Ti	Polysulfide	25.97	0.752	0.644	12.57	222
Cu–In–Ga–Se	MC/Ti	Polysulfide	25.01	0.740	0.621	11.49	223
CuInSe <sub>x</sub> S <sub>2-x</sub>	Cu <sub>2</sub> S/FTO	Polysulfide	16.8	0.56	0.59	5.51	78
Cu <sub>2</sub> ZnSnS <sub>4</sub>	Cu <sub>2</sub> S/brass	Polysulfide	17.48	0.47	0.40	3.29	224

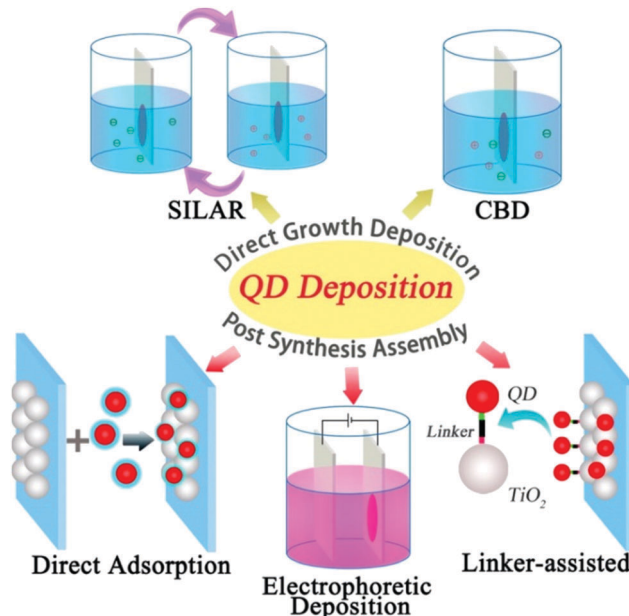


Fig. 11 Schematic illustration of QD deposition approaches. Direct growth method (above): (i) SILAR and (ii) CBD. Postsynthesis assembly deposition method (below): (i) direct adsorption, (ii) electrophoretic deposition (EPD), and (iii) linker-assisted assembly. Reprinted with permission from ref. 36. Copyright (2015) American Chemical Society.

doubt that high-quality QDs possess great potential for obtaining high-efficiency QDSCs. The main challenge for the use of pre-synthesized QDs in QDSCs is how to deposit them onto the metal oxide film in a high loading amount. The most common methods to immobilize pre-synthesized QDs onto a metal oxide substrate, include: (i) direct adsorption,<sup>95,96,228–231</sup> (ii) electrophoretic deposition (EPD),<sup>232,233</sup> and (iii) linker-molecule-assisted self-assembly.<sup>36,44,163,228,234,235</sup> In the initial stage, direct adsorption and EPD methods are commonly used to bind pre-synthesized QDs on to the metal oxide film. However, the obtained PCEs are usually low, mainly due to the low QD-loading amount, therefore they are a shadow of the high quality nature of the pre-synthesized QDs.

As already commented, the capping-ligand-induced self-assembly (CLIS) approach allowed the deposition of pre-synthesized QDs onto a TiO<sub>2</sub> electrode with a high loading amount.<sup>36,74,85,111,113–119</sup> High-quality QDs were first prepared in an organic phase, followed with a ligand-exchange process to obtain linker-molecule-capped water-soluble QDs, which could be then effectively deposited on to TiO<sub>2</sub> film electrodes. As early as the 1990s, Alivisatos *et al.* immobilized CdS and CdSe QDs on gold or aluminum surfaces in virtue of bifunctional group molecules containing thiol and carboxylate groups.<sup>236</sup> Later work borrowed this technique to assemble QDs on TiO<sub>2</sub> film electrodes in the fabrication of QDSCs.<sup>110,163,230,237–240</sup>

Despite the advantages of the CLIS approach, researchers still failed to achieve a high loading amount of QD sensitizers on to a TiO<sub>2</sub> electrode or to achieve a high photovoltaic performance of the resulting QDSCs. Through improving the ligand-exchange techniques as well as optimizing QD deposition

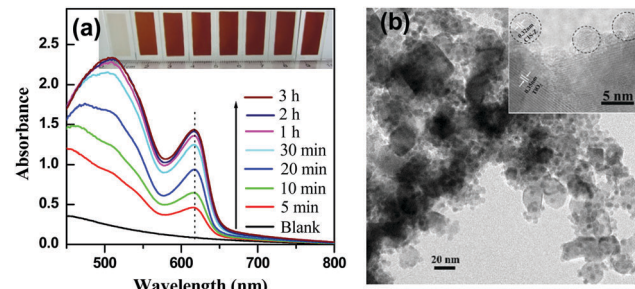


Fig. 12 (a) Temporal evolution of the absorption spectra of a CdSe QD-sensitized TiO<sub>2</sub> film. Inset: Photographs of the films with an increase in deposition time in turn. Reprinted with permission from ref. 110. Copyright (2012) Royal Society of Chemistry. (b) TEM image of CulnS<sub>2</sub>/ZnS QD (the small particles, ~5 nm)-sensitized TiO<sub>2</sub> film (the large particles ~20 nm). Inset: HRTEM micrograph. Reprinted with permission from ref. 116. Copyright (2014) American Chemical Society.

conditions, in 2012 Zhong's group exploited this deposition approach to develop a practicable and effective one to realize a fast and high loading amount of QDs on TiO<sub>2</sub> films.<sup>109,110</sup> Some special factors, including the choice of capping ligand, excess linker molecule in the final QD solution, and the pH of the QD solution, were found to be crucial to realize effective QD deposition. This novel deposition method was proven to be capable of realizing a fast, uniform, and high loading amount of QDs on a TiO<sub>2</sub> electrode (Fig. 12). Since then, the record PCE of QDSCs has rapidly improved to nearly 13% now.<sup>112</sup>

Although the CLIS deposition approach is very effective for the fabrication of high-efficiency QDSCs, this process involves a tedious additional step of ligand exchange using a short-chain mercapto-alkylcarboxyl ligand as a phase transfer reagent to displace the initial long carbon chain ligands around QDs prepared *via* an organometallic high-temperature route. The synthesis of colloidal QDs capped with a short-chain mercapto-alkylcarboxyl ligand directly in aqueous media (denoted as aqueous QDs henceforth) provides a straightforward access to immobilize QD sensitizers onto the TiO<sub>2</sub> surface in photoanodes. This approach obviates the additional step for ligand exchange, thereby simplifying the QD sensitization process. Attempts at using aqueous QDs in the fabrication of QDSCs can be dated back as early as 2009,<sup>241</sup> but no photovoltaic performances were reported. In 2011, Meng and coworker employed aqueous CuInS<sub>2</sub> in the fabrication of QDSCs with a PCE of 1.47%.<sup>242</sup> Following this, a series of higher PCEs have been obtained through optimizing the deposition conditions (such as pH values of QD solution, introduction of free ligand) and tuning the electronic structure of QD sensitizers, *etc.*<sup>198,211,216,243–248</sup> Up to date, the reported highest PCE using an aqueous QD sensitizer under the irradiation of one full sun light is 8.0%, while a PCE of 8.15% has also been obtained but under light intensity of 30 mW cm<sup>-2</sup>.<sup>249,250</sup> It is noted that the aqueous QD sensitizers were mostly concentrated on CuInS<sub>2</sub>- and CdTe-based QDs due to the relatively mature aqueous synthesis methods for these two kinds of QDs.

**4.2.2. Binary QDs.** Binary QDs are widely used as sensitizers in the initial stage of QDSCs due to their mature synthesis

recipe and well-known photoelectronic properties. A variety of binary QDs, such as InP,<sup>95,209</sup> InAs,<sup>96</sup> CdS,<sup>146,202,251,252</sup> CdSe,<sup>99,100,110,200,203</sup> CdTe,<sup>206,253</sup> PbS,<sup>127,207,213,254–259</sup> and Ag<sub>2</sub>S,<sup>169,210,260–262</sup> have been applied as sensitizers in QDSCs. Among these, CdS and CdSe QDs are the most popular choice due to their simple preparation. Another distinct advantage of the binary QDs is that they can be directly grown on a metal oxide substrate through the corresponding anions and cations in solution at low temperature, enabling a convenient route to prepare the photoanode. However, the key problem with binary QDs is that it is difficult to balance the narrower band gap and higher conduction band edge. For example, the conduction band edge of both CdS and CdSe is suitable for charge separation, whereas their band gap is relatively wide so that their light-harvesting range is narrow. On the contrary, PbS or PbSe QDs possess a narrower band gap, but their conduction band edge is low and their electron-injection efficiency is thus compromised. Therefore, the development of QD sensitizers has turned to explore composite QDs to balance the light-harvesting efficiency and electron-injection efficiency.

**4.2.3. Core/shell QDs.** Since the first report of the wet chemical synthesis of core/shell QDs by Hines *et al.* in 1996, core/shell-structured QDs have attracted much attention due to their unique properties.<sup>263–271</sup> This core/shell strategy has also been shown to be effective in enhancing the chemical, thermal, and photochemical stability because the inorganic shell can provide a more robust protection to the core QDs with respect to typical organic capping ligands.<sup>268–271</sup> Furthermore, in core/shell QDs, the band edge alignment of the core and shell QDs enable tuning of the light-absorption range, charge separation, and the recombination processes in QDSCs.

In QDSCs, core/shell QDs were first used as a sensitizer by Lee *et al.* in 2009.<sup>101</sup> In that work, the authors deposited CdS/CdSe core/shell QDs through a SILAR approach and obtained a PCE of 4.22%. It was shown that the re-organization of energy levels between CdS and CdSe formed a stepwise structure of band edge levels, which was advantageous to the electron injection and hole-recovery of CdS and CdSe QDs. Since then, CdS/CdSe core/shell QDs have been widely used in QDSCs and a highest efficiency of 6.6% has been achieved based on this kind of QD sensitizer.<sup>192</sup> Kim *et al.* prepared a PbS/CdS core/shell QD-sensitized photoanode through a SILAR method, showing a PCE of 3.25%, using insulating oxide materials (MgO and Al<sub>2</sub>O<sub>3</sub>) as a barrier layer on bare TiO<sub>2</sub>.<sup>272</sup>

It is noted that the SILAR and CBD method are not feasible to construct other kinds of core/shell QDs, especially Te-based core/shell QDs, due to the difficulty to prepare a stable Te precursor. In addition, the direct growth route is unable to obtain exact core/shell-structured QDs due to the uncontrollability of the nucleation and growth of the QDs in the confined mesoporous space. Therefore, a variety of core/shell QD sensitizers used in QDSCs are pre-synthesized and then deposited on the TiO<sub>2</sub> electrode. On the basis of the band alignment of core and shell QDs, core/shell QDs can be classified into three types: type-I, reverse type-I, and type-II structures (Fig. 13).<sup>270</sup> All of these three kinds of core/shell QDs have been investigated as

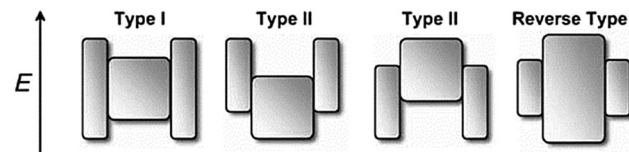


Fig. 13 Schematic representation of the energy-level alignment in different core/shell systems realized with semiconductor NCs to date. The upper and lower edges of the rectangles correspond to the positions of the conduction- and valence-band edges of the core (center) and shell materials, respectively. Reprinted with permission from ref. 270. Copyright (2009) Wiley.

sensitizers in QDSCs. For example, in a type-I-structured QD, the CB of the shell material is higher than the core material and the shell is usually used to passivate the surface of the core so as to improve the optical properties and chemical stability. Parkinson *et al.* used type-I-structured CdSe/ZnS QDs to sensitize single crystal TiO<sub>2</sub> for the first time and found that the stability of the photoanode could be significantly improved compared to the core QD-based one.<sup>234</sup> Zhong *et al.* prepared type-I-structured “green” CuInS<sub>2</sub>/ZnS QDs through a cation-exchange approach.<sup>116</sup> The thin ZnS layer was found to be beneficial for reducing the defect density of QDs and inhibiting charge-recombination processes in the QDSCs (Fig. 14a). As a result, an impressive record PCE of 7.04% was obtained based on the CuInS<sub>2</sub>/ZnS QDs, whereas the plain CuInS<sub>2</sub> QDs-based cell only showed a highest PCE of 5.05%. Zhong’s group also reported type-I-structured CdSeTe/CdS-based QDSCs, which exhibited a PCE of 9.48%, which was distinctly higher than the PCE for the plain CdSeTe QD-based one (8.02%). It was shown that the improved photovoltaic performance was mainly attributed to the suppressed charge-recombination rates inside the QDs and at the QD/TiO<sub>2</sub>/electrolyte interface due to the reduced trapping state defects in the QDs.<sup>273</sup>

In type-II-structured core/shell QDs, both the CB and VB of the shell material are higher or lower than the core material. As a result, the electron and hole are spatially separated, enabling fast electron transfer from the QD sensitizer to the oxide matrix.<sup>270,271</sup> Furthermore, type-II QDs show a remarkable

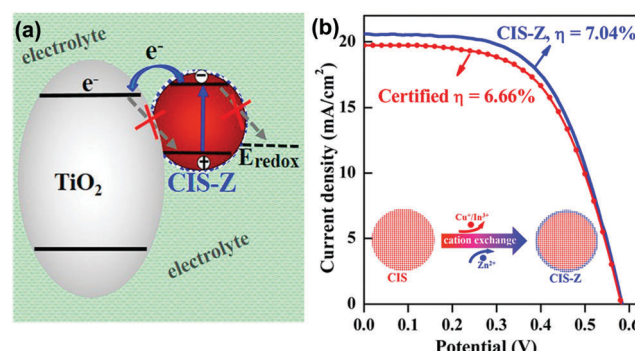


Fig. 14 (a) Schematic illustration of the charge-recombination-inhibition mechanism of CuInS<sub>2</sub>/ZnS QDSCs. (b) *J*–*V* curves of CuInS<sub>2</sub>/ZnS-based champion cells (blue) and the certified cell (red). Reprinted with permission from ref. 116. Copyright (2014) American Chemical Society.

red-shift of the absorption edge due to the effect of the exciplex state. These attractive properties suggest type-II core/shell QDs are promising light-harvesting materials to be used in QDSCs. For example, Ning *et al.* constructed type-II ZnSe/CdS core/shell QD-sensitized solar cells, which showed an efficiency of 0.27%.<sup>217</sup> Kuang's group reported a one-step linker-assisted CBD method to prepare CdTe/CdS QD-sensitized TiO<sub>2</sub> electrodes, and achieved an efficiency of 3.8%.<sup>215</sup> Meng *et al.* applied a microwave-assisted aqueous method to prepare type-II-structured CdSe<sub>x</sub>Te<sub>1-x</sub>/CdS core/shell QDs, exhibiting a PCE of 5.04%.<sup>247</sup> Zhong's group explored CdTe/CdSe type-II core/shell QDs as a sensitizer in QDSCs using a postsynthesis assembly approach and obtained a record PCE of 6.76% (Fig. 15a-d).<sup>74</sup> It was demonstrated that the type-II core/shell QDs could not only extent the light-absorption range of the solar cells, but also accelerate electron-injection and suppress charge-recombination processes. Furthermore, Zhong and coworkers developed another type-II core/shell QDs, ZnTe/CdSe, which possessed a much larger conduction band offset in comparison with that of CdTe/CdSe, and used this as a sensitizer, which led to further improving the record PCE to 7.17% (Fig. 15e).<sup>85</sup>

**4.2.4. Alloyed QDs.** Compared to binary QDs, ternary- or quaternary-alloyed QD are an attractive alternative to binary QD sensitizers since their optoelectronic properties can be tuned by controlling their composition without changing the particle size, and their band gap has the possibility to be narrower than that of their binary constituents due to the non-linear relationship between the composition and band gap.<sup>274-277</sup> Furthermore, alloyed QDs also show higher chemical stability than their constituents due to their hardened lattice structure and decreased interdiffusion.<sup>274</sup>

The alloyed QDs used in QDSCs are mainly focused on II-VI (Cd<sub>x</sub>Se<sub>1-x</sub>, CdSe<sub>x</sub>Te<sub>1-x</sub> etc.) and I-III-VI (AgInS<sub>2</sub>, CuInS<sub>2</sub>, CuInSe<sub>2</sub> etc.) group QDs. Among these, Cd<sub>x</sub>Se<sub>1-x</sub>-alloyed QDs were first explored as sensitizers in QDSCs. For example, Wang *et al.* prepared CdSe QDs in solution and deposited them on TiO<sub>2</sub> nanowires for the first time, achieving a PCE of 0.6%.<sup>278</sup> Hossain *et al.* deposited Cd<sub>x</sub>Se<sub>1-x</sub>-alloyed QDs on TiO<sub>2</sub> by alternately depositing CdS and CdSe layers through a SILAR approach, yielding a PCE of 4.05%.<sup>279</sup> Kamat *et al.* designed multiple absorber layers of CdSeS QDs with varying band gaps within the TiO<sub>2</sub> film.<sup>218</sup> This multiple absorber architecture was found to be advantageous for improving the light-harvesting capability of the solar cells and PCEs of 3.2% and 3.0% were obtained for QDSCs with two and three layers of QDs, respectively (Fig. 16). The main limitation of CdSeS QDs is their narrow light-absorption range, resulting in a relatively poor photovoltaic performance. As another II-VI group-alloyed QD, the CdSe<sub>x</sub>Te<sub>1-x</sub> QD sensitizer, developed by Zhong's group, showed superior characteristics, such as a wide absorption range extending to the near-IR region, high conduction band edge, and good chemical stability (Fig. 17).<sup>111</sup> A record PCE of 6.36% was obtained in 2013 based on this kind of alloyed QD sensitizer. Since then, a series of record PCEs have been reported based on this kind of QDs.<sup>113,114,117,118</sup>

I-III-VI group semiconductors, such as CuInS<sub>2</sub> (CIS) and CuInSe<sub>2</sub> (CISe), are considered as "green" light-adsorption materials as they are without Cd or Pb heavy metal elements. In addition, I-III-VI group semiconductors possess several prominent advantages, such as a high absorption coefficient and narrow band gap, rendering them excellent photovoltaic

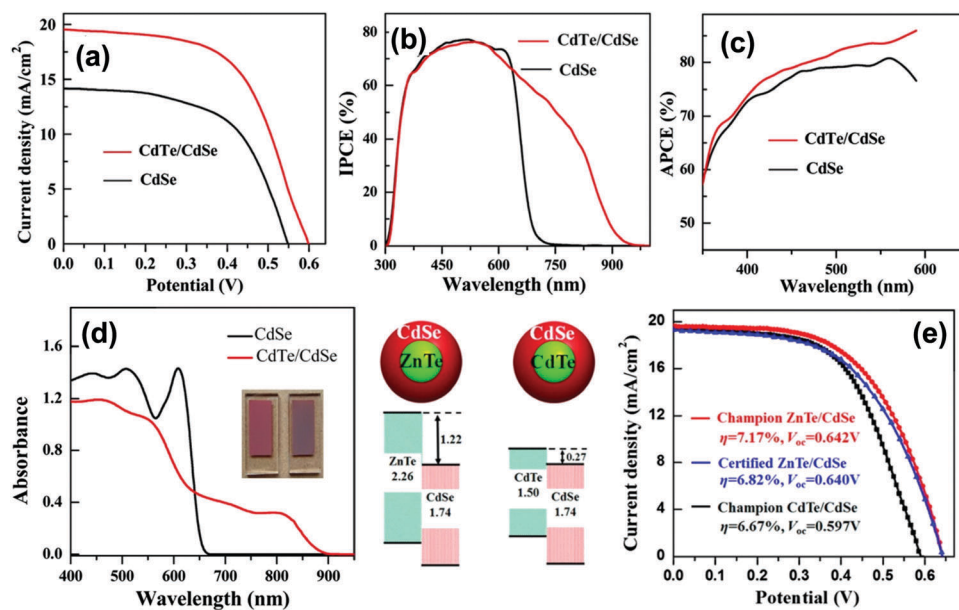


**Fig. 15** (a) J-V, (b) IPCE, and (c) APCE curves of CdSe and CdTe/CdSe QD-based QDSCs. (d) Diffuse reflectance absorption spectra of identically-sized CdTe/CdSe and CdSe QD-sensitized TiO<sub>2</sub> film electrodes. Insets: Photographs of CdTe/CdSe (right) and CdSe (left) QD-sensitized TiO<sub>2</sub> film electrodes. Reprinted with permission from ref. 74. Copyright (2013) American Chemical Society. (e) Schematic diagram of the band gap and band offsets (in eV) for the interfaces between bulk ZnTe/CdSe and CdTe/CdSe and the J-V curves of the corresponding QDSCs. Reprinted with permission from ref. 85. Copyright (2015) American Chemical Society.

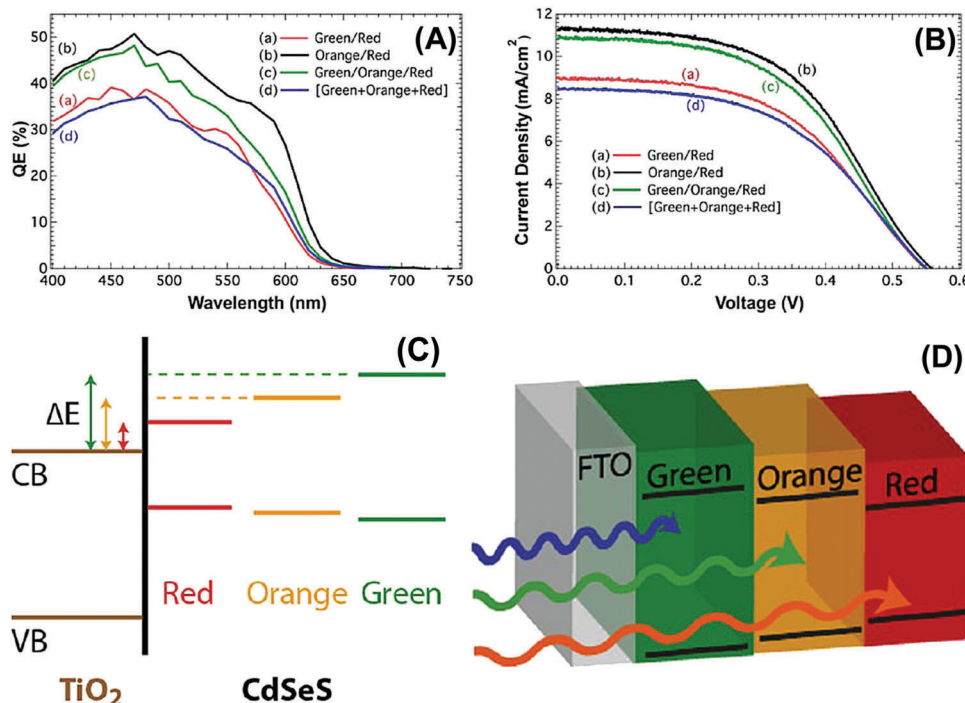


**Fig. 16** (A) IPCE spectra and (B)  $J$ – $V$  characteristics of different composite working electrodes containing: (a) green/red, (b) orange/red, or (c) green/orange/red sequential layers, or (d) a layer of premixed [green + orange + red] CdSeS QDs deposited by EPD. (C) Schematic illustration of the conduction- and valence-band positions of the green, orange, and red CdSeS QDs relative to TiO<sub>2</sub>. (D) Schematic illustration of the light-absorption way in the tandem anode. Reprinted with permission from ref. 218. Copyright (2013) American Chemical Society.

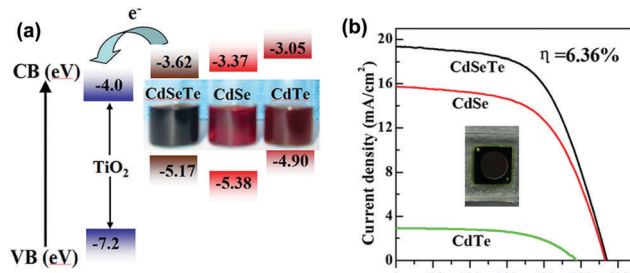


**Fig. 17** (a) Schematic energy-level diagram of TiO<sub>2</sub>, CdSeTe<sub>800</sub>, CdSe<sub>614</sub>, and CdTe<sub>680</sub> QDs. (b)  $J$ – $V$  curves of QDSCs based on different QD sensitizers. Reprinted with permission from ref. 111. Copyright (2013) American Chemical Society.

performance in thin film solar cells.<sup>11,280–282</sup> However, the fabrication of I–III–VI group light-harvesting materials in thin film solar cells typically is *via* applying magnetron sputtering or thermal evaporation in a vacuum condition, which is costly and involves a high energy consumption. Therefore, in recent years, I–III–VI group QDs have attracted much attention in QDSCs as a low-cost photovoltaic technology.<sup>77–79,221,242,246,283–293</sup>

In 2009, Chen *et al.* used CIS and CIS/ZnS QDs to sensitize ZnO nanowires, obtaining a PCE of 0.71% using I<sup>-</sup>/I<sub>3</sub><sup>-</sup> electrolyte.<sup>288</sup> Meng *et al.* synthesized CuInS<sub>2</sub> QDs in aqueous media and employed them as a sensitizer in QDSCs, achieving a PCE of 1.47%.<sup>242</sup> Teng's group proposed a heterojunction architecture using CIS and CdS QDs as sensitizers, boosting

the PCE of CIS-based QDSCs to 4.2%.<sup>287</sup> It was shown that the introduction of a CdS layer around CIS QDs can extend the optical absorption range and suppress charge recombination. Afterwards, Meng *et al.* doped Mn in the CdS layer, improving the PCE to 5.38%.<sup>246</sup> A key limitation of the CIS-based QDSCs is the low QD-loading amount, arising from the adopted dodecanethiol (DDT) ligand in the QD preparation. Since DDT cannot be completely displaced during the phase transfer procedure, this results in difficulty in immobilizing QDs on the TiO<sub>2</sub> film electrode. To address this, Zhong *et al.* developed a DDT-free synthetic approach for CIS QDs and constructed type-I-structured CIS/ZnS QDs through a cation-exchange approach, boosting the PCE of Cd-free CIS-based QDSCs to 7.04% (Fig. 14).<sup>116</sup> Furthermore, they developed a Zn–Cu–In–S-alloyed QD sensitizer, exhibiting a PCE of 8.55%.<sup>220</sup> It was demonstrated that the alloyed structure is superior to that of the CIS/ZnS core/shell and pristine CIS QDs as a sensitizer, benefiting from the suppression of charge recombination as well as an acceleration of the electron-injection efficiency. Up to now, this is the best efficiency reported for CIS QD-based QDSCs.

CISe QDs, which possess a narrower band gap compared to CIS QDs (1.05 vs. 1.52 eV), have shown great potential as sensitizers in QDSCs with the possibility to extend the light-absorption edge to the near-infrared region (NIR), therefore enabling obtaining a higher  $J_{sc}$  value.<sup>280,294,295</sup> Hyeon *et al.* presented a new synthetic process for CISe QDs through a Lewis acid-base reaction of metal iodides and selenocarbamate, showing a PCE of 4.3% for the Cd-free QDSCs.<sup>292</sup> Klimov *et al.* reported a

CuInSe<sub>1-x</sub>S<sub>x</sub>-alloyed I-III-VI group QD sensitizer and achieved a PCE of 5.5% with the aid of a cation-exchange process with Zn<sup>2+</sup> or Cd<sup>2+</sup> in the prepared CISe QDs.<sup>78,79</sup> Hyeon *et al.* boosted the PCE of CISe QDSCs to 8.1% through optimization of the ZnS passivation-layer thickness and obtained a  $J_{sc}$  as high as 26.93 mA cm<sup>-2</sup>.<sup>221</sup> Notably, Zhong's group explored an alloyed Zn-Cu-In-Se (ZCISe) QD sensitizer possessing a narrow band gap and high conduction band edge simultaneously, achieving a record PCE of 11.61% when combined with a Ti-mesh-supported mesoporous-carbon counter electrode (Fig. 18a-c).<sup>115</sup> It should be noted that this was the first report of QDSCs with a PCE over 10%. Afterwards, Zhong *et al.* found that the non-stoichiometry of the ZCISe QDs showed remarkable effects on the performance of the constructed QDSCs and that Cu-deficient ZCISe QDs were favorable for the improvement of the photovoltaic performance.<sup>222</sup> The PCE of ZCISe QD-based QDSCs was further improved to 12.57% with optimization of the Cu content in the QDs. They proposed that the enhanced PCE was mainly derived from the defect-state-related donor-acceptor pair (DAP) in the ZCISe QDs due to the Cu deficiency (Fig. 18d).

According to the above-mentioned QD sensitizers, it is reasonable to conclude that alloyed QDs, especially I-III-VI group-alloyed QDs, seem to be a better choice as a sensitizer in QDSCs. The reported PCEs of over 10% were mainly derived from I-III-VI group-alloyed QD sensitizers, benefiting from the narrow band gap, appropriate band edge, and facile synthetic process of this kind of QDs. In addition, they also present a better environmental behavior than other QDs containing

heavy metals. Therefore, it is believed that the I-III-VI group-alloyed QDs possess great potential to promote the further development of QDSCs in the near future.

**4.2.5. Doped QDs.** The introduction of a dopant into QDs is another way to tune the electronic and photophysical properties of QDs. The effect of dopants on the photoelectronic properties of QDs and the underlying mechanism have been widely studied.<sup>296-301</sup> The effect of dopants in QD sensitizers has also been investigated in QDSCs.<sup>107,185,191,203,246,302-312</sup> In 2012, Kamat and coworkers introduced the doping strategy in QDs and studied the doping effect on the photovoltaic performance of QDSCs (Fig. 19).<sup>107</sup> They applied a Mn dopant in a CdS core layer through a SILAR approach to form Mn:CdS/CdSe QD sensitizers. The Mn d-d transition was both spin and orbital forbidden, resulting in a long electron lifetime. This unique feature was believed to favor prolonging the lifetime of the photogenerated electrons. As a result, an impressive PCE of 5.4% was obtained and also the cell showed good stability. Meng *et al.* prepared CIS QDs first in aqueous media and then fabricated a CIS/Mn:CdS-sensitized photoanode by a SILAR approach.<sup>246</sup> The obtained PCE for the QDSCs based on the doped QDs (5.38%) was higher than for the undoped one (4.69%). Santra *et al.* investigated the role of a Mn dopant in QDSCs,<sup>307</sup> and demonstrated that the Mn dopant decreases the recombination within the QDs. The long lifetime of the photo-excited electron eventually leads to an improvement of the  $J_{sc}$  and  $V_{oc}$  values by raising the Fermi energy to a higher negative potential. Zhong *et al.* applied a Mn dopant in both a pre-synthesized CdSe<sub>x</sub>Te<sub>1-x</sub> QD sensitizer and the ZnS passivation layer, improving the PCE of the corresponding QDSCs from 8.55% to 9.40%.<sup>312</sup> Experimental results demonstrated that the presence of the Mn dopant could reduce the trap states in QD sensitizers, consequently suppressing the charge-recombination process in the QDSCs. Apart from the Mn dopant, other dopants, such as Co, have also been used in QD sensitizers. For example, Firooz *et al.* investigated the effect of Co<sup>2+</sup> ion incorporation into CdS/CdSe QDs on the performance of QDSCs, and found the PCE could be distinctly improved from 2.33% to 3.16% with the optimization of the Co doping amount.<sup>309</sup>

**4.2.6. Other QD sensitizers.** Apart from the above-mentioned QD sensitizers, there are several novel sensitizers that have also been explored in QDSCs. For example, Kamat *et al.* found that gold clusters with diameters of 1.0–1.6 nm could also inject electrons into TiO<sub>2</sub> under visible excitation.<sup>211</sup> The fabricated QDSCs based on the gold clusters exhibited a PCE of 2.36% using a Co(II)/Co(III) redox couple as the electrolyte. Bang *et al.* investigated the effect of the size of Au clusters on the performance of sensitized solar cells.<sup>313</sup> They constructed cell devices using I<sup>-</sup>/I<sub>3</sub><sup>-</sup> as the electrolyte and obtained a PCE of 3.8% using Au<sub>18</sub>(SR)<sub>14</sub> as a sensitizer due to its relatively good light-absorption capability and low recombination rate.

Another kind of novel sensitizer is the carbon QD (CQD), which is more low-cost and environmental friendly.<sup>212,314-319</sup> In 2010, Li *et al.* synthesized solution-processable, black graphene QDs and applied them as a sensitizer for solar cells.<sup>318</sup> The calculated band edge position of the graphene QDs was found

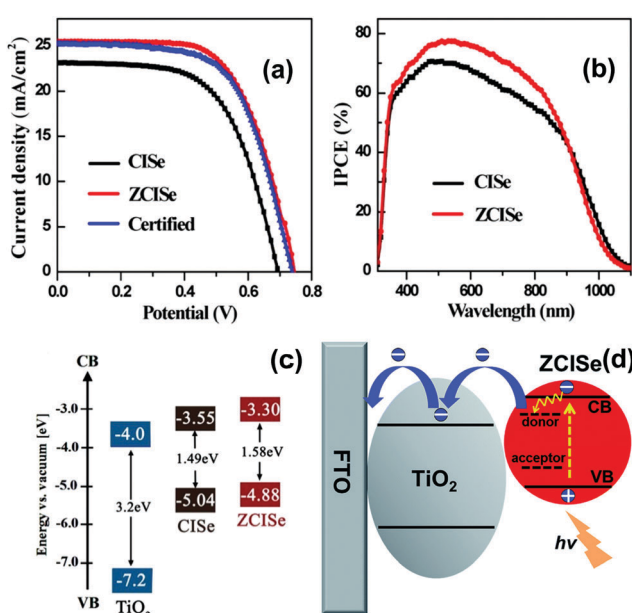


Fig. 18  $J-V$  (a) and IPCE (b) curves for the champion cells of ZCISe and CISe QD-based QDSCs. (c) Schematic energy-level diagrams of TiO<sub>2</sub>, 4.1 nm CISe, and ZCISe QDs. Reprinted with permission from ref. 115. Copyright (2016) American Chemical Society. (d) Schematic diagram illustrating the effect of the donor-acceptor pair (DAP) in the QDs on the charge-transfer process in the QDSCs. Reprinted with permission from ref. 222. Copyright (2017) Royal Society of Chemistry.

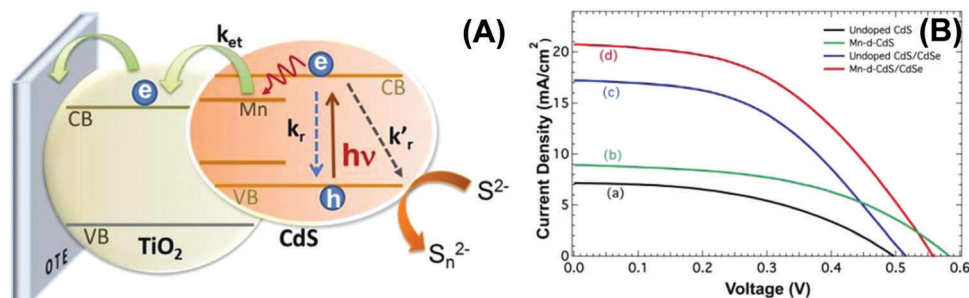


Fig. 19 (A) Schematic diagram illustrating the electron transfer ( $k_{et}$ ) from doped CdS into TiO<sub>2</sub> nanoparticles, where  $k_r$  and  $k'_r$  represent electron recombination with holes and the redox couple, respectively. (B)  $J$ - $V$  characteristics of different working electrodes measured under an AM 1.5 global filter of 100 mW cm<sup>-2</sup> sunlight: (a) undoped CdS, (b) Mn-doped-CdS, (c) undoped CdS/CdSe, and (d) Mn-doped-CdS/CdSe. Reprinted with permission from ref. 107. Copyright (2012) American Chemical Society.

to be suitable for electron injection and QDs regeneration. The fabricated solar cell exhibited a  $J_{sc}$  of 0.2 mA cm<sup>-2</sup>, a  $V_{oc}$  of 0.48 V, and an FF of 0.58. Ozin *et al.* synthesized CQDs via the dehydration of  $\gamma$ -butyrolactone with concentrated sulfuric acid.<sup>317</sup> The CQDs were employed as a sensitizer in QDSCs and achieved a PCE of 0.13%. Zhang *et al.* presented a simple *in situ* strategy of growing CQDs directly onto TiO<sub>2</sub> surfaces, obtaining an impressive PCE of 0.87%, which is the best PCE for CQD-based QDSCs to date.<sup>319</sup>

**4.2.7. Co-sensitization strategy.** Unlike the case of DSC, the coverage of QDs on TiO<sub>2</sub> is usually not complete, and indeed, the reported highest coverage of QDs is only about 34%.<sup>110</sup> That is to say, a large portion of the TiO<sub>2</sub> surface is bare and directly exposed to the electrolyte.<sup>36</sup> This low coverage of QDs leads to a decrease in the light-harvesting efficiency and the aggravation of charge recombination. One strategy to improve the QD-loading amount is *via* co-sensitization using different QDs or dye molecules. Furthermore, a co-sensitization strategy using different light-harvesting materials can achieve a higher light-harvesting efficiency since different materials have different properties, such as light-absorption range and extinction coefficient.<sup>32,240,320-327</sup>

For example, in 2008, Han *et al.* applied two different-sized CdSe QDs to co-sensitize vertically aligned TiO<sub>2</sub> nanotubes, obtaining a PCE of 1.2%, which was higher than the PCE for the single-sized CdSe QD-sensitized cells.<sup>240</sup> The improved PCE was mainly derived from the increase in  $J_{sc}$  values due to the

broader light-absorption range. Lei *et al.* achieved a similar result by depositing two different-sized CdSe QDs on a TiO<sub>2</sub> electrode,<sup>323</sup> showing that the improved photovoltaic performance could be attributed to the broader light-absorption range and the reduced charge-recombination loss at the interface due to the better coverage of CdSe QDs on the TiO<sub>2</sub> film. Qiao *et al.* also demonstrated the effectiveness of this co-sensitization strategy on improving solar cell performance using dual-sized CdSe QDs as sensitizers.<sup>321</sup> Recently, Zhong *et al.* displayed a co-sensitization strategy employing Zn–Cu–In–Se (ZCISe) and CdSe QDs as sensitizers (Fig. 20).<sup>112</sup> The synergistic effect of the ZCISe QDs with a wide light-absorption range and CdSe QDs with a high extinction coefficient contributed to the improvement of the light-harvesting efficiency as well as inhibition of charge recombination. As a result, a new record PCE of 12.75% ( $V_{oc} = 0.752$  V,  $J_{sc} = 27.39$  mA cm<sup>-2</sup>, FF = 0.619) was achieved for QDSCs. Meanwhile, metal–semiconductor nanohybrid materials (NHMs) were also used for enhancing the light-harvesting capability and photovoltaic performance of the resulting cells by Ghosh and coworkers.<sup>328</sup> Their experimental results showed that the absorption onset of CdSe/Au was red-shifted to 800 nm. A higher recombination resistance and longer electron lifetime were also confirmed by EIS measurements at the TiO<sub>2</sub>–CdSe/Au interface in comparison with TiO<sub>2</sub>–CdSe. Consequently, a PCE of 4.39% was obtained for CdSe/Au QDSC, which was ~30% higher than that of the plain CdSe QDSC.

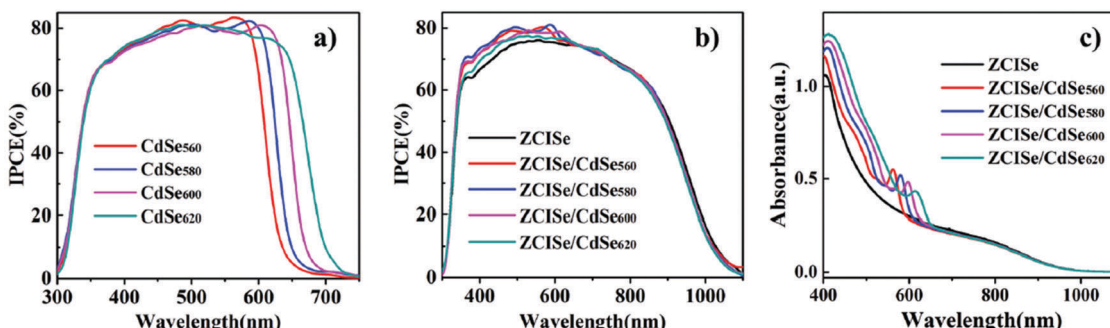


Fig. 20 IPCE spectra of QDSCs co-sensitized with various photoanodes: (a) CdSe QD-based QDSCs; (b) ZCISe- and ZCISe/CdSe-based QDSCs. (c) UV-vis absorption spectra of ZCISe and ZCISe/CdSe QD-sensitized TiO<sub>2</sub> film electrodes with an active area of 1.6 cm<sup>2</sup>. Reprinted with permission from ref. 112. Copyright (2018) Wiley.

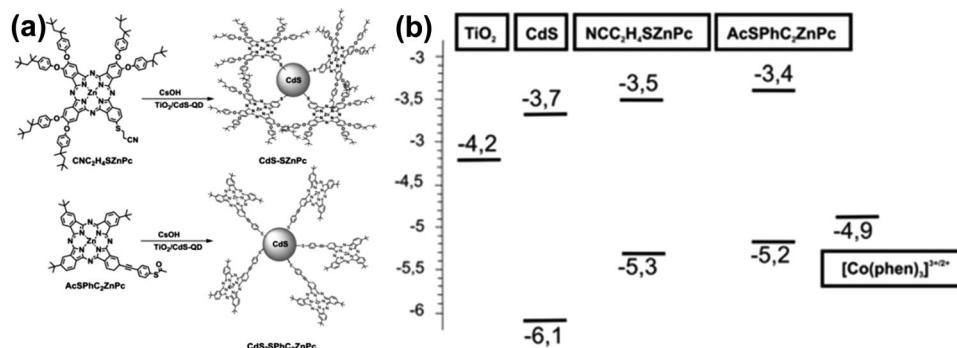


Fig. 21 (a) Preparation of  $\text{CdS-SZnPc}$  and  $\text{CdS-SPhC}_2\text{ZnPc}$  hybrid systems. (b) Energy levels of  $\text{TiO}_2$ ,  $\text{CdS}$ ,  $\text{CNC}_2\text{H}_4\text{SZnPc}$ ,  $\text{AcSPhC}_2\text{ZnPc}$  and  $[\text{Co}(\text{phen})]^{3+2+}$ . Reprinted with permission from ref. 320. Copyright (2015) Wiley.

The co-sensitization strategy can also be carried out using QDs and organic dyes as sensitizers.<sup>320,324–327</sup> Zaban and co-workers constructed a QDs and dye co-sensitized photoanode and showed that the QDs could serve as “antennas” to funnel the absorbed energy to nearby dye molecules *via* FRET.<sup>326</sup> The incorporation of the QDs and dye significantly enhanced the light absorption and broadened the absorption range. Kamat and coworkers employed  $\text{CdS}$  QDs and a NIR-absorbing squaraine dye (JK-216) as co-sensitizers, delivering a PCE of 3.14%, which was distinctly higher than that of the individual sensitizer-based ones.<sup>325</sup> Sastre-Santos and coworkers fabricated a cascade co-sensitization photoanode using  $\text{CdS}$  QDs and zinc phthalocyanines (ZnPcs) dyes (Fig. 21).<sup>320</sup> Unlike the previously co-sensitization method, in which QDs and dyes were separated by a barrier layer or the dyes were anchored to  $\text{TiO}_2$ , the dyes in this work were directly anchored on the  $\text{CdS}$  QDs through the thiol (SH) group in the dye. It was demonstrated that this cascade co-sensitization could not only expand the light-absorption range, but also benefited the reduction of charge recombination since the dye acted as a passivating agent. Finally, the PCE was increased from 0.8% to 2.5% for the cells using single  $\text{CdS}$  QD and co-sensitizers, respectively. Overall, the obtained photovoltaic performance of QDSCs fabricated with the co-sensitization strategy using QDs and organic dyes is relatively poor. This can be mainly ascribed to the limitation of the choice of QDs as well as the electrolyte that can stabilize both the QDs and dyes. Further work on this strategy should focus on the exploration of superior QDs and a suitable liquid or solid-state redox couple.

#### 4.3 Counter electrodes

The main function of a counter electrode CE in QDSCs is to catalyze the reduction reaction of the oxidized electrolyte by electrons from the external circuit.<sup>7,42,51</sup> A preferred CE should possess the following properties: (1) good conductivity to transfer electrons from the external circuit to the active sites; (2) high catalytic activity toward the reduction reaction of the oxidized electrolyte; and (3) good chemical and mechanical stability to ensure the whole stability of the device. The studied CE catalytic materials for QDSCs can be mainly divided into four kinds: noble metals, metal chalcogenides, carbon materials,

and composite materials. The representative photovoltaic performances for QDSCs based on the different CEs are summarized in Table 4. The CE was one of the biggest limitations on the QDSC performance in the early stages of their development and its consequent continuous optimization has contributed significantly to the latest increases reported in cell efficiency.

**4.3.1. Noble metals.** In DSCs, the thermally-deposited Pt electrode is the most common CE due to its superior catalytic ability for the reduction of the  $\text{I}^-/\text{I}_3^-$  electrolyte. Accordingly, this classical CE has been borrowed to make QDSCs.<sup>48,49,51</sup> For instance, Lee *et al.* employed a Pt CE to construct  $\text{CdS/CdSe}$  QDSCs in 2009 and obtained a record PCE of 3.7%.<sup>101</sup> Kuang *et al.* achieved a PCE of 4.81% in 2011 by applying a Pt CE in electrodeposited  $\text{CdS/CdSe}$  QDSCs.<sup>233</sup> Yang *et al.* showed a PCE of 5.25% for Pt CE-based QDSCs sensitized with a  $\text{ZnSe/CdSe/ZnSe}$  quantum well.<sup>188</sup> To the best of our knowledge, this is the best efficiency reported to date for noble metal CE-based QDSCs. Besides Pt, researchers found that another noble metal, *i.e.*, Au, was a more superior CE catalytic material.<sup>101,215,329–332</sup> For example, Lee *et al.* showed that under identical conditions, the PCE of QDSCs employing a Au CE (4.22%) was significantly higher than QDSCs with a Pt-based CE (3.70%).<sup>101</sup> The improvement in the photovoltaic performance was mainly attributed to the weak adsorption of  $\text{S}^{2-}$  to the Au surface as confirmed by cyclic voltammetry tests (Fig. 22). Kuang *et al.* also demonstrated the superiority of Au relative to Pt as a CE catalytic material in QDSCs.<sup>215</sup>

Typically, QDSCs based on a noble metal CE exhibit moderate PCEs. This is mainly induced by the adsorption of  $\text{S}^{2-}$  onto the surface of Pt or Au, leading to poisoning of the CE and hence reducing its catalytic activity as well as the stability of the cell device.<sup>51</sup> Furthermore, the high price of the noble metals increases the production cost of the device, thus limiting its commercial application. Therefore, much effort has been devoted to developing efficient low-cost CEs in QDSCs.

**4.3.2. Metal chalcogenides.** As early as 1980, Hodes *et al.* pointed out that metal sulfides were more suitable catalysts for the polysulfide redox reaction compared to the conventional Pt CE.<sup>333</sup> Afterward, it was indeed demonstrated that metal chalcogenides are superior materials for the fabrication of CE in QDSCs. Among these, copper chalcogenide is the most

**Table 4** Summary of the representative photovoltaic performances of QDSCs based on different CEs

CE	QDs	Electrolyte	$J_{sc}$ (mA cm $^{-2}$ )	$V_{oc}$ (V)	FF	PCE (%)	Ref.
Pt	ZnSe/CdSe/ZnSe	Polysulfide	17.8	0.741	0.398	5.25	152
Au	CdS/CdSe	Polysulfide	16.8	0.514	0.49	4.22	101
Cu <sub>2</sub> S/brass	Zn–Cu–In–Se	Polysulfide	26.91	0.629	0.607	10.27	391
Cu <sub>x</sub> S/FTO	CdSe <sub>x</sub> Te <sub>1-x</sub>	Polysulfide	20.78	0.702	0.636	9.28	113
Cu <sub>x</sub> Se/FTO	CdSe <sub>x</sub> Te <sub>1-x</sub>	Polysulfide	21.09	0.673	0.614	8.72	357
ITO/Cu <sub>2</sub> S	CdSe <sub>x</sub> Te <sub>1-x</sub>	Polysulfide	15.23	0.688	0.584	6.12	346
GH-CuS/Ti	CdSe <sub>x</sub> Te <sub>1-x</sub>	Polysulfide	20.69	0.786	0.66	10.74	392
CoS	CdS/CdSe	Polysulfide	14.44	0.510	0.565	4.16	365
PbS	CuInS <sub>2</sub> /CdS	Polysulfide	18.3	0.58	0.45	4.70	359
NiS	CdS/CdSe	Polysulfide	13.70	0.502	0.48	3.30	393
FeS <sub>2</sub>	ZnSe/CdSe	Polysulfide	13.58	0.743	0.387	3.90	370
MoS <sub>2</sub>	CdS/CdSe	Polysulfide	15.65	0.588	0.449	4.13	394
Cu <sub>2</sub> SnSe <sub>3</sub>	CdSe	Polysulfide	16.29	0.563	0.54	4.93	395
CZTS	ZnSe/CdSe	Polysulfide	11.06	0.822	0.41	3.73	379
CZTSe	CdSe	Polysulfide	15.49	0.54	0.52	4.35	377
Cu <sub>2</sub> S/carbon	CdS/CdSe	Polysulfide	13.69	0.593	0.48	3.87	396
Cu <sub>2</sub> S/RGO	CdS/CdSe	Polysulfide	18.4	0.520	0.46	4.40	397
PbS/CB	CdS/CdSe	Polysulfide	13.32	0.509	0.58	3.91	398
CuInS <sub>2</sub> /CB	CdS/CdSe	Polysulfide	14.16	0.512	0.60	4.32	399
Cu <sub>1.18</sub> S/GOR	CdTe/CdS/Cds	Polysulfide	20.55	0.626	0.53	6.81	400
C <sub>60</sub>	CdS/CdSe	Polysulfide	12.6	0.546	0.60	4.18	388
CNTs	CdS/CdSe	Polysulfide	16.09	0.586	0.495	4.67	387
HCMS	CdSe	Polysulfide	12.41	0.60	0.52	3.90	383
OMPC	CdSe	Polysulfide	12.34	0.63	0.56	4.36	103
MCNF	CdSe	Polysulfide	11.99	0.62	0.60	4.81	104
MC-Ti	CdSe <sub>x</sub> Te <sub>1-x</sub>	Polysulfide	20.69	0.807	0.689	11.51	118
N-MC-Ti	Zn–Cu–In–Se	Polysulfide	25.67	0.759	0.639	12.45	119

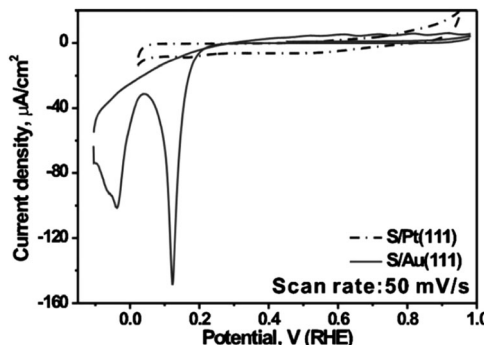
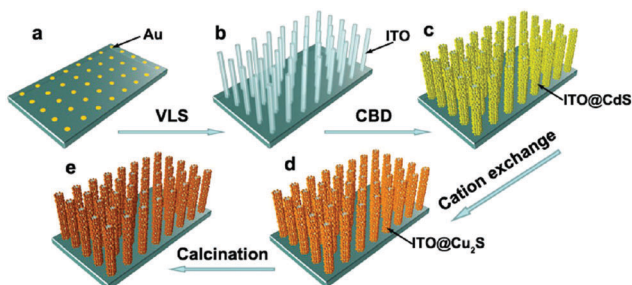


Fig. 22 Cyclic voltammograms for S-modified Au(111) and Pt(111) electrodes recorded at 50 mV s $^{-1}$  in 0.1 M HClO<sub>4</sub> solution. Reprinted with permission from ref. 101. Copyright (2009) Wiley.

widely studied CE in QDSCs. Mora-Seró and Toyoda and co-workers attempted to fabricate QDSCs using a Cu<sub>2</sub>S CE and found that the PCE could be improved from 0.65% (Pt CE) to 1.83% (Cu<sub>2</sub>S CE).<sup>229</sup> The improvement was derived from the reduction in the charge-transfer resistance at the CE/electrolyte interfaces, which dramatically affected the fill factor of the device. Afterward, Shen and Toyoda and coworkers reported a brass-substrate-based Cu<sub>2</sub>S CE (simplified as Cu<sub>2</sub>S/brass), which could be facilely prepared by directly immersing the brass foil in polysulfide electrolyte.<sup>122</sup> They obtained a PCE of 1.8% based on a CdSe QD-sensitized TiO<sub>2</sub>-nanotube working electrode. It should be noted that this brass-based Cu<sub>2</sub>S CE has been the most commonly used CE in QDSCs since then and most of the high PCEs reported were derived from this CE-based system.<sup>74,85,106,111,113,116,117,203</sup> Up to now, the highest

reported PCE for Cu<sub>2</sub>S/brass-based QDSCs is 10.75% based on ZCISe QD sensitizers.<sup>112</sup> Nevertheless, the key problem with this Cu<sub>2</sub>S/brass CE is that the polysulfide electrolyte can continually react with the brass substrate, leading to a poor long-term stability of the CE and the resultant device.

Aiming at resolving the stability issue of Cu<sub>2</sub>S/brass CEs, much work has focused on the preparation of Cu<sub>2</sub>S on a rigid substrate through electrodeposition, spray pyrolysis, or screen printing, etc. approaches to facilitate the sealing of the device.<sup>334–351</sup> For example, Zhong and coworkers prepared a Cu<sub>2</sub>S/FTO CE by electrodeposition of the copper film via a multipotential step technique, followed by dipping into polysulfide methanol solution to form Cu<sub>2</sub>S.<sup>349</sup> These electrodeposited-Cu<sub>2</sub>S/FTO CE-based QDSCs exhibited a PCE of 5.21%, which was comparable to the PCE of the Cu<sub>2</sub>S/brass CE-based one (5.41%). In particular, the stability of the cell under one sun illumination was significantly improved for over 10 h without performance degradation. Selopal *et al.* showed a spray pyrolysis approach to prepare Cu<sub>2</sub>S/FTO CE and achieved a PCE of 3.75%.<sup>345</sup> The spray pyrolysis deposition method possessed the advantages of being simple, cheap, time-saving, and had good reproducibility. Wang *et al.* reported a novel method to prepare Cu<sub>2</sub>S/ITO CE by ion exchange.<sup>340</sup> They first deposited ZnS on an ITO substrate through a SILAR approach, followed by immersing into a saturated CuCl acetonitrile solution for ion exchange to form a Cu<sub>2</sub>S film. A final PCE of 4.78% was achieved, which was comparable to that of the Cu<sub>2</sub>S/brass CE-based one. Meng *et al.* prepared a Cu<sub>2</sub>S/FTO CE through a screen-printing method using a Cu<sub>2</sub>S nanoparticle paste, exhibiting a PCE of 3.71%.<sup>351</sup> Zhang *et al.* used CuS/Cu<sub>1.8</sub>S composite nanomaterials to fabricate a Cu<sub>x</sub>S/FTO CE, obtaining a PCE of 6.28%, which was



**Fig. 23** Scheme for directly preparing ITO@Cu<sub>2</sub>S nanowire arrays on FTO glass: (a) sputtering of Au catalysts on the FTO substrate; (b) CVD synthesis of the ITO nanowire arrays; (c) chemical bath deposition of the CdS shell on the ITO nanowire arrays; (d) cation exchange to form ITO@Cu<sub>2</sub>S nanowire arrays; (e) calcination for improving the interfaces between the ITO nanowire core and the Cu<sub>2</sub>S nanocrystal shell. Reprinted with permission from ref. 347. Copyright (2014) American Chemical Society.

slightly higher than the Cu<sub>2</sub>S/brass CE-based one.<sup>350</sup> Furthermore, the constructed cell showed good stability over 225 h, benefiting from the good mechanical and chemical stability of the CE.

Wan and coworkers developed a novel ITO/Cu<sub>2</sub>S nanowire-arrays CE for QDSCs.<sup>335,346,347</sup> As shown in Fig. 23, the ITO nanowire arrays were first grown on a Au-coated FTO substrate *via* CVD and then a layer of CdS, in a thickness of about 20 nm, was coated on the as-prepared ITO nanowires *via* the CBD technique. After that, the ITO/Cu<sub>2</sub>S nanowire arrays were formed through a solution-based cation exchange. The constructed QDSC showed a PCE of 4.06%, which was significantly higher than the conventional Cu<sub>2</sub>S/FTO CE-based one (3.04%).<sup>347</sup> The improvement of the photovoltaic performance can be ascribed to the decrease in sheet resistance and charge-transfer resistance, benefiting from the high-quality tunnel junctions formed between the n-type ITO nanowires and p-type Cu<sub>2</sub>S nanocrystals, as well as the more active catalytic sites due to the three-dimensional structure of the nanowire arrays. In addition, they further explored an hierarchically-assembled ITO/Cu<sub>2</sub>S nanowire-arrays CE for the deposition of more Cu<sub>2</sub>S nanocrystals as active sites, boosting the PCE to 6.12% using CdSeTe QDs as a sensitizer.<sup>346</sup>

Apart from Cu<sub>2</sub>S, CuSe or Cu<sub>x</sub>Se have also been applied to fabricate CEs for QDSCs.<sup>352–357</sup> For example, Cui *et al.* prepared a Cu<sub>x</sub>Se/FTO CE through a novel route.<sup>353</sup> They first deposited red selenium on an FTO by disproportionation of Na<sub>2</sub>SeSO<sub>3</sub> aqueous solution with an ethanol spray, and then manipulated the red selenium as both a template and reaction center to fabricate a cuprous-embedded Cu<sub>x</sub>Se composite CE upon the selenium self-redox reaction with copper ions. The constructed QDSCs exhibited a PCE of 3.80%, which was slightly higher than the Cu<sub>2</sub>S/brass CE-based one (3.72%). Bang and coworkers prepared various metal selenide CEs by a SILAR method and investigated their performance in QDSCs.<sup>352</sup> They found that the Cu<sub>1.8</sub>Se-based CE was superior to the other kinds of metal-selenides-based CEs, achieving a PCE of 5.0%. Tian and coworkers developed a Cu<sub>3</sub>Se<sub>2</sub> CE composed of nanorod arrays and nanosheets, delivering a PCE of 5.05%, higher than the

Cu<sub>2</sub>S/brass-based one (4.10%).<sup>354</sup> Wang and coworkers prepared Cu<sub>2-x</sub>Se nanoparticles and nanowires catalysts by facile wet chemical methods and then used these as CEs in QDSCs.<sup>356</sup> The results showed that the Cu<sub>2-x</sub>Se nanoparticle-based CE could remarkably enhance the efficiency by 17.1% (6.50% vs. 5.55%) compared to Cu<sub>2</sub>S CE. Zhong and coworkers deposited Cu<sub>x</sub>Se nanoparticles on an FTO substrate and found that the copper-deficient Cu<sub>x</sub>Se favored an improvement in the electrochemical properties of the CE as well as in the photovoltaic performance of the solar cells.<sup>357</sup> A PCE of 8.72% was obtained with this Cu<sub>x</sub>Se/FTO CE and the cell showed good stability over 168 h.

Apart from copper-chalcogenides-based CEs, other binary or alloyed metal chalcogenides, such as PbS,<sup>358–362</sup> CoS,<sup>363–366</sup> FeS,<sup>367–370</sup> NiS,<sup>371,372</sup> and Cu<sub>2</sub>ZnSnS<sub>4</sub> (CZTS) or Cu<sub>2</sub>ZnSnSe<sub>4</sub> (CZTSe),<sup>373–379</sup> have also been used to fabricate CEs for QDSCs. For example, Zaban and coworkers used PbS as a CE catalytic material in QDSCs. They demonstrated that the PbS CE had higher catalytic activity toward the polysulfide electrolyte compared to the Pt CE.<sup>362</sup> Teng and coworkers applied a photoactive p-type PbS film as a CE to construct QDSCs. The authors proposed that the p-type characteristics of the PbS film formed a partial tandem junction between the PbS and the anode, resulting in an increase in the  $V_{oc}$  and FF values, achieving a PCE of 4.7%.<sup>359</sup> Jin and coworkers reported a CE based on a CoS<sub>2</sub> thin film on borosilicate glass prepared by thermal sulfidation. The CoS<sub>2</sub> film exhibited high catalytic activity toward a polysulfide electrolyte and good reproducibility and stability in the polysulfide electrolyte, giving a PCE of 4.16%.<sup>365</sup> Another kind of metal chalcogenide that has been widely investigated as a CE catalytic material is quaternary CZTS or CZTSe, which are also famous light-harvesting materials in thin film solar cells. Lee and coworkers applied a CZTS microspheres-coated FTO substrate as a CE in QDSCs and achieved a PCE of 3.73%.<sup>379</sup> It was shown that the catalytic activity of CZTS toward the S<sup>2-</sup>/S<sub>n</sub><sup>2-</sup> redox couple was distinctly higher than for the conventional Pt CE. Cheng *et al.* prepared a porous-structured CZTSe CE by a spray deposition method, achieving a PCE of 4.35%.<sup>380</sup>

**4.3.3. Carbon materials.** Carbon materials are considered attractive catalysts due to their advantages of low cost, high durability, and good conductivity. Thus, carbon materials are potential candidates for the construction of CEs in DSCs and QDSCs. As early as 1996, Grätzel and coworkers first explored a graphitic-carbon black mixture as a CE material in DSCs and obtained a PCE of 6.67%.<sup>381</sup> In fact, various carbon materials have been explored as CEs in QDSCs.<sup>103,104,382–390</sup> For example, Meng *et al.* deposited a mixture of activated carbon and conductive carbon black on an FTO substrate as a CE, exhibiting a PCE of 1.47% for CdS QDSCs.<sup>390</sup> Ko and coworkers devoted much work to carbon materials-based CEs in QDSCs. For example, Ko and coworkers employed hierarchical-nanostructured spherical carbon with a hollow core/mesoporous shell (HCMS) to prepare a CE for use in QDSCs. It was found that the charge-transfer resistance ( $R_{ct}$ ) at the interface of the CE/polysulfide electrolyte was decreased in comparison with Pt CE, delivering a PCE of 3.90% using CdSe QDs as a sensitizer.<sup>383</sup> Furthermore,

they explored ordered multimodal porous carbon (OMPC) as a CE material in both DSCs and QDSCs. The OMPC possessed a large surface area and well-developed 3D interconnected ordered macropore framework with open mesopores embedded in the macropore walls, exhibiting high catalytic activities and fast mass-transfer kinetics toward both  $I^-/I_3^-$  and  $S^{2-}/S_n^{2-}$  redox couples. As a result, an impressive PCE of 4.36% was obtained based on CdSe QDs in 2010.<sup>103</sup> Besides, they also developed a mesoporous-carbon nanofibers (MCNFs)-based CE in QDSCs, showing a PCE of 4.81%.<sup>104</sup>

Even though various carbon materials have been explored as CEs in QDSCs, the obtained solar cell performances are still unsatisfactory compared to the conventional Cu<sub>2</sub>S CE-based one. This can be attributed to the limited catalytic activity, internal resistance, and stability of the carbon-film-based CEs. Accordingly, Zhong's group developed a Ti-mesh-supported carbon film as a CE to improve the catalytic activity, conductivity, and mechanical stability of the CEs.<sup>118,119</sup> For example, as shown in Fig. 24, they used mesoporous carbon (MC) to fabricate a Ti-mesh-supported MC (MC/Ti) CE in QDSCs. It was found that the MC/Ti CE presented superior performance compared to the state-of-art Cu<sub>2</sub>S/FTO CE. On the one hand, the excellent performance of this MC/Ti CE could be attributed to the robust carbon film with good conductivity and the submillimeter thickness due to the confined area in the Ti mesh substrate, ensuring a high catalytic capacity. On the other hand, the 3D interconnected mesoporous framework structure of MC helps realize fast electrolyte mass-transfer kinetics. Finally, a PCE up to 11.51% (11.16% as a certified value) was obtained, representing nearly a 30% improvement relative to the Cu<sub>2</sub>S/FTO CE-based one.<sup>118</sup> Furthermore, they also explored nitrogen-doped mesoporous-carbon (N-MC) materials to prepare CEs in QDSCs. The incorporation of nitrogen heteroatoms into the MC could further improve its catalytic activity toward a polysulfide electrolyte, yielding a PCE of over 12%.<sup>119</sup> It is noted that the exploration of effective CEs based on carbon materials has dramatically promoted the development of QDSCs in recent years.

**4.3.4. Composite CEs.** Usually, the performance of a CE is limited by the unsatisfactory function of a single component material. Therefore, an efficient way to overcome the shortcomings of CEs based on single materials is to fabricate composite CEs using multi-component materials.<sup>329,397–412</sup> For example,

Kamat and coworkers designed a reduced graphene oxide (RGO)-Cu<sub>2</sub>S composite CE.<sup>397</sup> The 2D structure of the RGO facilitated the shuttling of electrons and provided a high surface area for the formation of Cu<sub>2</sub>S reactive sites. As a result, an impressive PCE of 4.4% was obtained based on CdS/CdSe QDSCs. Meng and coworkers prepared PbS/carbon black composite CEs on an FTO substrate.<sup>398</sup> The nanosized PbS provided a large area of catalytic sites, while the carbon black improved both the mechanical strength and the electrical conductivity of the CE. The constructed cell based on this composite CE exhibited a PCE of 3.91% using a CdS/CdSe QD sensitizer. Furthermore, the cell showed outstanding stability over 1000 h under room conditions without degradation. They also prepared a CuInS<sub>2</sub>/carbon composite CE, obtaining a higher PCE of 4.32% and good stability over 1000 h.<sup>399</sup> Choi and coworkers prepared a carbon-dot-Au nanoraspberries CE, exhibiting a high electrocatalytic activity, lower charger-transfer resistance, and larger exchange current density than the reference Au CE and obtained a PCE of 5.4%.<sup>329</sup> Bhattacharyya and coworkers reported a composite CE containing microwave-synthesized Cu<sub>x</sub>S and graphene oxide nanoribbon (GOR) for QDSCs.<sup>400</sup> The composite CE exhibited a higher electrocatalytic activity toward a polysulfide electrolyte, benefiting from the presence of organic functional groups, graphitic edge sites, and a quasi-one-dimensional structure of the GOR. Finally, PCEs of 5.42% and 6.81% were obtained for CdS/CdSe and CdTe/CdS/CdS dual-sensitized QDSCs, respectively.

#### 4.4 Electrolyte- or hole-transporting materials

The electrolyte redox couple or hole-transporting material (HTM) is also one of the most crucial components in QDSCs, serving to regenerate QDs and shuttle the photogenerated holes to the CE.<sup>6,51</sup> To evaluate a redox couple or HTM in QDSCs, the following characteristics should be considered: (1) a low corrosivity to the QDs to maintain the good long-term stability of the cell device; (2) an appropriate redox potential to regenerate QDs effectively and to maintain a high  $V_{oc}$  value at the same time; (3) high ion conductivity to facilitate hole transfer; (4) good stability of itself and high transparency in the visible-light window; and (5) fully regenerative, avoiding the use of non-regenerative hole scavengers. Generally, an electrolyte or HTM can significantly influence the solar cell performance and

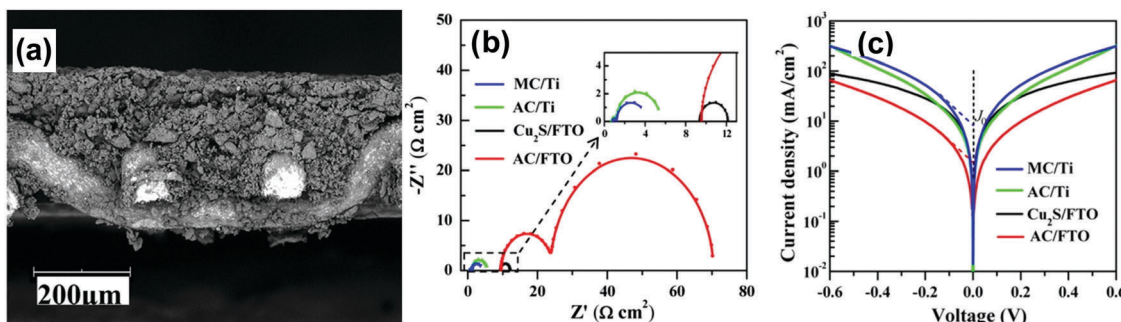


Fig. 24 (a) SEM image of a cross-section of MC/Ti CE. (b) Nyquist plots and (c) Tafel polarization curves of symmetric cells based on identical CEs. Reprinted with permission from ref. 118. Copyright (2016) American Chemical Society.

**Table 5** Summary of the representative photovoltaic performances of QDSCs based on different redox couples and solid-state HTMs

Redox couple or HTMs	QDs	CE	$J_{sc}$ (mA cm $^{-2}$ )	$V_{oc}$ (V)	FF	PCE (%)	Ref.
Polysulfide [(CH <sub>3</sub> ) <sub>4</sub> N] <sub>2</sub> S/[[(CH <sub>3</sub> ) <sub>4</sub> N] <sub>2</sub> S <sub>n</sub>	ZC1Se-CdSe	MC/Ti	27.39	0.752	0.619	12.75	112
	CdS	Pt	3.0	1.2	0.89	3.2	415
Polyulfide-IL Fe(CN) <sub>6</sub> <sup>3-/4-</sup>	CdSe	Pt	13.85	0.42	0.32	1.86	417
	CdS	Pt	3.8	0.8	0.66	2.0	418
[Co(bpy) <sub>3</sub> ] <sup>2+/3+</sup> [Co(bpy) <sub>3</sub> ] <sup>2+/3+</sup>	CdS	Pt	2.34	0.704	0.62	1.01	325
	Au <sub>x</sub>	Pt	3.96	0.832	0.716	2.36	211
[Co( <i>o</i> -phen) <sub>3</sub> ] <sup>2+/3+</sup>	CdSe <sub>x</sub> Te <sub>1-x</sub>	Pt	4.94	0.67	0.54	1.77	102
	ZnSe/CdS	Pt	2.25	0.66	0.58	0.86	416
Tetramethylthiourea [DHexBIm][SCN] <sup>a</sup>	CdS/CdSe	PbSe	12.58	0.60	0.56	4.26	420
	CdSe	Au	4.00	~0.50	—	2.3	421
CuSCN Spiro-OMeTAD <sup>b</sup>	PbS	Au	13.56	0.52	0.579	4.10	133
	PbS/CuS	Au	20.7	0.60	0.65	8.07	422
PCPDTBT <sup>d</sup>	Sb <sub>2</sub> S <sub>3</sub>	Au	15.3	0.616	0.657	6.18	423

<sup>a</sup> 1,3-Dihexylbenzimidazolium cation combined with the SCN anions. <sup>b</sup> 2,2',7,7'-Tetrakis-(*N,N*-di-*p*-methoxyphenylamine)-9,9'-spirobifluorene.  
<sup>c</sup> Poly(3-hexylthiophene). <sup>d</sup> Poly(2,6-(4,4-bis(2-ethylhexyl)-4*H*-cyclopenta[2,1-*b*;3,4-*b'*]dithiophene)-alt-4,7(2,1,3-benzothiadiazole)).

long-term stability of the device. According to the apparent characteristics, electrolytes or HTMs in QDSCs can be summarized into three kinds: liquid, quasi-solid-state, and solid-state. The representative photovoltaic performances for QDSCs based on the different electrolytes or HTMs are summarized in Table 5.

**4.4.1. Liquid electrolytes.** A liquid electrolyte is composed of a redox couple. Even though the well-studied I<sup>-</sup>/I<sub>3</sub><sup>-</sup> redox couple is the state-of-art electrolyte in DSCs, its high corrosivity to most QDs limits its application in QDSCs. Nevertheless, researchers found that the sulfide/polysulfide redox couple (S<sup>2-</sup>/S<sub>n</sub><sup>2-</sup>) was a suitable choice to stabilize most QDs.<sup>94,413,414</sup> Therefore, the polysulfide electrolyte is the most popular choice in QDSCs, and most of the obtained high PCEs have been derived with this electrolyte-based system.<sup>414</sup> However, the unwanted disadvantages of the polysulfide electrolyte has limited the development of QDSCs: (i) the redox potential of the polysulfide electrolyte is relatively high, leading to energy lose and consequently a low  $V_{oc}$ ; (ii) the QDs regeneration rate is slow, leading to an accumulation of holes in QDs and therefore decreasing the QDs stability and increasing the recombination rate.<sup>32</sup> Thus, considerable research efforts have been devoted to explore

new kinds of redox couples, or to modify the polysulfide electrolyte using additives to improve its electrochemical properties.

Much work so far has focused on the exploration of new kinds of redox couples in QDSCs.<sup>102,415-418</sup> One of these is a cobalt-complex-based electrolyte, which is also an efficient electrolyte in DSCs.<sup>102,320,325,419</sup> For example, Grätzel and coworkers introduced the cobalt redox couple of [Co(*o*-phen)<sub>3</sub>]<sup>2+/3+</sup> as an electrolyte in QDSCs.<sup>102</sup> The cell using CdSeTe QD sensitizers showed a PCE of 4.18% at 0.1 sun illumination. Ning and coworkers developed a tetramethylthiourea (TMTU)-based organic electrolyte for QDSCs.<sup>416</sup> It was found that the charge-transfer resistance at the electrolyte/CE interface was distinctly smaller for the cell based on this organic electrolyte than for the polysulfide-electrolyte-based one. Sun and coworkers employed an organic polysulfide redox couple, [(CH<sub>3</sub>)<sub>4</sub>N]<sub>2</sub>S/[[(CH<sub>3</sub>)<sub>4</sub>N]<sub>2</sub>S<sub>n</sub>], as an electrolyte in CdS QDSCs.<sup>415</sup> The oxidation potential of this organic polysulfide redox couple was 1.045 V vs. NHE, which was about 0.5 V lower than that of the S<sup>2-</sup>/S<sub>n</sub><sup>2-</sup> redox couple, exhibiting a  $V_{oc}$  as high as 1.2 V and an FF of 0.89 (Fig. 25). Mora-Seró and coworkers designed a novel pyrrolidinium-based ionic liquid as an electrolyte in QDSCs.<sup>417</sup> The CdSe QDSCs based on this ionic

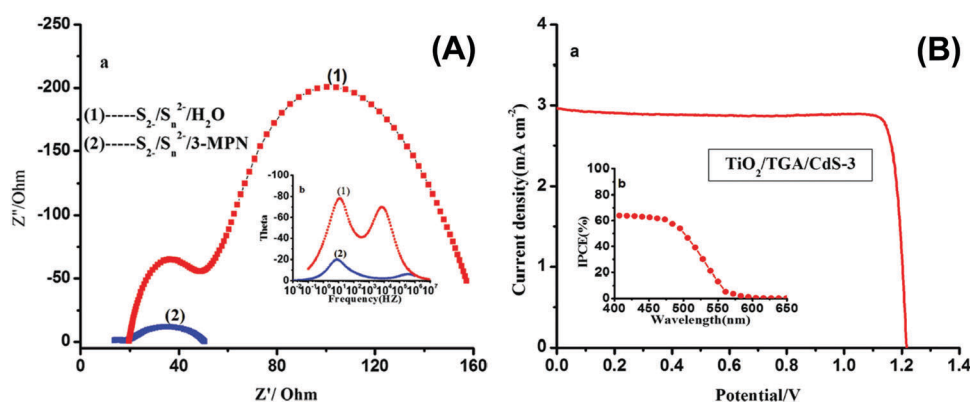


**Fig. 25** (A) Electrochemical impedance spectra of (1) 0.5 M Na<sub>2</sub>S + 2.0 M S in H<sub>2</sub>O and (2) [(CH<sub>3</sub>)<sub>4</sub>N]<sub>2</sub>S/[(CH<sub>3</sub>)<sub>4</sub>N]<sub>2</sub>S<sub>n</sub> in 3-methoxypropionitrile (MPN): (a) complex plane impedance plots; (b, inset) Bode phase plots. (B) J-V characteristics of the TiO<sub>2</sub>/TGA/CdS-3-based cell measured under one sun illumination (a) and IPCE spectrum (b, inset) of the cell based on the TiO<sub>2</sub>/TGA/CdS-3 electrode. Reprinted with permission from ref. 415. Copyright (2011) American Chemical Society.

liquid electrolyte reached a PCE of 1.86%, with good stability over 10 days. Tachibana and coworkers employed a ferricyanide/ferrocyanide ( $\text{Fe}(\text{CN})_6^{3-}/4-$ ) redox couple, which had a relatively positive redox potential (around 0.25 V vs. Ag/AgCl), as an electrolyte for QDSCs. This electrolyte contributed to an enhancement of the  $V_{\text{oc}}$  to 0.8 V.<sup>418</sup>

However, according to the above-mentioned works, even though the application of novel redox couples have brought about an obvious improvement in  $V_{\text{oc}}$  values, the PCEs still lag far behind the polysulfide-electrolyte-based ones. This may be partially due to the limited stability of QDs in the electrolyte or due to the slow QDs regeneration rate. Thus, it remains challenging to develop an efficient redox couple to boost the PCE of QDSCs beyond that based on the state-of-the-art polysulfide electrolyte. This is an important challenge for QDSCs in order to further increase their performance in the future.

Apart from searching for new redox couples, modification of the polysulfide electrolyte using additives to improve its electrochemical properties is another way to improve the performance of QDSCs. This strategy has been intensively investigated in DSCs, and various additives, such as 4-*tert*-butylpyridine (TBP), lithium ions, and guanidinium thiocyanate (GuSCN), have been explored to modify the  $\text{I}^-/\text{I}_3^-$  electrolyte.<sup>6</sup> It has been demonstrated that these additives can distinctly contribute to an improvement in the photovoltaic performance by either inhibiting charge recombination at the photoanode/electrolyte interface or by shifting the conduction band edge of  $\text{TiO}_2$ . Furthermore, the redox potential of the redox couple can also be changed, thus influencing the  $V_{\text{oc}}$  of the cells. Recently, some initial attempts were made to modify the polysulfide electrolyte using additives in QDSCs.<sup>205,391,424,425</sup> For example, Zhong's group adopted water-soluble polymers, including poly(ethylene glycol) (PEG) and poly(vinyl pyrrolidone) (PVP), as additives in the polysulfide electrolyte and observed a remarkable enhancement in the PCE, especially in terms of the  $V_{\text{oc}}$  and FF values.<sup>205,424</sup> Meng's group reported a fumed  $\text{SiO}_2$  nanoparticles-modified polysulfide electrolyte,<sup>425</sup> and revealed that the addition of  $\text{SiO}_2$  nanoparticles in the electrolyte could create an energy barrier for the recombination at QDs/electrolyte as well as  $\text{TiO}_2$ /electrolyte interfaces. Finally, a PCE of 11.23% was achieved, 28.6% higher than the reference cell. Zhong and coworkers employed tetraethyl orthosilicate (TEOS) as an additive in the polysulfide electrolyte and investigated its effect on the charge-transfer dynamics at the photoanode/electrolyte interface.<sup>391</sup> The PCE of the corresponding cell could be improved from 11.75% to 12.34% with the aid of TEOS addition, arising from a reduction of the recombination loss.

**4.4.2. Quasi-solid-state electrolytes.** The drawbacks of easy leakage and volatilization of liquid electrolytes can lead to a poor stability of the cell device and so limit their application. The fabrication of quasi-solid-state QDSCs employing a gel electrolyte is a promising way to obtain highly stable QDSCs.<sup>426–432</sup> Meng and coworkers reported for the first time a quasi-solid-state polysulfide electrolyte using a polyacrylamide-based hydrogel as the polymer matrix and obtained a PCE of 4.0%.<sup>427</sup> It was demonstrated that the 3D continuous porous network of the

polymer was very effective to enhance the absorbent ability toward the liquid electrolyte and the ion-transportation capability. The gel electrolyte exhibited a high ionic conductivity of 0.093 S cm<sup>-1</sup>, which was very close to that of the liquid polysulfide electrolyte (0.104 S cm<sup>-1</sup>). Kuang and coworkers prepared a gel polysulfide electrolyte using dextran as a gelator.<sup>429</sup> This gel electrolyte had a similar conductivity to the liquid one through optimization of the gelator concentration, and the corresponding QDSCs exhibited a PCE of 3.23%. Meng and coworkers applied the natural polysaccharide konjac glucomannan (KGM) as the polymer matrix to prepare the gel electrolyte and the electrolyte, with the  $\text{Cu}_2\text{S}$  counter electrode prepared in one step without a mold.<sup>428</sup> The QDSCs based on this gel electrolyte showed a comparable PCE (4.06%) with the liquid-electrolyte-based one (4.22%) while the cell stability was remarkably improved. Tang and coworkers synthesized graphene-implanted polyacrylamide (PAAm-G) conducting gel electrolytes for quasi-solid-state QDSCs.<sup>430</sup> They utilized osmotic press across the PAAm-G and capillary force within the 3D micropores as driving forces to improve the dosage of the  $\text{S}^{2-}/\text{S}_n^{2-}$  redox couple and obtained a PCE of 2.34% based on the  $\text{CdS}$  QD sensitizer. Huo and coworkers employed 12-hydroxystearic acid as a low molecular mass organogelator to gelate the polysulfide electrolyte and also found an improvement in the cell stability.<sup>431</sup> Zhong's group used sodium polyacrylate (PAAS) and sodium carboxymethylcellulose (CMC-Na) as gelators to prepare quasi-solid-state gel polysulfide electrolytes for QDSCs (Fig. 26), and both of the gel electrolytes contributed to an improvement in the cell stability under continuous irradiation for 90 h.<sup>426,432</sup>

**4.4.3. All-solid-state QDSCs.** All-solid-state devices can thoroughly overcome the drawbacks of the leakage and volatilization of a liquid electrolyte, thus having the potential to realize the long-term stability of the constructed QDSC.<sup>6</sup> The architecture

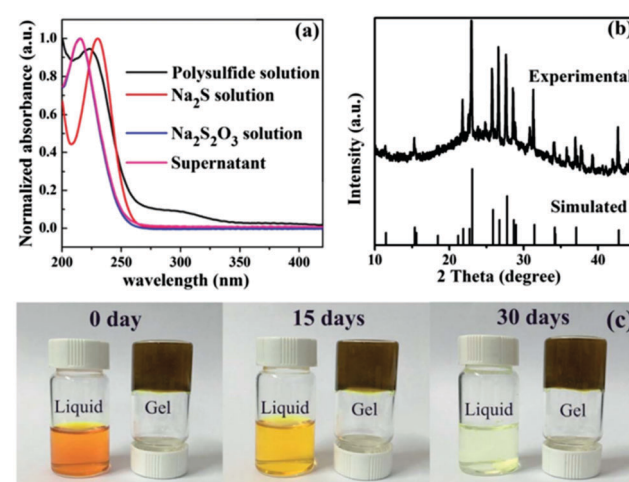


Fig. 26 (a) UV-Vis spectra of the polysulfide electrolyte,  $\text{Na}_2\text{S}$ ,  $\text{Na}_2\text{S}_2\text{O}_3$  solution, and the supernatant. (b) Experimental powder X-ray diffraction (PXRD) spectrum of the precipitates in the liquid polysulfide electrolyte solution, and simulated PXRD spectrum of b-sulfur. (c) The color change of the electrolytes over 30 days. Reprinted with permission from ref. 426. Copyright (2016) Royal Society of Chemistry.

of all-solid-state QDSCs is a little different from liquid-junction QDSCs.<sup>433</sup> Typically, a solid-state hole-transporting material (HTM) instead of a liquid redox couple is used as the hole-transport medium and an evaporated back electrode is applied instead of a counter electrode to collect charge carriers.

For solid-state QDSCs, PbS QD is one of the most commonly used sensitizers.<sup>97,133,251,422,434,435</sup> The first report about all-solid-state QDSCs was by Grätzel and coworkers, in which they employed spiro-OMeTAD as the HTM and obtained an efficiency of 0.49% under 0.1 sun illumination using PbS QDs.<sup>97</sup> Afterward, they improved the PCE to 1.46% through optimization of the pore size of the TiO<sub>2</sub> films and the PbS deposition cycles.<sup>251</sup> Seok and coworkers deposited multiple-layered PbS QDs on a TiO<sub>2</sub> electrode and fabricated solid-state QDSCs using poly(3-hexylthiophene) (P3HT) as the HTM.<sup>434</sup> The cell performance was further improved by a post-EDT treatment, achieving a PCE of 2.9% under 1 sun illumination. Kim and coworkers synthesized CuS-embedded PbS QDs (PbS/CuS) by a cation-exchange reaction and applied them as a sensitizer in solid-state QDSCs (Fig. 27).<sup>422</sup> It was shown that the introduction of CuS around PbS can prolong the exciton lifetime and increase the absorption due to the surface plasmon effect. As a result, a PCE of 8.07% was obtained with an architecture of TiO<sub>2</sub>/PbS/CuS/P3HT/Au.

II-VI group CdS or CdSe QDs were also used to fabricate solid-state QDSCs.<sup>421,436–440</sup> For example, in 2005, Hodes and coworkers sensitized ZnO nanowires with CdSe and fabricated solid-state QDSCs using CuSCN as an HTM, yielding a PCE of 2.3% under 360 W m<sup>-2</sup>.<sup>421</sup> Laramona and coworkers used a CdS QD-sensitized TiO<sub>2</sub> porous film to construct solid-state QDSCs based on CuSCN HTM, obtaining a PCE of 1.3% at 1 sun.<sup>436</sup> Bach and coworkers applied diisooctyl phosphonic

acid (DIOPA) and benzenethiol (BT) derivatives to modify the surface of a CdS/CdSe-sensitized TiO<sub>2</sub> electrode and obtained a PCE of 0.88%, which was higher than the reference cell (0.65%).<sup>437</sup> Song and coworkers employed P3HT, acting as both a HTM and assistant light absorber, in CdS solid-state QDSCs, exhibiting a PCE of 1.42%.<sup>438</sup> Lianos and coworkers demonstrated that the combination of ZnSe in CdSe QDs was beneficial for the improvement of the photovoltaic performance of the corresponding solid-state QDSCs, arising from the more favorable arrangement of the energy levels.<sup>439</sup> Furthermore, it was found that the addition of a small quantity of Na<sub>2</sub>S in P3HT HTM also contributed to an improved PCE of 3.4%.

Sb<sub>2</sub>S<sub>3</sub> is another promising light-harvesting material used in the construction of all-solid-state QDSCs due to its suitable band gap (1.7 eV), strong absorption coefficient ( $1.8 \times 10^5 \text{ cm}^{-1}$ ), and environmental friendly characteristics.<sup>94,208,423,441–455</sup> Initially, Sb<sub>2</sub>S<sub>3</sub> was used as a light-harvesting material in liquid-junction cells.<sup>94</sup> However, it was found that the stability of Sb<sub>2</sub>S<sub>3</sub> in liquid electrolyte was very poor. The first report about all-solid-state Sb<sub>2</sub>S<sub>3</sub> QDSCs was presented by Hodes's group.<sup>441</sup> They deposited Sb<sub>2</sub>S<sub>3</sub> on TiO<sub>2</sub> mesoporous film through a CBD method, and a PCE of 3.37% was obtained using CuSCN as the HTM. The cell also showed good stability over 3 days of illumination under load. Afterward, Hodes and Grätzel and coworkers employed spiro-MeOTAD instead of CuSCN as the HTM, delivering PCEs of 5.2% and 3.1% at 0.1 and 1 sun irradiation, respectively.<sup>443</sup> Seok and Grätzel and coworkers found that P3HT was a suitable HTM in solid-state Sb<sub>2</sub>S<sub>3</sub> QDSCs.<sup>442</sup> The P3HT in the device could act as both a hole conductor and light-harvesting material, achieving a IPCE of 80% and a PCE of 5.13% under 1 sun illumination. Since then, Sb<sub>2</sub>S<sub>3</sub> has attracted much attention as a light-harvesting material to fabricate

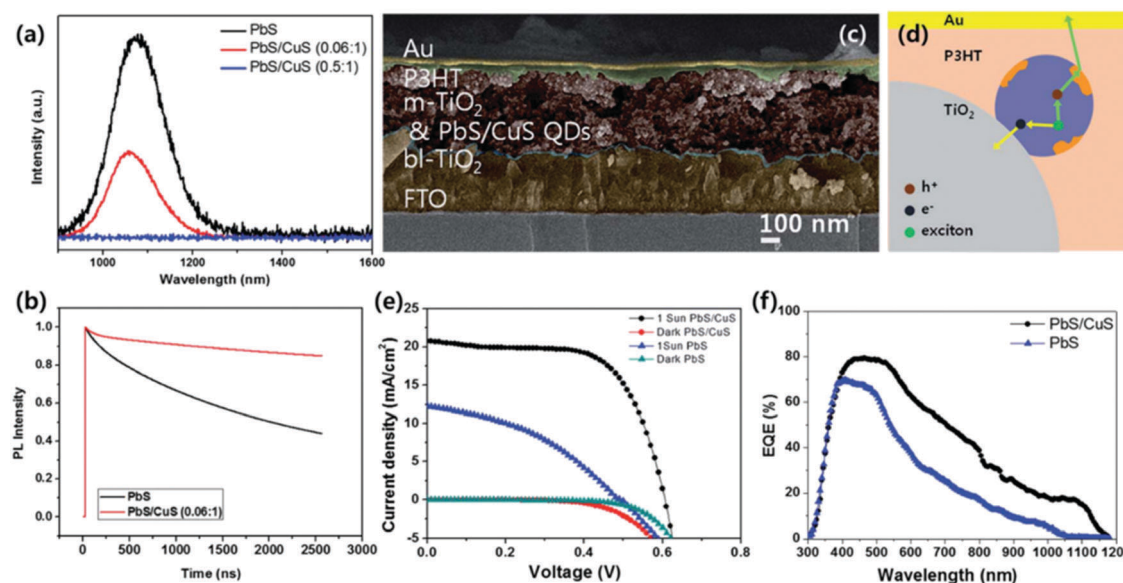


Fig. 27 (a) Static PL spectra of PbS, PbS[CuS], and CuS; (b) luminescence decays (TCSPC) of pristine PbS solution (black) and PbS[CuS] solution (red); (c) SEM cross-sectional images of QD-SSCs; (d) illustration of the proposed working mechanism, whereby excitons generated by light illumination are rapidly separated into free charge carriers; (e) J-V curve of pristine PbS QD-SSCs (blue, dark cyan) and PbS[CuS] QD-SSCs (black, red); (f) EQE spectra of pristine PbS QD-SSCs (blue) and PbS[CuS] QD-SSCs. Reprinted with permission from ref. 422. Copyright (2016) Royal Society of Chemistry.

all-solid-state QDSCs since the obtained PCE is comparable to solid-state DSCs.<sup>6</sup>

Seok's group has devoted much effort to improve the PCE of  $\text{Sb}_2\text{S}_3$ - or  $\text{Sb}_2\text{Se}_3$ -based solid-state QDSCs through optimization of the HTM and the light-harvesting material layer. For example, they investigated the effect of several HTMs on the cell performance of solid-state  $\text{Sb}_2\text{S}_3$  QDSCs, including P3HT, PCPDTBT, PCDTBT, and PTAA,<sup>423</sup> and found that the cell performance was strongly dependent on the chelation of the thiophene moieties in the HTMs toward  $\text{Sb}_2\text{S}_3$ . Finally, the cell based on PCPDTBT HTM gave the best PCE of 6.18% under 1 sun illumination. To overcome the filter effect caused by the absorption of P3HT in the visible-light window, Seok and coworkers constructed a PCBM electron channel that could bridge mp-TiO<sub>2</sub> and P3HT to transfer the generated charge carriers in P3HT to mp-TiO<sub>2</sub>.<sup>445</sup> Moreover, PCPDTBT was used in the device as an additional low-band-gap hole-conducting polymer that could absorb light in the near-infrared region. As a result, the  $J_{\text{sc}}$  could be improved to 16.0 mA cm<sup>-2</sup> and a PCE of 6.3% was obtained. Afterward, Seok *et al.* introduced the surface sulfurization of  $\text{Sb}_2\text{S}_3$  by thioacetamide (TA) before deposition of the HTM layer (Fig. 28).<sup>208</sup> It was found that the PCE of the cell could be significantly improved from 5.5% to 7.1% after the TA treatment. Deep-level transient spectroscopy (DLTS) revealed that the improved photovoltaic performance was mainly derived from the reduction of trap sites in  $\text{Sb}_2\text{S}_3$ .

The CBD method is generally used to deposit  $\text{Sb}_2\text{S}_3$  on a TiO<sub>2</sub> substrate. However, this approach is time-consuming and the experimental conditions need to be precisely controlled (below 10 °C) to avoid impurity phases. Gödel *et al.* reported a modified

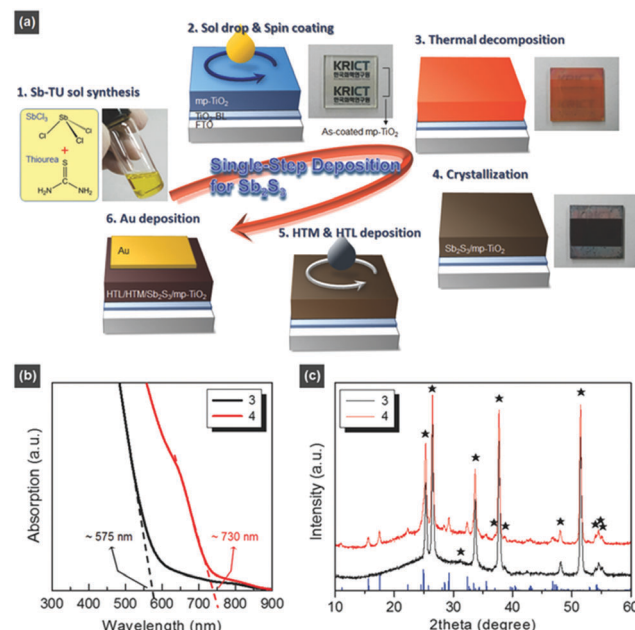


Fig. 29 (a) Schematic diagram of the fabrication process of the fabricated devices via Sb-TU complex solution processing. (b) UV-vis absorption spectra and (c) XRD patterns of the samples obtained after steps 3 and 4. Reprinted with permission from ref. 452. Copyright (2015) Wiley.

CBD approach to deposit  $\text{Sb}_2\text{S}_3$  under room temperature, showing a lower sub-band-gap trap state density and delivering a PCE of 5.1%.<sup>454</sup> Seok and coworkers developed a single-step process to deposit  $\text{Sb}_2\text{S}_3$  on TiO<sub>2</sub> by spin-coating an S/Sb ratio-controlled  $\text{SbCl}_3$ -thiourea complex solution on the substrate (Fig. 29).<sup>452</sup> This single-step approach was demonstrated to be efficient and reproducible to fabricate a high-quality  $\text{Sb}_2\text{S}_3$  layer, and a comparable PCE of 6.4% was obtained relative to the conventional CBD-method-based one (6.3%). Herein, it is noted that the size of  $\text{Sb}_2\text{S}_3$  obtained through this single-step approach was about 60 nm, which is not in the range of quantum dot size. Thus, this kind of cell is usually named as a: semiconductor-sensitized solar cell (SSC).<sup>433</sup>

Apart from  $\text{Sb}_2\text{S}_3$ ,  $\text{Sb}_2\text{Se}_3$ , which has a narrower band gap (1.1 eV), has also been applied as a light-harvesting material to fabricate solid-state sensitized solar cells. Seok and coworkers applied a single-step to deposit  $\text{Sb}_2\text{Se}_3$  on mesoporous TiO<sub>2</sub> by simple multiple cycles of spin-coating of a Se-SSP solution followed by thermal decomposition.<sup>456</sup> The light-absorption range could be expanded to 1050 nm due to the narrower band gap of  $\text{Sb}_2\text{Se}_3$ . The cell device exhibited a  $J_{\text{sc}}$  of 22.3 mA cm<sup>-2</sup>, a  $V_{\text{oc}}$  of 304.5 mV, an FF of 47.2%, and a PCE of 3.21% under a full one-sun illumination. Besides, they also constructed  $\text{Sb}_2(\text{S}/\text{Se}_{1-x})_3$ -graded-composition-sensitizers-based solid-state inorganic-semiconductor-sensitized solar cells,<sup>450</sup> for which they first deposited  $\text{Sb}_2\text{Se}_3$  on a TiO<sub>2</sub> substrate by spin-coating a Se precursor and then  $\text{Sb}_2\text{S}_3$  was grown on the  $\text{Sb}_2\text{Se}_3$ -sensitized film through a CBD method. The cell exhibited a best PCE of 6.6% with a high  $J_{\text{sc}}$  value of 24.9 mA cm<sup>-2</sup>.

In general, although all-solid-state QDSCs or SSCs possess prominent advantages, especially their potential to realize

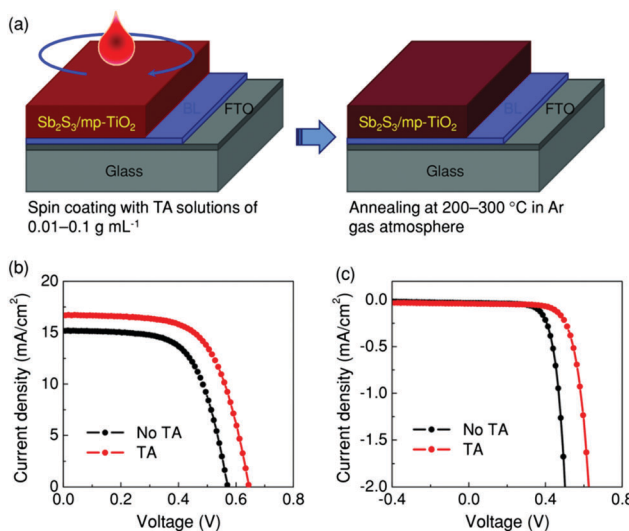


Fig. 28 Thioacetamide (TA) surface sulfurization and its effects on photovoltaic performance. (a) Schematic diagram for the TA-surface-sulfurization process in  $\text{Sb}_2\text{S}_3$ -sensitized inorganic–organic heterojunction solar cells. (b) Effects of TA sulfurization on the  $J$ – $V$  characteristics measured under AM 1.5 G solar irradiance (100 mW cm<sup>-2</sup>) and (c) corresponding dark  $J$ – $V$  curves. In (b and c), the devices with and without TA treatment are denoted as TA and No TA, respectively. Reprinted with permission from ref. 208. Copyright (2014) Wiley.

long-term stability of a device, their obtained PCEs are still low compared to the liquid-junction QDSCs. To date, the highest PCE for an all-solid-state QDSC or SSC is about 8%. The component materials are the main limitations for solid-state QDSC, including the light-harvesting materials as well as HTMs. Further work should focus on the exploration of high-quality light-harvesting materials with a suitable band gap and proper HTM, combined with optimization of the device structure.

## 5. Recombination control

In QDSCs, apart from the preferred charge-transfer processes, there are also several recombination paths competing with these favorable processes. It is well known that non-radiative charge recombination can seriously deteriorate the performance of a device.<sup>33,38</sup> For QDSCs, charge recombination is particularly serious compared to DSCs due to the existence of defect states in QD sensitizers, the low QD-loading amount inducing a large portion of bare TiO<sub>2</sub> surface to be directly exposed to the electrolyte, and the complex chemical activity of the commonly used polysulfide electrolyte. Therefore, the suppression of charge recombination in QDSCs is a big issue that should be addressed to obtain the desirable photovoltaic performance.

As shown in Fig. 30 with dashed arrows, there are four main recombination pathways in QDSCs: (1) charge recombination inside the QD through defect states, (2) recombination of excited electron in the QD with oxidized species in the electrolyte at the QD/electrolyte interface, (3) back transfer of electrons in the TiO<sub>2</sub> to the QD at the TiO<sub>2</sub>/QD interface, and (4) recombination of electrons in TiO<sub>2</sub> with the electrolyte at the TiO<sub>2</sub>/electrolyte interface.<sup>38</sup> It can be seen that the defect states in the QD and the large area of bare TiO<sub>2</sub> surface aggravate the charge recombination in QDSCs compared to DSCs, where TiO<sub>2</sub> is practically fully covered by the dye, or polymer solar cells. In recent years, considerable efforts have been made to address the recombination issue. In general, the reported means for recombination controlling in QDSCs can be summarized into

two kinds: material engineering and interface engineering, which are discussed in detail in the following section.

### 5.1 Material engineering

Since one of the major charge-recombination processes takes place inside QDs through defect states, a high-quality QD sensitizer has become a prerequisite for high-efficiency solar cells. In the early investigation stage of QDSCs, QDs were usually grown directly on the TiO<sub>2</sub> substrate through SILAR or CBD methods.<sup>36,101</sup> As mentioned in the above section, QDs formed by this *in situ* approach usually possess a high density of defect states due to the poor crystallinity and large number of dangling bonds at the surface, leading to severe charge recombination inside QDs or back electron transfer from TiO<sub>2</sub> to QDs. Therefore, the adoption of a high-quality pre-synthesized QD sensitizer is an effective route to improve the photovoltaic performance of QDSCs.<sup>36,457</sup> On the one hand, pre-synthesized colloidal QDs possess a lower density of inner and surface defect states, benefiting from the well-developed organometallic synthesis method. On the other hand, pre-prepared QDs provide more opportunities to realize a better control over the composition and structure of the QDs. Thus, it's not surprising that the adoption of pre-synthesized QDs as a sensitizer have prominently promoted the development of QDSCs in the past five years.<sup>74,85,109,111,115–118,219,425</sup> Accordingly, much effort has been made to design the optimum composition and structure of QDs to ensure charge-recombination control. Among the solutions, the construction of a core/shell structure and the alloying strategy have been demonstrated to be efficient means to reduce charge-recombination loss.

Core/shell-structured QDs are an attractive material to use in recombination design since their photoelectric properties can be facilely tailored through the shell materials.<sup>270,271</sup> Among these, type-II-structured QDs possess the potential to reduce charge recombination inside QDs. For type-II-structured QDs, both the CB and VB of the core material are located either lower or higher than the shell material, resulting in the spatial separation of charge carriers. Accordingly, if the CB and VB of the core material are both higher than the shell material, the electron is mostly confined to the shell layer and the hole is mostly confined to the core layer.<sup>268,270,271</sup> It is noted that this spatial separation of electrons and holes reduces the possibility of charge recombination within QDs. Inspired by these unique properties, several attempts have been made to apply type-II QDs as sensitizers in QDSCs, including ZnSe/CdS, ZnTe/ZnSe, CdTe/CdSe, and ZnTe/CdSe, and a record PCE of 7.17% has been achieved for ZnTe/CdSe-based QDSCs.<sup>74,85,217,416</sup> The details of the related works have been discussed in the above section. It is noted that the obtained  $V_{oc}$  of QDSCs based on these type-II QDs are especially higher compared to other QDs, partially due to the inhibited charge-recombination inside the QDs.

Besides, type-I-structured core/shell QDs also show their superiority in controlling the charge-recombination process. In type-I-structured QDs, the shell materials have a higher CB edge and lower VB edge than those of the core materials.<sup>270</sup> On the one hand, the wide-band-gap shell acts as a barrier layer,

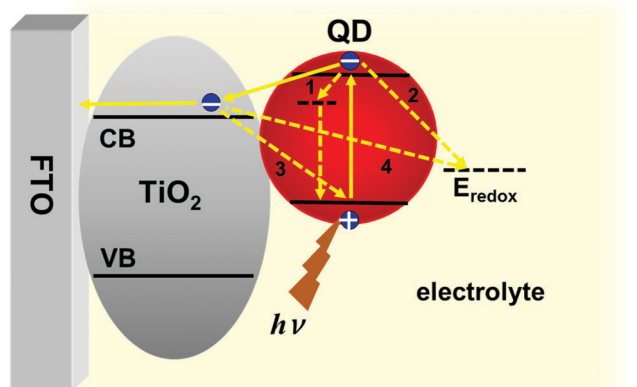
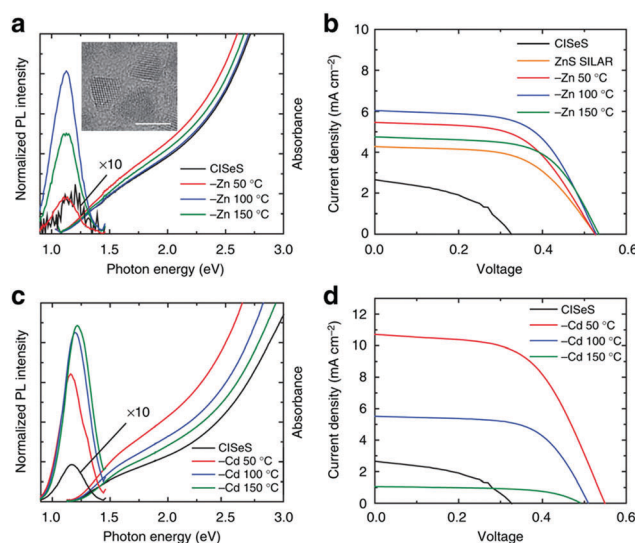


Fig. 30 Schematic illustration of the main charge-recombination routes in QDSCs.

which can prevent photogenerated electron leakage from the QD to the electrolyte. On the other hand, the epitaxial growth of the wide-band-gap shell material significantly reduces the trap state density of the core QD, so the processes of internal charge recombination inside the QD and electron back transfer from  $\text{TiO}_2$  to the trap states of QDs are consequently retarded.<sup>38</sup> However, it should be noted that the shell can also act as a barrier in preventing electron injection from the QD to the electron acceptor.<sup>116</sup> Therefore, the thickness of the shell material should be thin enough (generally less than 1–2 nm) to guarantee efficient electron extraction. The cation-exchange method is one convenient way to fabricate a thin shell layer around the core QDs to form the quasi-type-I structure. For example, Zhong and coworkers applied a cation-exchange approach to prepare type-I  $\text{CuInS}_2/\text{ZnS}$  core/shell QDs.<sup>116</sup> The photoluminescence (PL) quantum yield of the as-prepared QDs was significantly improved after the formation of the ZnS shell layer through the cation-exchange process. Accordingly, the PCE of the cell was improved from 5.05% ( $\text{CuInS}_2$  based) to 7.04% ( $\text{CuInS}_2/\text{ZnS}$  based) benefiting from the inhibited charge recombination and prolonged electron lifetime. Klimov and coworkers compared the different effects of cation exchange in  $\text{CuInSe}_{1-x}\text{S}_x$  QDs using  $\text{Zn}^{2+}$  and  $\text{Cd}^{2+}$  ions as the exchange cation.<sup>78</sup> It was found that both  $\text{Zn}^{2+}$  and  $\text{Cd}^{2+}$  cation exchange could contribute to an improvement in the PL quantum yield as well as in the resultant solar cell performance, with the enhancement greater for the  $\text{Cd}^{2+}$ -based one, and a certified PCE of 5.1% was obtained (Fig. 31).



**Fig. 31** (a) Absorption and photoluminescence (PL) spectra of the QDs before and after exposure to Zn-oleate at various temperatures after recapping with tert-butylamine (tBA). Inset: TEM image of 4.5 nm  $\text{CulnSe}_{1.4}\text{S}_{0.6}$  QDs. Scale bar, 5 nm. (b)  $J$ – $V$  curves for QDs with varying degrees of Zn-cation exchange, or with ZnS SILAR post-treatment of the QD-infused anode (orange line). (c) Absorption and PL spectra of the QDs before and after exposure to Cd-oleate and recapping with tBA. (d)  $J$ – $V$  curves for QDs with varying degrees of Cd-cation exchange controlled by the reaction temperature. Reprinted with permission from ref. 78. Copyright (2013) Macmillan Publishers Limited.

Recently, the alloying strategy has been demonstrated as a convenient way to improve the photoelectronic properties of QDs as well as the photovoltaic performance of the related solar cells.<sup>115,223,274</sup> As discussed above, there are two conflicting effects of the shell layer in type-I-structured core/shell QDs: reducing surface trapping defects but retarding electron injection and hole scavenging simultaneously. Furthermore, the formation of the thin shell layer can only reduce the surface defect states of QDs, while it is powerless to tailor the defect states inside the QDs. In contrast, alloying a wide-band-gap material into the native QD can resolve these problems simultaneously. It has been shown that the alloying strategy could not only reduce the density of trap defects both at the surface and inside the QD due to the hardened lattice structure and decreased atomic intradiffusion, but could also favor electron injection due to the upshift of the CB edge. Zhong and coworkers alloyed ZnSe and  $\text{Ga}_2\text{Se}_3$  in native CISe QDs to form Zn-Cu-In-Se or Ga-Cu-In-Se QDs through a “simultaneous nucleation and growth” approach.<sup>115,223</sup> The PCE of the QDSCs could be improved by more than 20% by using the alloying strategy with the QD sensitizers and a record PCE of 11.66% was obtained. The enhancement in the solar cell performance could be mainly attributed to the lower density of trap states in the QDs, thus inhibiting the charge-recombination process, and the upshift of the CB edge, thus improving the electron-injection efficiency.

## 5.2 Interface engineering

In charge-recombination control, besides the amelioration of the quality of QD sensitizers to suppress the QD-related recombination processes, other attention has been mainly paid to the recombination processes taking place at the  $\text{TiO}_2$ /QD/electrolyte interface.<sup>32,33,38</sup> In the photoanode, QDs and the bare  $\text{TiO}_2$  surface contact directly with the electrolyte. This facilitates electrons being captured by the oxidized species in the electrolyte. Thus, the modification of the  $\text{TiO}_2$ /QD/electrolyte interface is crucial to realize the high photovoltaic performance of QDSCs. As a whole, interface modification techniques can be classed into three kinds: coating strategy using inorganic wide-band-gap materials, organic molecular treatment, and electrolyte modification.

**5.2.1. Coating strategy.** The coating strategy on the photoanode using wide-band-gap materials to prevent direct contact between the photoanode and electrolyte is believed to be an efficient way to reduce electron-recombination losses at the photoanode/electrolyte interface. Among the materials, the ZnS-coating layer is the most popular and commonly used one in QDSCs and has had a dramatically positive effect in improving solar cell performance.<sup>117,459–464</sup> The concept of ZnS-coating treatment on a semiconductor to tailor the interface characteristics was first carried out by Huang and coworkers, in which they coated a  $\text{TiO}_2/\text{PbS}/\text{CdS}$  electrode by a ZnS layer through a SILAR method to protect the PbS and CdS particles from photocorrosion.<sup>460</sup> They found that the photovoltaic performance of solar cells could be improved significantly after the ZnS treatment, especially in terms of the  $V_{oc}$  value. This work indicated that the ZnS-coating layer could not only protect

the QDs from photocorrosion, but also showed a suppressing effect on the charge-recombination process. After that, Toyoda and Shen and coworkers introduced this treatment to QDSCs and systematically investigated the effect of a ZnS-coating layer on the solar cell performance.<sup>99,459,464</sup> It was demonstrated that the ZnS treatment plays two roles in the performance of QDSCs: one is to passivate the QDs' surface and the other is to block the bare TiO<sub>2</sub> surface. As a result, an improvement of 74% in the final PCE can be achieved. Since then, the ZnS-coating treatment has been adopted as a typical process in the fabrication of QDSCs. Meanwhile, ZnSe has also been used as a passivation layer in QDSCs.<sup>465–469</sup> For example, Cao and coworkers compared the effect of a ZnS and ZnSe passivation layer on the performance of QDSCs.<sup>466</sup> They found that the ZnSe passivation layer was superior to the ZnS passivation layer in terms of improving the PCE of QDSCs. The ZnSe passivation layer could not only improve the light-harvesting capability of the photoanode, but also showed a better charge-recombination inhibition effect. Finally, a PCE of 6.4% was achieved for CdS/CdSe QDSCs with a ZnSe passivation layer, about 30% higher than the ZnS-passivation-layer-based one (4.9%).

Apart from ZnS or ZnSe passivation layer, metal oxides with a wide band gap have also been investigated as a coating layer to inhibit charge recombination at the photoanode/electrolyte interface in QDSCs.<sup>113,114,117,256,458,470–473</sup> This was motivated by the corresponding works in DSCs, in which insulating metal oxide treatment on the photoanode has been widely investigated for the purpose of recombination control.<sup>474–477</sup> It was revealed that the main function of the metal oxide layer coating is to block the electron back transfer process, thus improving the  $V_{oc}$  of the cell device. Zaban and coworkers deposited a thin amorphous TiO<sub>2</sub> layer on a QD-sensitized film.<sup>471</sup> The results showed that both the PCE and the stability of the CdS-based QDSCs were remarkably improved in I<sup>-</sup>/I<sub>3</sub><sup>-</sup> electrolyte. Besides, Zaban and coworkers also used a MgO coating to modify the interfaces.<sup>472</sup> They deposited conformal MgO by the EPD method on a TiO<sub>2</sub> electrode before or after QDs deposition, illustrating that the interface between the TiO<sub>2</sub> and QDs is also crucial for the recombination process as well as for the other interfaces in the TiO<sub>2</sub>/QDs/electrolyte triple junction. Bent and coworkers deposited Al<sub>2</sub>O<sub>3</sub> barrier layers either before or after the QD deposition on a TiO<sub>2</sub> film by the ALD method to fabricate CdS- or PbS-based solid-state QDSCs (Fig. 32),<sup>458</sup> and found that the Al<sub>2</sub>O<sub>3</sub> barrier layer could act as a tunneling barrier to suppress charge recombination and increase electron lifetimes in TiO<sub>2</sub>. With optimization of the Al<sub>2</sub>O<sub>3</sub> layer thickness, the obtained  $V_{oc}$  and PCE were increased obviously.

Zhong and coworkers reported a robust coating treatment to tailor the interface charge-recombination processes, in which they applied a novel double-coating layer by sequentially depositing ZnS and SiO<sub>2</sub> on a QD-sensitized TiO<sub>2</sub> electrode (Fig. 33).<sup>117</sup> Density functional theory (DFT) calculations were performed and unraveled that the ZnS or SiO<sub>2</sub> single coating layer could reduce the surface electron density of states (DOS) by 2 orders of magnitude, while the double-coating layer could further reduce the DOS by 3 orders of magnitude. As a result,

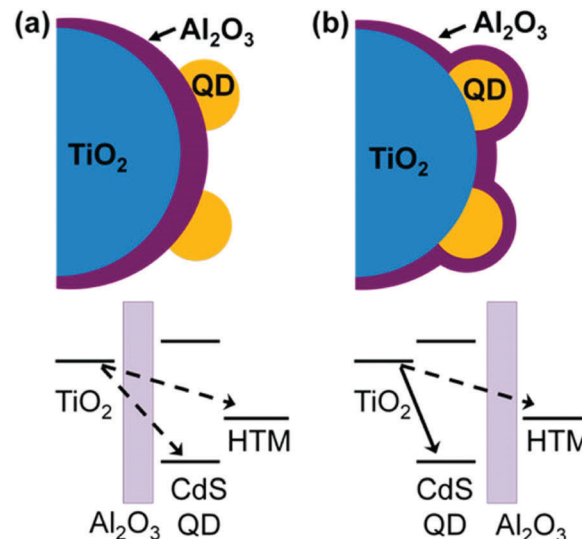


Fig. 32 Schematic of the barrier-layer configurations (not to scale) available in quantum dot-sensitized solar cells: (a) TiO<sub>2</sub>/Al<sub>2</sub>O<sub>3</sub>/QD and (b) TiO<sub>2</sub>/QD/Al<sub>2</sub>O<sub>3</sub>, resulting, respectively, from deposition of the Al<sub>2</sub>O<sub>3</sub> layer before and after the CdS QDs. Spiro-OMeTAD is employed as the hole-transport material (HTM). Arrows indicate the undesirable recombination pathways, and pathways that may be blocked by the Al<sub>2</sub>O<sub>3</sub> barrier layer are shown by dashed arrows. Reprinted with permission from ref. 458. Copyright (2013) American Chemical Society.

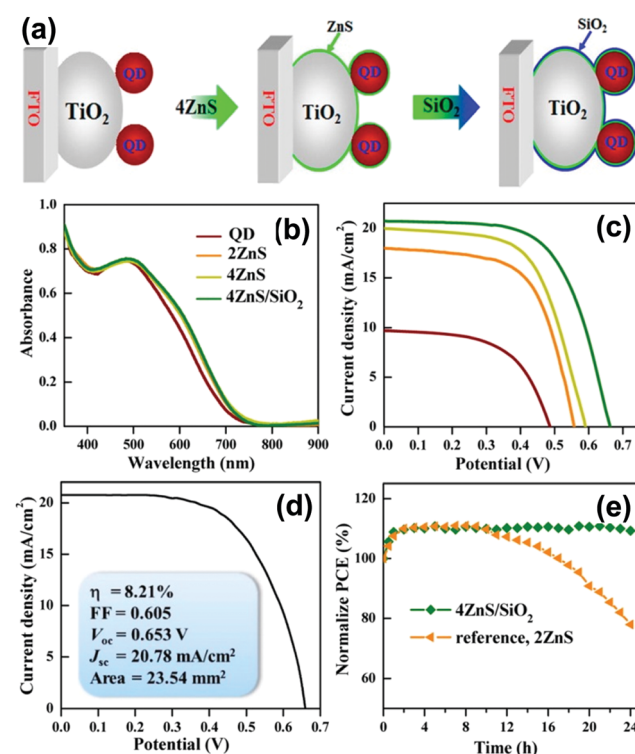


Fig. 33 (a) Schematic showing the sequential overcoating of a ZnS and SiO<sub>2</sub> thin layer around a QD-sensitized TiO<sub>2</sub> film electrode. (b) Absorption spectra of photoanode films after different coatings. (c) J-V curve of samples prepared with different coatings after QD sensitization. (d) Certified efficiency of a QDSC prepared with 4ZnS/SiO<sub>2</sub> coating. (e) Cell efficiency normalized to the initial efficiency for samples with different coatings measured during a 24 h period under continuous 1 sun illumination. Reprinted with permission from ref. 117. Copyright (2015) American Chemical Society.

the PCE of the constructed cell was boosted from 7.17% (single ZnS layer) to 8.55% (ZnS/SiO<sub>2</sub> double layer). Besides, they introduced an additional amorphous metal oxyhydroxide as a buffer layer between the QD-sensitized film and ZnS/SiO<sub>2</sub> blocking layer to further suppress charge recombination at the interface.<sup>113,114</sup> A series of metal oxyhydroxides were overcoated on CdSeTe QD-sensitized photoanodes *via* a hydrolysis and condensation process from the corresponding metal chloride aqueous solution to investigate their effect on the photovoltaic performance. It was found that the introduction of am-TiO<sub>2</sub>, am-ZrO<sub>2</sub>, and am-Nb<sub>2</sub>O<sub>5</sub> as buffer layers showed beneficial effects in terms of an improvement of the cell performance due to further suppression of charge-recombination processes, and the PCE was further boosted to 9.73% with ZrOCl<sub>2</sub> treatment on the photoanode.

Unlike the above-mentioned wide-band-gap semiconductor or insulating inorganic materials overcoating strategy aiming at isolating the photoanode from the electrolyte, and thus reducing photogenerated electron leakage at the photoanode/electrolyte interface, a p-type semiconductor CuS overlayer has been used to facilitate hole transfer to the electrolyte from QD sensitizers.<sup>192,462,478</sup> In an example reported by Ghosh *et al.*,<sup>479</sup> a CdS layer was first overcoated around a QD-sensitized photoanode, and then Cd<sup>2+</sup> was partially replaced by Cu<sup>2+</sup> to form a CuS layer. With the formation of the CuS layer, the PCE of the champion cell was 4.03%, which was about 12% higher than the one with a normal ZnS coating. EIS measurements disclosed that the CuS layer acted as a hole-transporting buffer layer, thus increasing the charge-collection efficiency. Therefore, this strategy could help to overcome the inherent disadvantage of the slower hole-transfer rate in standard QDSCs, which is one of the key factors limiting the performance of QDSCs.

**5.2.2. Organic molecular treatment.** Apart from the inorganic coating layer treatment, photoanode interface modification using organic molecules was also demonstrated to be effective for the suppression of charge recombination.<sup>480–485</sup> For example, Mora-Seró and coworkers showed that molecular dipole (DT)-assisted ZnS treatment could give a better control of the recombination dynamics as well as the charge-injection process.<sup>480</sup> They found that the sequence of DT and ZnS treatment could significantly influence the final performance of solar cells, whereby the optimized sequence of the treatment (DT + ZnS) resulted in a dramatic 600% increase in the PCE compared to the reference cell without treatment. Furthermore, they also investigated the passivation effect of different organic molecules, including ethanedithiol (EDT), ethylenediamine (ETDA), thioglycolic acid (TGA), dimethylamine (DMA), and formic acid (FA),<sup>481</sup> and found that the treatment using molecules containing amine or thiol groups could enhance the PCE of QDSCs, while the treatment by molecules with acid groups would lead to a negative effect. It should be noted that investigation of the organic molecular treatment on QD-sensitized photoanodes was performed *via* the *in situ* growth of QD sensitizers on a TiO<sub>2</sub> film electrode. In this condition, no capping ligand was present on the surface of the QD sensitizers, so that the organic molecules could easily absorb on the QDs. It is not

certain whether this organic molecular treatment could provide a similar positive effect in ligand-capped pre-prepared QD-sensitizer-based QDSCs. In the case of *ex situ* prepared QD sensitizers, thiol coadsorbents (such as thioglycolic acid (TGA), 3-mercaptopropionic acid (MPA), glutathione (GSH), and cysteine) were added into the QD solution prepared in aqueous media during the QD deposition process.<sup>248</sup> The experimental results indicated that the photovoltaic performance of the resulting QDSCs were dependent on the type and concentration of the thiol coadsorbent used. With the use of TGA coadsorbents, the PCE of the CuInS<sub>2</sub> QDSCs (5.90%) was 20 times higher than that of the control cell without TGA coadsorbents (0.29%). The versatility of this strategy was demonstrated in the fabrication of QDSCs using AgInS<sub>2</sub> or CdSeTe QDs prepared in aqueous media. The improved performance was ascribed to reducing the disulfides, and varying the conduction band edge of TiO<sub>2</sub>. However the effect of coadsorbents in increasing the QD-loading amount was prominent, and this could explain the enhanced  $J_{sc}$  and  $V_{oc}$ .

**5.2.3. Electrolyte modification.** As discussed above, the complex nature of the polysulfide electrolyte brings about severe charge recombination. Previous work has demonstrated that the rate of charge recombination from TiO<sub>2</sub> to the polysulfide electrolyte is at least 2 orders of magnitude greater than that in the I<sup>-</sup>/I<sub>3</sub><sup>-</sup> redox couple based system.<sup>32</sup> This should, therefore, be seriously taken into account when designing high-efficiency QDSCs. An alternative way to suppress the charge recombination is by modification of the polysulfide electrolyte using additives to tune its electrochemical properties.

Zhong *et al.* found that the addition of water-soluble polymers, such as PEG and PVP, in the polysulfide electrolyte could distinctly inhibit the charge-recombination rate at the TiO<sub>2</sub>/QD/electrolyte interface.<sup>205,424</sup> They proposed that the polymer additives in the polysulfide electrolyte could serve as a protective layer over both the TiO<sub>2</sub> and QDs surfaces by a steric hindrance effect, thus inhibiting the unwanted charge recombination from TiO<sub>2</sub> to the polysulfide electrolyte and improving the resultant photovoltaic performance. Meng *et al.* reported that the addition of fumed SiO<sub>2</sub> nanoparticles in the polysulfide electrolyte also resulted in an inhibition effect for the charge recombination.<sup>425</sup> They demonstrated that the SiO<sub>2</sub> nanoparticles in the electrolyte could create an energy barrier at the QDs/electrolyte and TiO<sub>2</sub>/electrolyte interfaces, consequently retarding the charge-recombination processes. However, it should be noted that the intrinsic mechanism of charge-recombination inhibition using these additives in the polysulfide electrolyte is not fully understood yet.

## 6. Stability issues

For all kinds of emerging solar cells, long-term stability is a prerequisite to realize their commercial application. Up to now, long-term stability is one of the bottlenecks limiting the practical application of almost all kinds of emerging solar cells.<sup>486–491</sup> In QDSCs, however, few studies have been focused on the

stability investigation, despite the cell stability still being far from satisfactory. Therefore, for the further development of this kind of solar cells, much effort should be devoted to address the stability issue. The stability of QDSCs is mainly determined by the following factors: (1) the chemical stability of the QDs in the electrolyte; (2) the chemical and mechanical stability of the counter electrode used in QDSCs; (3) the stability of the redox couple in the electrolyte; and (4) the sealing technology used to avoid the leakage and volatilization of the electrolyte (for liquid-junction devices). A summary of stability tests for QDSCs is shown in Table 6.

The  $I^-/I_3^-$  redox couple is the most popular choice in DSCs, but most QDs are unstable in this system. Although the polysulfide electrolyte ( $S^{2-}/S_n^{2-}$ ) was found to be suitable for stabilizing QDs and therefore could offer a relatively stable cell device, photocorrosion of the QDs in the polysulfide electrolyte could still take place due to the complex chemical properties of the polysulfide redox couple, consequently resulting in a deterioration of the cell stability.<sup>75,253</sup> In addition, the chemical and mechanical stability of the CEs can also affect the stability of the cell device. For example, brass-foil-based Cu<sub>2</sub>S is commonly used as a CE in QDSCs, even though this CE suffers from continuous corrosion by the polysulfide electrolyte, resulting in leakage of the electrolyte eventually.<sup>397</sup> Therefore, to improve the stability of QDSCs, the exploitation of highly stable QDs, a robust CE, and an effective cell-sealing technique should be taken into account simultaneously.

The good chemical stability of QDs toward light, heat, and the electrolyte is a prerequisite to realize good device stability. Various QDs, such as PbS, CdTe, and Sb<sub>2</sub>S<sub>3</sub>, have been proven to be unstable in the traditional polysulfide electrolyte.<sup>97,253,448</sup> Zhong *et al.* demonstrated an improvement in the solar cell stability by using an alloyed CdSe<sub>x</sub>Te<sub>1-x</sub> QD with good stability

in the polysulfide electrolyte.<sup>111</sup> The fabricated QDSCs exhibited good stability for more than 500 h (Fig. 34). It is noted that many subsequent studies on the stability improvement have also been based on this kind of state-of-the-art sensitizer.<sup>205,425,426,432,473</sup> In addition, the doping strategy in QD sensitizers was also found to favor the stability of QDSCs.<sup>107,305,492</sup> For example, Kamat *et al.* reported that QDSCs using Mn-doped CdS/CdSe QDs as a sensitizer showed good stability under continuous illumination of 100 mW cm<sup>-2</sup> for 2 h.<sup>107</sup> Gopi *et al.* also demonstrated that the cells based on Mn-doped CdS QDs displayed a better stability compared to an undoped one.<sup>305</sup>

Another way to improve the stability of QDSCs is by photoanode post-treatment with an overcoating of an isolating wide-band-gap semiconductor.<sup>117,460,471,473,493,494</sup> On the one hand, the coating layer can prevent QDs from having direct contact with the electrolyte, thus reducing photocorrosion of the QDs in the electrolyte, while on the other hand, the coating layer around the photoanode can protect the QDs from the attack by oxygen molecules, thus improving the chemical stability of the QDs. For example, a commonly used ZnS or ZnSe passivation layer was found to be capable of improving the stability of QDSCs.<sup>460,493,494</sup> In addition, a metal oxide coating layer on the photoanode can also favor the stability of the device.<sup>471</sup> For instance, Zaban *et al.* presented a coating strategy on a CdS-sensitized TiO<sub>2</sub> film using an amorphous TiO<sub>2</sub> layer to improve the cell stability in  $I^-/I_3^-$  electrolyte.<sup>471</sup> The amorphous TiO<sub>2</sub> coating protected the QDs from severe corrosion by the  $I^-/I_3^-$  redox couple and therefore allowed obtaining a better performance compared to the uncoated one. Zhong *et al.* found that a ZnS/SiO<sub>2</sub> double-layer coating on the photoanode was beneficial for improving the stability of QDSCs.<sup>117</sup> The constructed cell with this double-layer coating exhibited no degradation over the course of 24 h under 1 sun continuous irradiation,

**Table 6** Summary of stability tests for QDSCs under different test conditions

QDs	CE	Electrolyte	Storage conditions	Period (h)	Degradation (%)	Ref.
CdS/CdSe	PbS-CB/FTO	Polysulfide	AC <sup>a</sup>	1000	No	398
CdS/CdSe	CuInS <sub>2</sub> -CB/FTO	Polysulfide	In dark at AC	1000	No	399
CdSe <sub>x</sub> Te <sub>1-x</sub>	CuS/FTO	Polysulfide/SiO <sub>2</sub>	In dark at AC	1000	6.3	425
CdS/CdSe	Cu <sub>2</sub> S/brass	Gel polysulfide	—	1000	27	428
CdS/CdSe	Cu <sub>2</sub> S-carbon/FTO	Polysulfide	In dark at AC	720	No	396
CdS/Au@PAA	C-Fabric/WO <sub>3-x</sub>	Polysulfide/SiO <sub>2</sub>	In dark at AC	720	3	204
CdS/CdSe	PbSe	[DHexBIm][SCN]	—	504	33	420
CdSe <sub>x</sub> Te <sub>1-x</sub>	Cu <sub>2</sub> S/FTO	Polysulfide	AC	500	No	111
CdS/CdSe	CuS/FTO	Gel polysulfide	—	240	No	342
CdS/CdSe	Pt	Gel polysulfide	In oven at 60 °C	220	8	431
CdSe <sub>x</sub> Te <sub>1-x</sub>	Cu <sub>2</sub> S/FTO	Polysulfide	AC	120	20	473
CdSe <sub>x</sub> Te <sub>1-x</sub>	Cu <sub>2</sub> S/FTO	Polysulfide/PVP	AC	80	15	205
CdSe	Cu <sub>2</sub> S/FTO	Polysulfide/TEOS	AC	76	6	391
CdSe <sub>x</sub> Te <sub>1-x</sub>	Cu <sub>2</sub> S/FTO	Gel polysulfide	1 sun illumination	90	20	426
CdSe	Cu <sub>x</sub> S/FTO	Gel polysulfide	1 sun illumination	77	23	432
Sb <sub>2</sub> S <sub>3</sub>	Au	CuSCN	0.6 sun illumination	72	10	441
CdSe <sub>x</sub> Te <sub>1-x</sub>	Cu <sub>x</sub> S/FTO	Gel polysulfide	1 sun illumination	46	31	432
CdSe	Cu <sub>x</sub> S/FTO	Polysulfide/PEG	1 sun illumination	30	No	424
CdSe <sub>x</sub> Te <sub>1-x</sub>	Cu <sub>2</sub> S/FTO	Polysulfide	1 sun illumination	24	No	117
CdSe	Cu <sub>2</sub> S/FTO	Polysulfide	1 sun illumination	10	No	349
CdS/CdSe	NiS-PbS/FTO	Polysulfide	1 sun illumination	10	No	411
CdS/Au@PAA	C-Fabric/WO <sub>3-x</sub>	Polysulfide/SiO <sub>2</sub>	1–2 sun illumination	5	18	204
Mn–CdSe/CdSe	Cu <sub>2</sub> S-RGO/FTO	Polysulfide	1 sun illumination	2	2	107

<sup>a</sup> Ambient condition under room light.

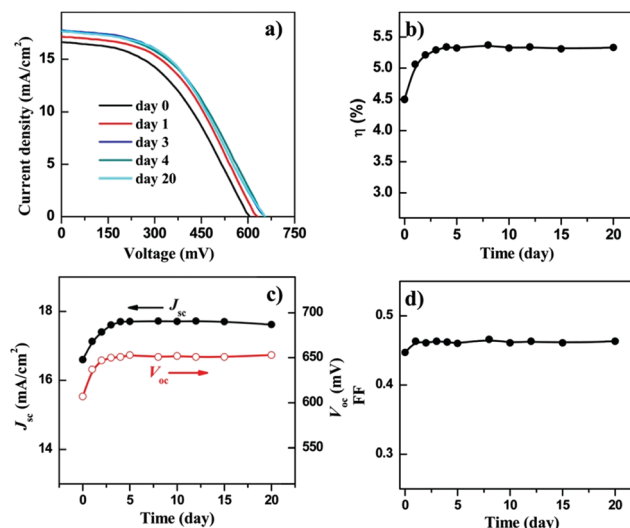


**Fig. 34** Temporal evolution of  $J$ - $V$  curves (a) and the photovoltaic parameter values,  $\eta$  (b),  $J_{sc}$ ,  $V_{oc}$  (c), and FF (d), for  $CdSeTe_{800}$  cells based on  $Cu_2S$  counter electrodes via the electrodeposition of Cu on FTO glass. Reprinted with permission from ref. 111. Copyright (2013) American Chemical Society.

significantly better than the single ZnS-coated one (Fig. 29d). They also demonstrated that a ZnS and metal hydroxide composite passivation layer favored the stability of QDSCs, benefiting from the better protection effect of the passivation layer for the QDs.<sup>473</sup>

Another factor that limits the stability of QDSCs is the nature of the CE catalytic materials used. To overcome the stability issue induced by brass-foil-based CEs, several groups developed novel CEs on an FTO substrate to improve the stability of the cell device.<sup>342,349,398,399,411,495</sup> For example, Meng's group prepared two kinds of composite CEs: PbS/carbon black and CuInS<sub>2</sub>/carbon black on an FTO substrate.<sup>398,399</sup> It was proposed that the framework of the carbon black used in the composite CE together with the PVDF binder provided good physical contact between the nanoparticles and the FTO substrate and therefore could improve the long-term stability of

the CE. The composite CE-based cells showed excellent stability over 1000 h without degradation under room light conditions (Fig. 35). It is noted that this was the longest reported period for the stability test for QDSCs. Wang *et al.* prepared hierarchical CuS/FTO CEs through a facile electrochemical deposition method, which exhibited excellent chemical and electrochemical stability in polysulfide electrolyte.<sup>342</sup> The corresponding QDSC device presented a high illumination and conservation stability for 2 and 240 h, respectively. Zhong *et al.* deposited a copper film on an FTO substrate through an electrodeposition method and then formed Cu<sub>2</sub>S/FTO CE by dipping the Cu/FTO into polysulfide solution.<sup>349</sup> The cell based on this Cu<sub>2</sub>S/FTO CE showed good stability over 10 h without degradation under continuous irradiation at 100 mW cm<sup>-2</sup> (Fig. 36). Gopi *et al.* prepared a NiS/PbS composite CE on FTO using a CBD technique and the PCE of the fabricated QDSC showed no degradation over 10 h under room light conditions.<sup>411</sup>

In addition to the above-mentioned methods to address the stability issue, another efficient way to improve the stability of QDSCs is by modification of the electrolyte.<sup>205,391,424–426,431,432,496</sup> As discussed above, the relatively high chemical activity of the polysulfide electrolyte leads to the corrosion of QDs, which therefore damages the stability of the resultant device. Hence, modification of the electrolyte by using additives to tune its chemical activity or the physical features is a potential way to improve the stability of QDSCs. Zhong's group adopted water-soluble polymers, such as poly(ethylene glycol) (PEG) and poly(vinyl pyrrolidone) (PVP), as additives in polysulfide electrolyte,<sup>205,424</sup> and found that both additives were favorable for the improvement of cell stability. Meng *et al.* reported a fumed SiO<sub>2</sub> nanoparticles-modified polysulfide electrolyte to improve the photovoltaic performance of QDSCs.<sup>425</sup> An improvement in the solar cell stability was achieved employing the SiO<sub>2</sub> NP-modified electrolyte, in which only a 6.3% drop in the PCE was found for a cell based on this modified electrolyte after 42 days of storage, whereas the PCE of the reference cell dropped by 23.3% during the same period. Similar results were also obtained by Zhong *et al.*, who used tetraethyl orthosilicate (TEOS) as an additive in polysulfide electrolyte to form a two-dimensional amorphous

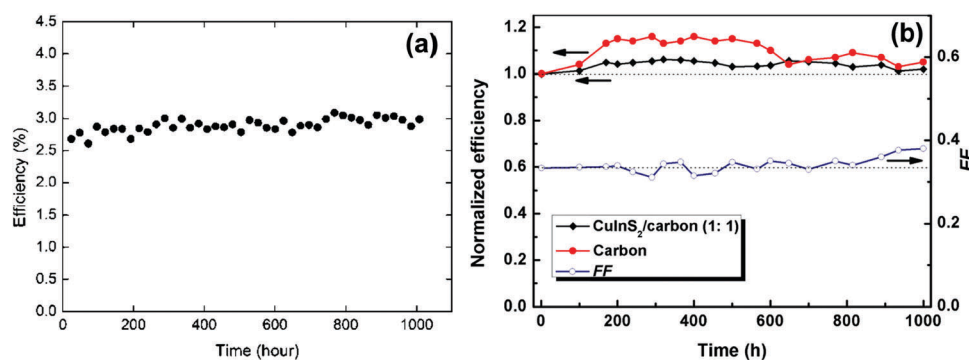


**Fig. 35** (a) Efficiency test of PbS/CB-composite CE-based sealed QDSCs over 1000 h. The cells were kept in room conditions and measured under AM 1.5 100 mW cm<sup>-2</sup> illumination every day. Reprinted with permission from ref. 398. Copyright (2012) American Chemical Society. (b) Normalized efficiency of CdS/CdSe QDSCs fabricated with a CuInS<sub>2</sub>/carbon composite (weight ratio 1:1) and carbon electrodes versus conservation time. Reprinted with permission from ref. 399. Copyright (2013) American Chemical Society.

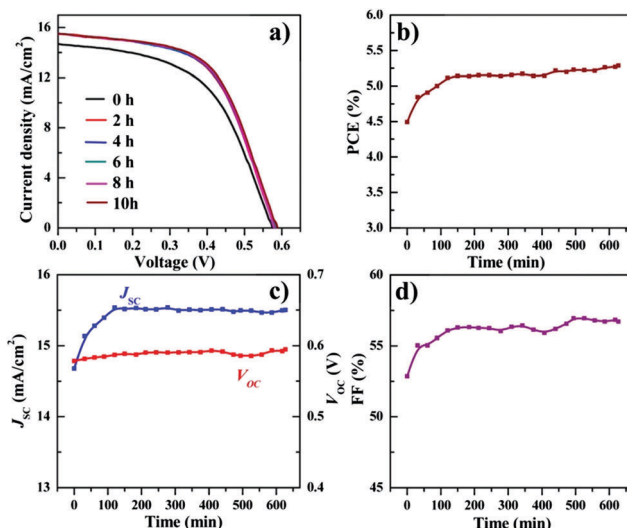


**Fig. 36** Temporal evolution of  $J$ - $V$  curves (a), PCE (b),  $J_{sc}$ ,  $V_{oc}$  (c), and FF (d) for the CdSe QDSCs based on Cu<sub>2</sub>S/FTO CE. The  $J$ - $V$  curves were tested under irradiation by an AM 1.5 G solar simulator at an intensity of 100 mW cm<sup>-2</sup>. Reprinted with permission from ref. 349. Copyright (2014) American Chemical Society.

SiO<sub>2</sub> film, showing a distinct improvement in the cell stability.<sup>391</sup> Besides, it is well known that liquid electrolytes suffer from the limitation of volatilization and leakage, thus seriously hampering the stability of the cell device. Therefore, the fabrication of solid-state or quasi-solid-state solar cells is another way to obtain highly stable QDSCs. For example, Meng *et al.* applied natural polysaccharide konjac glucomannan (KGM) as a polymer matrix to prepare a gel electrolyte, which significantly improved the cell stability.<sup>428</sup> Kim *et al.* also found an improvement in stability by using a poly(ethylene glycol) dimethyl-ether (PEGDME)-supported gel polysulfide electrolyte.<sup>497</sup> Zhong *et al.* used sodium polyacrylate (PAAS) and sodium carboxymethylcellulose (CMC-Na) as gelators to prepare quasi-solid-state gel electrolytes for QDSCs, and both of the gel electrolytes contributed to an improvement in the cell stability under continuous irradiation for 90 h (Fig. 37).<sup>426,432</sup>

On the whole, despite the stability of QDSCs being distinctly improved in recent years, it is still far from satisfactory for their practical application or in comparison with other kinds of emerging solar cells. Up to now, the best reported stability test result for QDSCs is 1000 h with the cells stored under room light conditions.<sup>398,399,425,428</sup> Issues about the long-term stability have been the main limitation for their industrial application. Even though a series of stability characterizations have been reported for QDSCs, they were conducted in non-standardized ways with incomparable data. Meanwhile, standard stability test conditions for QDSCs are still lacking. Although rigorous industrial standard stability measurement conditions for commercial photovoltaic panels were defined by the IEC 61646 protocol, the stability assessment of a novel solar panel with its own peculiarities might require an adjustment of the common standards.<sup>487</sup> Therefore, it is still a great challenge to realize recognized stability and test conditions for QDSCs in the future.

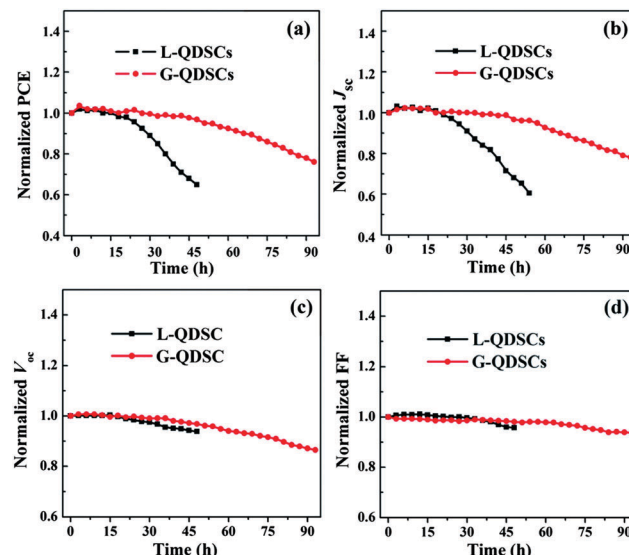


**Fig. 37** Normalized performance variation of liquid (L-QDSCs) and gel (G-QDSCs) electrolyte-based cells under successive irradiation by an AM 1.5 G solar simulator with an intensity of 100 mW cm<sup>-2</sup> under room conditions: (a) PCE; (b)  $J_{sc}$ ; (c)  $V_{oc}$ ; (d) FF. Reprinted with permission from ref. 426. Copyright (2016) Royal Society of Chemistry.

## 7. Summary and outlook

In recent years, QDSCs have emerged as attractive candidates for the third-generation solar cells. During the past five years, we have witnessed a fast improvement in the obtained record PCEs for QDSCs, arising both from material and technical advances. The record PCE is about 13% now, which is a competitive level relative to other kinds of emerging solar cells. This motivates us to further promote this kind of solar cells to a higher level aiming at commercial application. In this review article, we presented a comprehensive overview of the progress, fundamental principles, and main research areas in QDSCs. Finally, we now discuss possible future directions for this field of research with the aim toward developing highly efficient QDSCs.

To further promote the development of QDSCs, the PCE and stability of the cells together with the toxicity of various constituents should be taken into consideration simultaneously, and improved to a new satisfactory level. Accordingly, the authors believe that the following aspects deserve great attention in the future:

(a) Development of completely “green” QDSCs. For the real applications of a new kind of solar cell, it is a prerequisite that the whole device is environmentally friendly. As for QDSCs, the environmental concerns come from various constituents, such as the high toxicity from the Cd- or Pb-containing QD materials, the toxicity from the nanoscaled materials and from the polysulfide redox. Therefore, the “green” concept should be taken into account in the study of all the components of QDSCs. Concretely, Cd- and Pb-free I-III-VI group QDs such as CuInS<sub>2</sub> and CuInSe<sub>2</sub>, are wise choices as light-absorbing sensitizers in QDSCs. In fact, I-III-VI group QDs have been demonstrated to be capable of obtaining a higher efficiency in comparison with

Cd- and Pb-based QDs.<sup>115,222</sup> For the counter electrode, carbon materials may be a good choice due to their environmentally friendly nature, high catalytic activity, and low cost. From the safety point of view, QDSCs with an aqueous electrolyte are more promising for commercial applications in comparison with DSCs with an organic electrolyte.

(b) Exploration of more superior QD sensitizers. The development of QD sensitizers has contributed to the huge enhancement of the PCE of QDSCs in recent years. Nevertheless, there is still a great need to explore new types of QD sensitizers, possessing the characteristics of a suitable band edge position, wide absorption range, lower density of trap states, environmentally friendly nature, and low cost. Specifically, the construction of composite-structured I–III–VI group QDs through alloying or a core/shell strategy is a promising way to obtain high-quality and low-toxicity environmentally friendly QD light absorbers in QDSCs.

(c) Improvement of the loading amount of QDs on the TiO<sub>2</sub> substrate. The highest reported surface coverage ratio of QDs on the TiO<sub>2</sub> electrode is only about 34%.<sup>110</sup> This means that a large portion of the TiO<sub>2</sub> electrode surface is bare and uncovered. A further improvement of the QD-loading amount would not only improve the light-harvesting efficiency, but also inhibit charge recombination. The co-sensitization strategy using two or more kinds of QDs to sensitize the TiO<sub>2</sub> film electrode may be a good choice to further improve the QD-loading amount. In addition, the application of solvent engineering to reasonably tailor the polarity of the QD solution may also be helpful for enhancing the QD-loading amount on metal oxide film electrodes.

(d) Suppression of the charge-recombination processes. The severe charge recombination in QDSCs still constitutes one of the main factors limiting cell performance. There is thereby an urgent need, albeit still a significant challenge, to explore a facile and robust method to realize a powerful control of the charge-recombination processes, and therefore to significantly reduce the energy loss during the charge-transfer and -transport processes. Up to now, the surface-coating strategy has been commonly used to modify the interfaces and to inhibit charge-recombination processes. This coating treatment is mainly carried out through a sol-gel route, but it's difficult to obtain a compact film on the photoanode surface through the sol-gel approach, resulting in an incomplete passivation effect at interfaces. Therefore, other surface-treatment techniques, such as atomic layer deposition (ALD), may provide a more robust passivation layer and thereby could improve the photovoltaic performance further.

(e) Exploration of new kinds of electrolytes or HTMs. Up to now, the development of electrolytes in QDSCs is still lagging behind other advances, thus restricting the  $V_{oc}$  and PCE values of QDSCs. This has become a key bottleneck for the further development of QDSCs. It is believed that a breakthrough in electrolyte exploration will dramatically improve the photovoltaic performance of QDSCs. In this regard, we expect that the Co<sup>2+/3+</sup> complexes redox couple and p-type inorganic semiconductors, such as CuI, CuSCN, and perovskite materials, are promising candidates as electrolytes or HTMs in QDSCs.

(f) Realization of the long-term stability of devices. The current stability of QDSCs is still far from the standard needed for real applications. Further effort is required to improve the long-term stability of QDSCs. The improvement of the device sealing technique for liquid-junction QDSCs or the fabrication of all-inorganic-solid-state QDSCs possess potential to realize satisfactory long-term stability. Additionally, standard stability test conditions for QDSCs are also needed to reasonably evaluate the stability of a device.

(g) Utilization of related works and technology. Concerning the commercialization of this technology, QDSCs can take advantage of the developments made in this line by DSCs.<sup>498</sup> There should be no technical difficulty to upscale and fabricate large modules for QDSCs since their analog DSCs have succeeded in these fields. As for DSCs, long-term stability is the major issue for QDSCs. Unfortunately, as far as we know, there are no specific works focusing on the life-cycle assessment of QDSCs to evaluate the cost and the environmental impacts produced by the upscaling of this technology in order to determine the main limiting factors in terms of cost, technology, toxicity, or stability, and this lack needs to be solved in the future.

The fascinating advantages combined with the fast evolution of QDSCs render them promising candidates for the next-generation solar cells. We are confident that with further breakthroughs in materials exploration and in device structure optimization, QDSC with a PCE of over 15% will be obtained in the near future.

## Conflicts of interest

There are no conflicts of interest to declare.

## Acknowledgements

This research is supported by the National Natural Science Foundation of China (No. 51732004, 21703071, 91433106) and the MINECO of Spain (MAT2016-76892-C3-1-R).

## References

- 1 R. E. Smalley, *Abstr. Pap. Am. Chem. Soc.*, 2003, **226**, U24.
- 2 O. Morton, *Nature*, 2006, **443**, 19–22.
- 3 N. S. Lewis and D. G. Nocera, *Proc. Natl. Acad. Sci. U. S. A.*, 2006, **103**, 15729–15735.
- 4 A. Hagfeldt, G. Boschloo, L. Sun, L. Kloo and H. Pettersson, *Chem. Rev.*, 2010, **110**, 6595–6663.
- 5 D. Chapin, C. Fuller and G. Pearson, *J. Appl. Phys.*, 1954, **25**, 676.
- 6 J. Wu, Z. Lan, J. Lin, M. Huang, Y. Huang, L. Fan and G. Luo, *Chem. Rev.*, 2015, **115**, 2136–2173.
- 7 J. Wu, Z. Lan, J. Lin, M. Huang, Y. Huang, L. Fan, G. Luo, Y. Lin, Y. Xie and Y. Wei, *Chem. Soc. Rev.*, 2017, **46**, 5975–6023.
- 8 C. Battaglia, A. Cuevas and S. De Wolf, *Energy Environ. Sci.*, 2016, **9**, 1552–1576.

- 9 T. Saga, *NPG Asia Mater.*, 2010, **2**, 96–102.
- 10 J. K. Rath, *Sol. Energy Mater. Sol. Cells*, 2003, **76**, 431–487.
- 11 P. Jackson, D. Hariskos, E. Lotter, S. Paetel, R. Wuerz, R. Menner, W. Wischmann and M. Powalla, *Prog. Photovoltaics*, 2011, **19**, 894–897.
- 12 K. Nakayama, K. Tanabe and H. A. Atwater, *Appl. Phys. Lett.*, 2008, **93**, 121904.
- 13 F. Dimroth, M. Grave, P. Beutel, U. Fiedeler, C. Karcher, T. N. D. Tibbits, E. Oliva, G. Siefer, M. Schachtner, A. Wekkeli, A. W. Bett, R. Krause, M. Piccin, N. Blanc, C. Drazen, E. Guiot, B. Ghyselen, T. Salvatet, A. Tauzin, T. Signamarcheix, A. Dobrich, T. Hannappel and K. Schwarzburg, *Prog. Photovoltaics*, 2014, **22**, 277–282.
- 14 A. Romeo, A. Terheggen, D. Abou-Ras, D. L. Batzner, F. J. Haug, M. Kalin, D. Rudmann and A. N. Tiwari, *Prog. Photovoltaics*, 2004, **12**, 93–111.
- 15 X. Z. Wu, *Sol. Energy*, 2004, **77**, 803–814.
- 16 M. Grätzel, *Acc. Chem. Res.*, 2009, **42**, 1788–1798.
- 17 Y.-J. Cheng, S.-H. Yang and C.-S. Hsu, *Chem. Rev.*, 2009, **109**, 5868–5923.
- 18 S. Guenes, H. Neugebauer and N. S. Sariciftci, *Chem. Rev.*, 2007, **107**, 1324–1338.
- 19 G. H. Carey, A. L. Abdelhady, Z. Ning, S. M. Thon, O. M. Bakr and E. H. Sargent, *Chem. Rev.*, 2015, **115**, 12732–12763.
- 20 A. J. Nozik, M. C. Beard, J. M. Luther, M. Law, R. J. Ellingson and J. C. Johnson, *Chem. Rev.*, 2010, **110**, 6873–6890.
- 21 A. Kojima, K. Teshima, Y. Shirai and T. Miyasaka, *J. Am. Chem. Soc.*, 2009, **131**, 6050–6051.
- 22 G. Hodes, *Science*, 2013, **342**, 317–318.
- 23 M. M. Lee, J. Teuscher, T. Miyasaka, T. N. Murakami and H. J. Snaith, *Science*, 2012, **338**, 643–647.
- 24 M. Kouhnnavard, S. Ikeda, N. A. Ludin, N. B. Ahmad Khairudin, B. V. Ghaffari, M. A. Mat-Teridi, M. A. Ibrahim, S. Sepeai and K. Sopian, *Renewable Sustainable Energy Rev.*, 2014, **37**, 397–407.
- 25 I. J. Kramer and E. H. Sargent, *ACS Nano*, 2011, **5**, 8506–8514.
- 26 P. V. Kamat, K. Tvrdy, D. R. Baker and J. G. Radich, *Chem. Rev.*, 2010, **110**, 6664–6688.
- 27 I. J. Kramer and E. H. Sargent, *Chem. Rev.*, 2014, **114**, 863–882.
- 28 O. E. Semionin, J. M. Luther, S. Choi, H.-Y. Chen, J. Gao, A. J. Nozik and M. C. Beard, *Science*, 2011, **334**, 1530–1533.
- 29 M. R. Kim and D. Ma, *J. Phys. Chem. Lett.*, 2015, **6**, 85–99.
- 30 S. Ruhle, M. Shalom and A. Zaban, *ChemPhysChem*, 2010, **11**, 2290–2304.
- 31 S. Emin, S. P. Singh, L. Han, N. Satoh and A. Islam, *Sol. Energy*, 2011, **85**, 1264–1282.
- 32 P. V. Kamat, *Acc. Chem. Res.*, 2012, **45**, 1906–1915.
- 33 I. Mora-Sero, S. Gimenez, F. Fabregat-Santiago, R. Gomez, Q. Shen, T. Toyoda and J. Bisquert, *Acc. Chem. Res.*, 2009, **42**, 1848–1857.
- 34 J. Duan, H. Zhang, Q. Tang, B. He and L. Yu, *J. Mater. Chem. A*, 2015, **3**, 17497–17510.
- 35 P. V. Kamat, *J. Phys. Chem. Lett.*, 2013, **4**, 908–918.
- 36 W. Li and X. Zhong, *J. Phys. Chem. Lett.*, 2015, **6**, 796–806.
- 37 I. Mora-Sero and J. Bisquert, *J. Phys. Chem. Lett.*, 2010, **1**, 3046–3052.
- 38 K. Zhao, Z. Pan and X. Zhong, *J. Phys. Chem. Lett.*, 2016, **7**, 406–417.
- 39 P. V. Kamat, J. A. Christians and J. G. Radich, *Langmuir*, 2014, **30**, 5716–5725.
- 40 J.-K. Sun, Y. Jiang, X. Zhong, J.-S. Hu and L.-J. Wan, *Nano Energy*, 2017, **32**, 130–156.
- 41 S. Kumar, M. Nehra, A. Deep, D. Kedia, N. Dilbaghi and K.-H. Kim, *Renewable Sustainable Energy Rev.*, 2017, **73**, 821–839.
- 42 M. Ye, X. Gao, X. Hong, Q. Liu, C. He, X. Liu and C. Lin, *Sustainable Energy Fuels*, 2017, **1**, 1217–1231.
- 43 G. Hodes, *J. Phys. Chem. C*, 2008, **112**, 17778–17787.
- 44 D. F. Watson, *J. Phys. Chem. Lett.*, 2010, **1**, 2299–2309.
- 45 Z. Yang, C. Y. Chen, P. Roy and H. T. Chang, *Chem. Commun.*, 2011, **47**, 9561–9571.
- 46 I. Hod and A. Zaban, *Langmuir*, 2014, **30**, 7264–7273.
- 47 J. Xu, Z. Chen, J. A. Zapien, C. S. Lee and W. Zhang, *Adv. Mater.*, 2014, **26**, 5337–5367.
- 48 I. Hwang and K. Yong, *ChemElectroChem*, 2015, **2**, 634–653.
- 49 K. Meng, G. Chen and K. R. Thampi, *J. Mater. Chem. A*, 2015, **3**, 23074–23089.
- 50 J. Tian and G. Cao, *J. Phys. Chem. Lett.*, 2015, **6**, 1859–1869.
- 51 M. Wu, X. Lin, Y. Wang and T. Ma, *J. Mater. Chem. A*, 2015, **3**, 19638–19656.
- 52 C. Shen, D. Fichou and Q. Wang, *Chem. – Asian J.*, 2016, **11**, 1183–1193.
- 53 R. Xia, S.-M. Wang, W.-W. Dong and X.-D. Fang, *Acta Phys.-Chim. Sin.*, 2017, **33**, 670–690.
- 54 H. Gerischer, M. E. Michel-Beyerle, F. Rebentrost and H. Tributsch, *Electrochim. Acta*, 1968, **13**, 1509–1515.
- 55 K. Kalyanasundaram, *Sol. Cells*, 1985, **15**, 93–156.
- 56 B. O'Regan and M. Grätzel, *Nature*, 1991, **353**, 737–740.
- 57 P. Wang, S. M. Zakeeruddin, J. E. Moser, M. K. Nazeeruddin, T. Sekiguchi and M. Grätzel, *Nat. Mater.*, 2003, **2**, 402–407.
- 58 M. Law, L. E. Greene, J. C. Johnson, R. Saykally and P. D. Yang, *Nat. Mater.*, 2005, **4**, 455–459.
- 59 X. Wang, L. Zhi and K. Müllen, *Nano Lett.*, 2008, **8**, 323–327.
- 60 A. Mishra, M. K. R. Fischer and P. Baeuerle, *Angew. Chem., Int. Ed.*, 2009, **48**, 2474–2499.
- 61 A. Yella, H.-W. Lee, H. N. Tsao, C. Yi, A. K. Chandiran, M. K. Nazeeruddin, E. W.-G. Diau, C.-Y. Yeh, S. M. Zakeeruddin and M. Grätzel, *Science*, 2011, **334**, 629–634.
- 62 S. Mathew, A. Yella, P. Gao, R. Humphry-Baker, B. F. E. Curchod, N. Ashari-Astani, I. Tavernelli, U. Rothlisberger, M. K. Nazeeruddin and M. Grätzel, *Nat. Chem.*, 2014, **6**, 242–247.
- 63 J. Bisquert, *The Physics of Solar Cells: Perovskites, Organics, and Photovoltaic Fundamentals*, CRC Press, Boca Raton, 2017.
- 64 P. V. Kamat, *J. Phys. Chem. C*, 2008, **112**, 18737–18753.
- 65 M. Pazoki, U. B. Cappel, E. M. J. Johansson, A. Hagfeldt and G. Boschloo, *Energy Environ. Sci.*, 2017, **10**, 672–709.

- 66 F. Fabregat-Santiago, G. Garcia-Belmonte, I. Mora-Sero and J. Bisquert, *Phys. Chem. Chem. Phys.*, 2011, **13**, 9083–9118.
- 67 K. Zheng, K. Zidek, M. Abdellah, P. Chabera, M. S. Abd El-Sadek and T. Pullerits, *Appl. Phys. Lett.*, 2013, **102**, 163119.
- 68 K. Zidek, K. Zheng, P. Chabera, M. Abdellah and T. Pullerits, *Appl. Phys. Lett.*, 2012, **100**, 243111.
- 69 K. Zidek, K. Zheng, C. S. Ponceca, Jr., M. E. Messing, L. R. Wallenberg, P. Chabera, M. Abdellah, V. Sundstrom and T. Pullerits, *J. Am. Chem. Soc.*, 2012, **134**, 12110–12117.
- 70 M. Abdellah, R. Marschan, K. Zidek, M. E. Messing, A. Abdelwahab, P. Chabera, K. Zheng and T. Pullerits, *J. Phys. Chem. C*, 2014, **118**, 25802–25808.
- 71 K. Zheng, K. Zidek, M. Abdellah, W. Zhang, P. Chabera, N. Lenngren, A. Yartsev and T. Pullerits, *J. Phys. Chem. C*, 2014, **118**, 18462–18471.
- 72 K. Zidek, K. Zheng, M. Abdellah, N. Lenngren, P. Chabera and T. Pullerits, *Nano Lett.*, 2012, **12**, 6393–6399.
- 73 A. Kongkanand, K. Tvrdy, K. Takechi, M. Kuno and P. V. Kamat, *J. Am. Chem. Soc.*, 2008, **130**, 4007–4015.
- 74 J. Wang, I. Mora-Sero, Z. Pan, K. Zhao, H. Zhang, Y. Feng, G. Yang, X. Zhong and J. Bisquert, *J. Am. Chem. Soc.*, 2013, **135**, 15913–15922.
- 75 V. Chakrapani, D. Baker and P. V. Kamat, *J. Am. Chem. Soc.*, 2011, **133**, 9607–9615.
- 76 K. Tvrdy, P. A. Frantsuzov and P. V. Kamat, *Proc. Natl. Acad. Sci. U. S. A.*, 2011, **108**, 29–34.
- 77 P. K. Santra, P. V. Nair, K. G. Thomas and P. V. Kamat, *J. Phys. Chem. Lett.*, 2013, **4**, 722–729.
- 78 H. McDaniel, N. Fuke, N. S. Makarov, J. M. Pietryga and V. I. Klimov, *Nat. Commun.*, 2013, **4**, 2887.
- 79 H. McDaniel, N. Fuke, J. M. Pietryga and V. I. Klimov, *J. Phys. Chem. Lett.*, 2013, **4**, 355–361.
- 80 D. R. Pernik, K. Tvrdy, J. G. Radich and P. V. Kamat, *J. Phys. Chem. C*, 2011, **115**, 13511–13519.
- 81 V. Gonzalez-Pedro, X. Xu, I. Mora-Sero and J. Bisquert, *ACS Nano*, 2010, **4**, 5783–5790.
- 82 A. Zaban, M. Greenshtein and J. Bisquert, *ChemPhysChem*, 2003, **4**, 859–864.
- 83 J. Bisquert, F. Fabregat-Santiago, I. Mora-Sero, G. Garcia-Belmonte and S. Gimenez, *J. Phys. Chem. C*, 2009, **113**, 17278–17290.
- 84 J. Fan, L. Li, H.-S. Rao, Q.-L. Yang, J. Zhang, H.-Y. Chen, L. Chen, D.-B. Kuang and C.-Y. Su, *J. Mater. Chem. A*, 2014, **2**, 15406–15413.
- 85 S. Jiao, Q. Shen, I. Mora-Sero, J. Wang, Z. Pan, K. Zhao, Y. Kuga, X. Zhong and J. Bisquert, *ACS Nano*, 2015, **9**, 908–915.
- 86 A. Salant, M. Shalom, Z. Tachan, S. Buhbut, A. Zaban and U. Banin, *Nano Lett.*, 2012, **12**, 2095–2100.
- 87 N. Serpone, E. Borgarello and M. Grätzel, *J. Chem. Soc., Chem. Commun.*, 1984, **0**, 342–344.
- 88 H. Gerischer and M. Lubke, *J. Electroanal. Chem.*, 1986, **204**, 225–227.
- 89 L. Spanhel, H. Weller and A. Henglein, *J. Am. Chem. Soc.*, 1987, **109**, 6632–6635.
- 90 K. R. Gopidas, M. Bohorquez and P. V. Kamat, *J. Phys. Chem.*, 1990, **94**, 6435–6440.
- 91 R. Vogel, K. Pohl and H. Weller, *Chem. Phys. Lett.*, 1990, **174**, 241–246.
- 92 S. Kohtani, A. Kudo and T. Sakata, *Chem. Phys. Lett.*, 1993, **206**, 166–170.
- 93 D. Liu and P. V. Kamat, *J. Phys. Chem.*, 1993, **97**, 10769–10773.
- 94 R. Vogel, P. Hoyer and H. Weller, *J. Phys. Chem.*, 1994, **98**, 3183–3188.
- 95 A. Zaban, O. I. Micic, B. A. Gregg and A. J. Nozik, *Langmuir*, 1998, **14**, 3153–3156.
- 96 P. Yu, K. Zhu, A. G. Norman, S. Ferrere, A. J. Frank and A. J. Nozik, *J. Phys. Chem. B*, 2006, **110**, 25451–25454.
- 97 R. Plass, S. Pelet, J. Krueger, M. Grätzel and U. Bach, *J. Phys. Chem. B*, 2002, **106**, 7578–7580.
- 98 A. J. Nozik, *Phys. E*, 2002, **14**, 115–120.
- 99 L. J. Diguna, Q. Shen, J. Kobayashi and T. Toyoda, *Appl. Phys. Lett.*, 2007, **91**, 023116.
- 100 Y.-L. Lee, B.-M. Huang and H.-T. Chien, *Chem. Mater.*, 2008, **20**, 6903–6905.
- 101 Y.-L. Lee and Y.-S. Lo, *Adv. Funct. Mater.*, 2009, **19**, 604–609.
- 102 H. Lee, M. Wang, P. Chen, D. R. Gamelin, S. M. Zakeeruddin, M. Grätzel and M. K. Nazeeruddin, *Nano Lett.*, 2009, **9**, 4221–4227.
- 103 S.-Q. Fan, B. Fang, J. H. Kim, B. Jeong, C. Kim, J.-S. Yu and J. Ko, *Langmuir*, 2010, **26**, 13644–13649.
- 104 B. Fang, M. Kim, S.-Q. Fan, J. H. Kim, D. P. Wilkinson, J. Ko and J.-S. Yu, *J. Mater. Chem.*, 2011, **21**, 8742–8748.
- 105 J. Xu, X. Yang, H. Wang, X. Chen, C. Luan, Z. Xu, Z. Lu, V. A. Roy, W. Zhang and C. S. Lee, *Nano Lett.*, 2011, **11**, 4138–4143.
- 106 Q. Zhang, X. Guo, X. Huang, S. Huang, D. Li, Y. Luo, Q. Shen, T. Toyoda and Q. Meng, *Phys. Chem. Chem. Phys.*, 2011, **13**, 4659–4667.
- 107 P. K. Santra and P. V. Kamat, *J. Am. Chem. Soc.*, 2012, **134**, 2508–2511.
- 108 E. Martinez-Ferrero, I. M. Sero, J. Albero, S. Gimenez, J. Bisquert and E. Palomares, *Phys. Chem. Chem. Phys.*, 2010, **12**, 2819–2821.
- 109 Z. Pan, H. Zhang, K. Cheng, Y. Hou, J. Hua and X. Zhong, *ACS Nano*, 2012, **6**, 3982–3991.
- 110 H. Zhang, K. Cheng, Y. M. Hou, Z. Fang, Z. X. Pan, W. J. Wu, J. L. Hua and X. H. Zhong, *Chem. Commun.*, 2012, **48**, 11235–11237.
- 111 Z. Pan, K. Zhao, J. Wang, H. Zhang, Y. Feng and X. Zhong, *ACS Nano*, 2013, **7**, 5215–5222.
- 112 W. Wang, W. Feng, J. Du, W. Xue, L. Zhang, L. Zhao, Y. Li and X. Zhong, *Adv. Mater.*, 2018, **30**, 1705746.
- 113 Z. Ren, J. Wang, Z. Pan, K. Zhao, H. Zhang, Y. Li, Y. Zhao, I. Mora-Sero, J. Bisquert and X. Zhong, *Chem. Mater.*, 2015, **27**, 8398–8405.
- 114 Z. Ren, Z. Wang, R. Wang, Z. Pan, X. Gong and X. Zhong, *Chem. Mater.*, 2016, **28**, 2323–2330.
- 115 J. Du, Z. Du, J. S. Hu, Z. Pan, Q. Shen, J. Sun, D. Long, H. Dong, L. Sun, X. Zhong and L. J. Wan, *J. Am. Chem. Soc.*, 2016, **138**, 4201–4209.

- 116 Z. Pan, I. Mora-Sero, Q. Shen, H. Zhang, Y. Li, K. Zhao, J. Wang, X. Zhong and J. Bisquert, *J. Am. Chem. Soc.*, 2014, **136**, 9203–9210.
- 117 K. Zhao, Z. Pan, I. Mora-Sero, E. Canovas, H. Wang, Y. Song, X. Gong, J. Wang, M. Bonn, J. Bisquert and X. Zhong, *J. Am. Chem. Soc.*, 2015, **137**, 5602–5609.
- 118 Z. Du, Z. Pan, F. Fabregat-Santiago, K. Zhao, D. Long, H. Zhang, Y. Zhao, X. Zhong, J. S. Yu and J. Bisquert, *J. Phys. Chem. Lett.*, 2016, **7**, 3103–3111.
- 119 S. Jiao, J. Du, Z. Du, D. Long, W. Jiang, Z. Pan, Y. Li and X. Zhong, *J. Phys. Chem. Lett.*, 2017, **8**, 559–564.
- 120 Y. Bai, I. Mora-Sero, F. De Angelis, J. Bisquert and P. Wang, *Chem. Rev.*, 2014, **114**, 10095–10130.
- 121 J. Zhang, J. H. Bang, C. Tang and P. V. Kamat, *ACS Nano*, 2010, **4**, 387–395.
- 122 Q. Shen, A. Yamada, S. Tamura and T. Toyoda, *Appl. Phys. Lett.*, 2010, **97**, 123107.
- 123 H. Han, P. Sudhagar, T. Song, Y. Jeon, I. Mora-Sero, F. Fabregat-Santiago, J. Bisquert, Y. S. Kang and U. Paik, *Chem. Commun.*, 2013, **49**, 2810–2812.
- 124 J. Zhang, C. Tang and J. H. Bang, *Electrochim. Commun.*, 2010, **12**, 1124–1128.
- 125 B. Liu, Y. Sun, X. Wang, L. Zhang, D. Wang, Z. Fu, Y. Lin and T. Xie, *J. Mater. Chem. A*, 2015, **3**, 4445–4452.
- 126 C. Dong, X. Li and J. Qi, *J. Phys. Chem. C*, 2011, **115**, 20307–20315.
- 127 L. Tao, Y. Xiong, H. Liu and W. Shen, *Nanoscale*, 2014, **6**, 931–938.
- 128 S. Huang, Q. Zhang, X. Huang, X. Guo, M. Deng, D. Li, Y. Luo, Q. Shen, T. Toyoda and Q. Meng, *Nanotechnology*, 2010, **21**, 375201.
- 129 W. Lee, S. H. Kang, J.-Y. Kim, G. B. Kolekar, Y.-E. Sung and S.-H. Han, *Nanotechnology*, 2009, **20**, 335706.
- 130 M. Akimoto, T. Toyoda, T. Okuno, S. Hayase and Q. Shen, *Thin Solid Films*, 2015, **590**, 90–97.
- 131 H. Huang, L. Pan, C. K. Lim, H. Gong, J. Guo, M. S. Tse and O. K. Tan, *Small*, 2013, **9**, 3153–3160.
- 132 L. Yu, Z. Li, Y. Liu, F. Cheng and S. Sun, *Appl. Surf. Sci.*, 2014, **309**, 255–262.
- 133 Z. Zhang, C. Shi, J. Chen, G. Xiao and L. Li, *Appl. Surf. Sci.*, 2017, **410**, 8–13.
- 134 Z. Zhang, C. Shi, G. Xiao, K. Lv, C. Ma and J. Yue, *Ceram. Int.*, 2017, **43**, 10052–10056.
- 135 Y. Chen, Q. Tao, W. Fu, H. Yang, X. Zhou, S. Su, D. Ding, Y. Mu, X. Li and M. Li, *Chem. Commun.*, 2014, **50**, 9509–9512.
- 136 C. Chen, M. Ye, M. Lv, C. Gong, W. Guo and C. Lin, *Electrochim. Acta*, 2014, **121**, 175–182.
- 137 R. Zhou, Y. Huang, L. Wan, H. Niu, F. Ji and J. Xu, *J. Alloys Compd.*, 2017, **716**, 162–170.
- 138 C. Wang, Z. Jiang, L. Wei, Y. Chen, J. Jiao, M. Eastman and H. Liu, *Nano Energy*, 2012, **1**, 440–447.
- 139 J. Wan, R. Liu, Y. Tong, S. Chen, Y. Hu, B. Wang, Y. Xu and H. Wang, *Nanoscale Res. Lett.*, 2016, **11**, 12.
- 140 W. Zhang, X. Zeng, H. Wang, R. Fang, Y. Xu, Y. Zhang and W. Chen, *RSC Adv.*, 2016, **6**, 33713–33722.
- 141 Z. Peng, Y. Liu, Y. Zhao, K. Chen, Y. Cheng and W. Chen, *Electrochim. Acta*, 2014, **135**, 276–283.
- 142 L. Yu, X. Ren, Z. Yang, Y. Han and Z. Li, *J. Mater. Sci.: Mater. Electron.*, 2016, **27**, 7150–7160.
- 143 A. Fatehmulla, M. A. Manthrammel, W. A. Farooq, S. M. Ali and M. Atif, *J. Nanomater.*, 2015, 358063.
- 144 H.-S. Rao, W.-Q. Wu, Y. Liu, Y.-F. Xu, B.-X. Chen, H.-Y. Chen, D.-B. Kuang and C.-Y. Su, *Nano Energy*, 2014, **8**, 1–8.
- 145 Y.-F. Xu, W.-Q. Wu, H.-S. Rao, H.-Y. Chen, D.-B. Kuang and C.-Y. Su, *Nano Energy*, 2015, **11**, 621–630.
- 146 D. R. Baker and P. V. Kamat, *Adv. Funct. Mater.*, 2009, **19**, 805–811.
- 147 Z. Zhang, C. Shi, J. Chen, G. Xiao and L. Li, *Appl. Surf. Sci.*, 2017, **410**, 8–13.
- 148 H. Zhou, L. Li, D. Jiang, Y. Lu and K. Pan, *RSC Adv.*, 2016, **6**, 67968–67975.
- 149 C. Li, L. Yang, J. Xiao, Y.-C. Wu, M. Sondergaard, Y. Luo, D. Li, Q. Meng and B. B. Iversen, *Phys. Chem. Chem. Phys.*, 2013, **15**, 8710–8715.
- 150 J. Xu, X. Yang, Q.-D. Yang, T.-L. Wong, S.-T. Lee, W.-J. Zhang and C.-S. Lee, *J. Mater. Chem.*, 2012, **22**, 13374–13379.
- 151 D. Wu, X. Wang, K. Cao, Y. An, X. Song, N. Liu, F. Xu, Z. Gao and K. Jiang, *Electrochim. Acta*, 2017, **231**, 1–12.
- 152 K. Yan, L. Zhang, J. Qiu, Y. Qiu, Z. Zhu, J. Wang and S. Yang, *J. Am. Chem. Soc.*, 2013, **135**, 9531–9539.
- 153 J. Xiao, Q. Huang, J. Xu, C. Li, G. Chen, Y. Luo, D. Li and Q. Meng, *J. Phys. Chem. C*, 2014, **118**, 4007–4015.
- 154 M. Raissi, Y. Pellegrin, S. Jobic, M. Boujtita and F. Odobel, *Sci. Rep.*, 2016, **6**, 24908.
- 155 H.-M. Cheng, K.-Y. Huang, K.-M. Lee, P. Yu, S.-C. Lin, J.-H. Huang, C.-G. Wu and J. Tang, *Phys. Chem. Chem. Phys.*, 2012, **14**, 13539–13548.
- 156 C. J. Raj, S. N. Karthick, K. V. Hemalatha, H.-J. Kim and K. Prabakar, *Thin Solid Films*, 2013, **548**, 636–640.
- 157 J. Deng, M. Wang, C. Yang, J. Liu and X. Song, *RSC Adv.*, 2014, **4**, 41141–41147.
- 158 F. S. Ghoreishi, V. Ahmadi and M. Samadpour, *J. Power Sources*, 2014, **271**, 195–202.
- 159 M.-S. Jeong, M.-K. Son, S.-K. Kim, S. Park, K. Prabakar and H.-J. Kim, *Thin Solid Films*, 2014, **570**, 310–314.
- 160 D. Karageorgopoulos, E. Stathatos and E. Vitoratos, *J. Power Sources*, 2012, **219**, 9–15.
- 161 J. Tian, Q. Zhang, E. Uchaker, R. Gao, X. Qu, S. Zhang and G. Cao, *Energy Environ. Sci.*, 2013, **6**, 3542–3547.
- 162 J. Tian, L. Lv, X. Wang, C. Fei, X. Liu, Z. Zhao, Y. Wang and G. Cao, *J. Phys. Chem. C*, 2014, **118**, 16611–16617.
- 163 K. S. Leschkies, R. Divakar, J. Basu, E. Enache-Pommer, J. E. Boercker, C. B. Carter, U. R. Kortshagen, D. J. Norris and E. S. Aydil, *Nano Lett.*, 2007, **7**, 1793–1798.
- 164 M. Seol, E. Ramasamy, J. Lee and K. Yong, *J. Phys. Chem. C*, 2011, **115**, 22018–22024.
- 165 P. Sudhagar, T. Song, D. H. Lee, I. Mora-Sero, J. Bisquert, M. Laudenslager, W. M. Sigmund, W. I. Park, U. Paik and Y. S. Kang, *J. Phys. Chem. Lett.*, 2011, **2**, 1984–1990.

- 166 H. Chen, L. Zhu, H. Liu and W. Li, *Nanotechnology*, 2012, **23**, 075402.
- 167 R. Zhang, Q.-P. Luo, H.-Y. Chen, X.-Y. Yu, D.-B. Kuang and C.-Y. Su, *ChemPhysChem*, 2012, **13**, 1435–1439.
- 168 C.-Y. Chou, C.-T. Li, C.-P. Lee, L.-Y. Lin, M.-H. Yeh, R. Vittal and K.-C. Ho, *Electrochim. Acta*, 2013, **88**, 35–43.
- 169 I. Hwang and K. Yong, *ChemPhysChem*, 2013, **14**, 364–368.
- 170 H. Kim, H. Jeong, T. K. An, C. E. Park and K. Yong, *ACS Appl. Mater. Interfaces*, 2013, **5**, 268–275.
- 171 X. Yin, W. Que, D. Fei, H. Xie and Z. He, *Electrochim. Acta*, 2013, **99**, 204–210.
- 172 X. Yin, W. Que, D. Fei, H. Xie, Z. He and G. Wang, *Electrochim. Acta*, 2013, **89**, 561–570.
- 173 M.-L. Zhang, F. Jin, M.-L. Zheng, J. Liu, Z.-S. Zhao and X.-M. Duan, *RSC Adv.*, 2014, **4**, 10462–10466.
- 174 W. Lee, S. Kang, T. Hwang, K. Kim, H. Woo, B. Lee, J. Kim, J. Kim and B. Park, *Electrochim. Acta*, 2015, **167**, 194–200.
- 175 M. Seol, H. Kim, Y. Tak and K. Yong, *Chem. Commun.*, 2010, **46**, 5521–5523.
- 176 H. Chen, W. Li, Q. Hou, H. Liu and L. Zhu, *Electrochim. Acta*, 2011, **56**, 8358–8364.
- 177 J. Chen, W. Lei, C. Li, Y. Zhang, Y. Cui, B. Wang and W. Deng, *Phys. Chem. Chem. Phys.*, 2011, **13**, 13182–13184.
- 178 J. Chen, C. Li, G. Eda, Y. Zhang, W. Lei, M. Chhowalla, W. I. Milne and W.-Q. Deng, *Chem. Commun.*, 2011, **47**, 6084–6086.
- 179 C.-Z. Yao, B.-H. Wei, L.-X. Meng, H. Li, Q.-J. Gong, H. Sun, H.-X. Ma and X.-H. Hu, *J. Power Sources*, 2012, **207**, 222–228.
- 180 L.-B. Li, Y.-F. Wang, H.-S. Rao, W.-Q. Wu, K.-N. Li, C.-Y. Su and D.-B. Kuang, *ACS Appl. Mater. Interfaces*, 2013, **5**, 11865–11871.
- 181 J. Tian, Q. Zhang, E. Uchaker, Z. Liang, R. Gao, X. Qu, S. Zhang and G. Cao, *J. Mater. Chem. A*, 2013, **1**, 6770–6775.
- 182 C. J. Raj, S. N. Karthick, S. Park, K. V. Hemalatha, S.-K. Kim, K. Prabakar and H.-J. Kim, *J. Power Sources*, 2014, **248**, 439–446.
- 183 J. Tian, E. Uchaker, Q. Zhang and G. Cao, *ACS Appl. Mater. Interfaces*, 2014, **6**, 4466–4472.
- 184 C. V. V. M. Gopi, M. Venkata-Haritha, Y.-S. Lee and H.-J. Kim, *J. Mater. Chem. A*, 2016, **4**, 8161–8171.
- 185 J. Hou, H. Zhao, F. Huang, Q. Jing, H. Cao, Q. Wu, S. Peng and G. Cao, *J. Power Sources*, 2016, **325**, 438–445.
- 186 C. V. V. M. Gopi, M. Venkata-Haritha, Y.-S. Lee and H.-J. Kim, *J. Mater. Chem. A*, 2017, **5**, 428–429.
- 187 Z. Zhu, J. Qiu, K. Yan and S. Yang, *ACS Appl. Mater. Interfaces*, 2013, **5**, 4000–4005.
- 188 K. Yan, L. Zhang, J. Qiu, Y. Qiu, Z. Zhu, J. Wang and S. Yang, *J. Am. Chem. Soc.*, 2013, **135**, 9531–9539.
- 189 V. Ganapathy, E.-H. Kong, Y.-C. Park, H. M. Jang and S.-W. Rhee, *Nanoscale*, 2014, **6**, 3296–3301.
- 190 S. Greenwald, S. Ruhle, M. Shalom, S. Yahav and A. Zaban, *Phys. Chem. Chem. Phys.*, 2011, **13**, 19302–19306.
- 191 A. Pimachev, U. Poudyal, V. Proshchenko, W. Wang and Y. Dahnovsky, *Phys. Chem. Chem. Phys.*, 2016, **18**, 26771–26776.
- 192 J. G. Radich, N. R. Peebles, P. K. Santra and P. V. Kamat, *J. Phys. Chem. C*, 2014, **118**, 16463–16471.
- 193 J. Park, M. T. Sajjad, P.-H. Jounneau, A. Ruseckas, J. Faure-Vincent, I. D. W. Samuel, P. Reiss and D. Aldakov, *J. Mater. Chem. A*, 2016, **4**, 827–837.
- 194 M. T. Sajjad, J. Park, D. Gaboriau, J. R. Harwell, F. Odobel, P. Reiss, I. D. W. Samuel and D. Aldakov, *J. Phys. Chem. C*, 2018, **122**, 5161–5170.
- 195 M. Raissi, M. T. Sajjad, Y. Pellegrin, T. J. Roland, S. Jobic, M. Boujtita, A. Ruseckas, I. D. W. Samuel and F. Odobel, *Nanoscale*, 2017, **9**, 15566–15575.
- 196 F. Odobel and Y. Pellegrin, *J. Phys. Chem. Lett.*, 2013, **4**, 2551–2564.
- 197 J. H. Rhee, Y. H. Lee, P. Bera and S. I. Seok, *Chem. Phys. Lett.*, 2009, **477**, 345–348.
- 198 T. J. Macdonald, Y. J. Mange, M. R. Dewi, H. U. Islam, I. P. Parkin, W. M. Skinner and T. Nann, *J. Mater. Chem. A*, 2015, **3**, 13324–13331.
- 199 Y.-Q. Mao, Z.-J. Zhou, T. Ling and X.-W. Du, *RSC Adv.*, 2013, **3**, 1217–1221.
- 200 M. A. Becker, J. G. Radich, B. A. Bunker and P. V. Kamat, *J. Phys. Chem. Lett.*, 2014, **5**, 1575–1582.
- 201 O. Niitsoo, S. K. Sarkar, C. Pejoux, S. Ruhle, D. Cahen and G. Hodes, *J. Photochem. Photobiol. A*, 2006, **181**, 306–313.
- 202 C.-H. Chang and Y.-L. Lee, *Appl. Phys. Lett.*, 2007, **91**, 053503.
- 203 J. Tian, L. Lv, C. Fei, Y. Wang, X. Liu and G. Cao, *J. Mater. Chem. A*, 2014, **2**, 19653–19659.
- 204 P. N. Kumar, A. Kolay, M. Deepa, S. M. Shivaprasad and A. K. Srivastava, *ACS Appl. Mater. Interfaces*, 2017, **9**, 25278–25290.
- 205 G. Jiang, Z. Pan, Z. Ren, J. Du, C. Yang, W. Wang and X. Zhong, *J. Mater. Chem. A*, 2016, **4**, 11416–11421.
- 206 J. Yang and X. Zhong, *J. Mater. Chem. A*, 2016, **4**, 16553–16561.
- 207 J.-W. Lee, D.-Y. Son, T. K. Ahn, H.-W. Shin, I. Y. Kim, S.-J. Hwang, M. J. Ko, S. Sul, H. Han and N.-G. Park, *Sci. Rep.*, 2013, **3**, 1050.
- 208 Y. C. Choi, D. U. Lee, J. H. Noh, E. K. Kim and S. I. Seok, *Adv. Funct. Mater.*, 2014, **24**, 3587–3592.
- 209 S. Yang, P. Zhao, X. Zhao, L. Qu and X. Lai, *J. Mater. Chem. A*, 2015, **3**, 21922–21929.
- 210 R. K. Chava and M. Kang, *Mater. Lett.*, 2017, **199**, 188–191.
- 211 Y.-S. Chen, H. Choi and P. V. Kamat, *J. Am. Chem. Soc.*, 2013, **135**, 8822–8825.
- 212 Q. Zhang, G. Zhang, X. Sun, K. Yin and H. Li, *Nanomaterials*, 2017, **7**, 130.
- 213 S. Jiao, J. Wang, Q. Shen, Y. Li and X. Zhong, *J. Mater. Chem. A*, 2016, **4**, 7214–7221.
- 214 F. Huang, L. Zhang, Q. Zhang, J. Hou, H. Wang, H. Wang, S. Peng, J. Liu and G. Cao, *ACS Appl. Mater. Interfaces*, 2016, **8**, 34482–34489.
- 215 X.-Y. Yu, B.-X. Lei, D.-B. Kuang and C.-Y. Su, *Chem. Sci.*, 2011, **2**, 1396–1400.
- 216 A. Sahasrabudhe and S. Bhattacharyya, *Chem. Mater.*, 2015, **27**, 4848–4859.

- 217 Z. Ning, H. Tian, C. Yuan, Y. Fu, H. Qin, L. Sun and H. Agren, *Chem. Commun.*, 2011, **47**, 1536–1538.
- 218 P. K. Santra and P. V. Kamat, *J. Am. Chem. Soc.*, 2013, **135**, 877–885.
- 219 G. Wang, H. Wei, J. Shi, Y. Xu, H. Wu, Y. Luo, D. Li and Q. Meng, *Nano Energy*, 2017, **35**, 17–25.
- 220 L. Yue, H. Rao, J. Du, Z. Pan, J. Yu and X. Zhong, *RSC Adv.*, 2018, **8**, 3637–3645.
- 221 J.-Y. Kim, J. Yang, J. H. Yu, W. Baek, C.-H. Lee, H. J. Son, T. Hyeon and M. J. Ko, *ACS Nano*, 2015, **9**, 11286–11295.
- 222 L. Zhang, Z. Pan, W. Wang, J. Du, Z. Ren, Q. Shen and X. Zhong, *J. Mater. Chem. A*, 2017, **5**, 21442–21451.
- 223 W. Peng, J. Du, Z. Pan, N. Nakazawa, J. Sun, Z. Du, G. Shen, J. Yu, J. S. Hu, Q. Shen and X. Zhong, *ACS Appl. Mater. Interfaces*, 2017, **9**, 5328–5336.
- 224 B. Bai, D. Kou, W. Zhou, Z. Zhou and S. Wu, *Green Chem.*, 2015, **17**, 4377–4382.
- 225 X. Michalet, F. F. Pinaud, L. A. Bentolila, J. M. Tsay, S. Doose, J. J. Li, G. Sundaresan, A. M. Wu, S. S. Gambhir and S. Weiss, *Science*, 2005, **307**, 538–544.
- 226 U. Resch-Genger, M. Grabolle, S. Cavaliere-Jaricot, R. Nitschke and T. Nann, *Nat. Methods*, 2008, **5**, 763–775.
- 227 P. Zrazhevskiy, M. Sena and X. H. Gao, *Chem. Soc. Rev.*, 2010, **39**, 4326–4354.
- 228 N. Guijarro, T. Lana-Villarreal, I. Mora-Sero, J. Bisquert and R. Gomez, *J. Phys. Chem. C*, 2009, **113**, 4208–4214.
- 229 S. Gimenez, I. Mora-Sero, L. Macor, N. Guijarro, T. Lana-Villarreal, R. Gomez, L. J. Diguna, Q. Shen, T. Toyoda and J. Bisquert, *Nanotechnology*, 2009, **20**, 295204.
- 230 H. J. Lee, J.-H. Yum, H. C. Leventis, S. M. Zakeeruddin, S. A. Haque, P. Chen, S. I. Seok, M. Grätzel and M. K. Nazeeruddin, *J. Phys. Chem. C*, 2008, **112**, 11600–11608.
- 231 W. Wang, G. Jiang, J. Yu, W. Wang, Z. Pan, N. Nakazawa, Q. Shen and X. Zhong, *ACS Appl. Mater. Interfaces*, 2017, **9**, 22549–22559.
- 232 A. Salant, M. Shalom, I. Hod, A. Faust, A. Zaban and U. Banin, *ACS Nano*, 2010, **4**, 5962–5968.
- 233 X.-Y. Yu, J.-Y. Liao, K.-Q. Qiu, D.-B. Kuang and C.-Y. Su, *ACS Nano*, 2011, **5**, 9494–9500.
- 234 J. B. Sambur and B. A. Parkinson, *J. Am. Chem. Soc.*, 2010, **132**, 2130–2131.
- 235 I. Mora-Sero, S. Gimenez, T. Moehl, F. Fabregat-Santiago, T. Lana-Villareal, R. Gomez and J. Bisquert, *Nanotechnology*, 2008, **19**, 424007.
- 236 V. L. Colvin, A. N. Goldstein and A. P. Alivisatos, *J. Am. Chem. Soc.*, 1992, **114**, 5221–5230.
- 237 I. Robel, V. Subramanian, M. Kuno and P. V. Kamat, *J. Am. Chem. Soc.*, 2006, **128**, 2385–2393.
- 238 B.-R. Hyun, Y.-W. Zhong, A. C. Bartnik, L. Sun, H. D. Abruna, F. W. Wise, J. D. Goodreau, J. R. Matthews, T. M. Leslie and N. F. Borrelli, *ACS Nano*, 2008, **2**, 2206–2212.
- 239 M.-H. Jung and M. G. Kang, *J. Mater. Chem.*, 2011, **21**, 2694–2700.
- 240 W. Lee, S. H. Kang, S. K. Min, Y.-E. Sung and S.-H. Han, *Electrochim. Commun.*, 2008, **10**, 1579–1582.
- 241 S. Peng, F. Cheng, J. Liang, Z. Tao and J. Chen, *J. Alloys Compd.*, 2009, **481**, 786–791.
- 242 X. Hu, Q. Zhang, X. Huang, D. Li, Y. Luo and Q. Meng, *J. Mater. Chem.*, 2011, **21**, 15903–15905.
- 243 K. M. Coughlin, J. S. Nevins and D. F. Watson, *ACS Appl. Mater. Interfaces*, 2013, **5**, 8649–8654.
- 244 J. S. Nevins, K. M. Coughlin and D. F. Watson, *ACS Appl. Mater. Interfaces*, 2011, **3**, 4242–4253.
- 245 H. Wang, C. Luan, X. Xu, S. V. Kershaw and A. L. Rogach, *J. Phys. Chem. C*, 2012, **116**, 484–489.
- 246 J. Luo, H. Wei, Q. Huang, X. Hu, H. Zhao, R. Yu, D. Li, Y. Luo and Q. Meng, *Chem. Commun.*, 2013, **49**, 3881–3883.
- 247 J. Luo, H. Wei, F. Li, Q. Huang, D. Li, Y. Luo and Q. Meng, *Chem. Commun.*, 2014, **50**, 3464–3466.
- 248 J. Y. Chang, C. H. Li, Y. H. Chiang, C. H. Chen and P. N. Li, *ACS Appl. Mater. Interfaces*, 2016, **8**, 18878–18890.
- 249 Y.-H. Chiang, K.-Y. Lin, Y.-H. Chen, K. Waki, M. A. Abate, J.-C. Jiang and J.-Y. Chang, *J. Mater. Chem. A*, 2018, **6**, 9629–9641.
- 250 A. Raevskaya, O. Rosovik, A. Kozytskiy, O. Stroyuk, V. Dzhagan and D. R. T. Zahn, *RSC Adv.*, 2016, **6**, 100145–100157.
- 251 H. Lee, H. C. Leventis, S.-J. Moon, P. Chen, S. Ito, S. A. Haque, T. Torres, F. Nüesch, T. Geiger, S. M. Zakeeruddin, M. Grätzel and M. K. Nazeeruddin, *Adv. Funct. Mater.*, 2009, **19**, 2735–2742.
- 252 W.-T. Sun, Y. Yu, H.-Y. Pan, X.-F. Gao, Q. Chen and L.-M. Peng, *J. Am. Chem. Soc.*, 2008, **130**, 1124–1125.
- 253 J. H. Bang and P. V. Kamat, *ACS Nano*, 2009, **3**, 1467–1476.
- 254 L. C. Spangler, L. Lu, C. J. Kiely, B. W. Berger and S. McIntosh, *J. Mater. Chem. A*, 2016, **4**, 6107–6115.
- 255 G. Niu, L. Wang, R. Gao, B. Ma, H. Dong and Y. Qiu, *J. Mater. Chem.*, 2012, **22**, 16914–16919.
- 256 T. P. Brennan, O. Trejo, K. E. Roelofs, J. Xu, F. B. Prinz and S. F. Bent, *J. Mater. Chem. A*, 2013, **1**, 7566–7571.
- 257 H. J. Lee, P. Chen, S.-J. Moon, F. Sauvage, K. Sivula, T. Bessho, D. R. Gamelin, P. Comte, S. M. Zakeeruddin, S. I. Seok, M. Grätzel and M. K. Nazeeruddin, *Langmuir*, 2009, **25**, 7602–7608.
- 258 J. Tian, T. Shen, X. Liu, C. Fei, L. Lv and G. Cao, *Sci. Rep.*, 2016, **6**, 23094.
- 259 J.-H. Yum, J.-W. Lee, Y. Kim, R. Humphry-Baker, N.-G. Park and M. Grätzel, *Sol. Energy*, 2014, **109**, 183–188.
- 260 B. Liu, D. Wang, Y. Zhang, H. Fan, Y. Lin, T. Jiang and T. Xie, *Dalton Trans.*, 2013, **42**, 2232–2237.
- 261 D. Wu, F. Wang, H. Wang, K. Cao, Z. Gao, F. Xua and K. Jiang, *Dalton Trans.*, 2016, **45**, 16275–16282.
- 262 A. Tubtimtae, K.-L. Wu, H.-Y. Tung, M.-W. Lee and G. J. Wang, *Electrochim. Commun.*, 2010, **12**, 1158–1160.
- 263 M. A. Hines and P. Guyot-Sionnest, *J. Phys. Chem.*, 1996, **100**, 468–470.
- 264 X. G. Peng, M. C. Schlamp, A. V. Kadavanich and A. P. Alivisatos, *J. Am. Chem. Soc.*, 1997, **119**, 7019–7029.
- 265 S. L. Cumberland, K. M. Hanif, A. Javier, G. A. Khitrov, G. F. Strouse, S. M. Woessner and C. S. Yun, *Chem. Mater.*, 2002, **14**, 1576–1584.

- 266 L. Manna, E. C. Scher, L. S. Li and A. P. Alivisatos, *J. Am. Chem. Soc.*, 2002, **124**, 7136–7145.
- 267 J. J. Li, Y. A. Wang, W. Z. Guo, J. C. Keay, T. D. Mishima, M. B. Johnson and X. G. Peng, *J. Am. Chem. Soc.*, 2003, **125**, 12567–12575.
- 268 W. Zhang, G. Chen, J. Wang, B.-C. Ye and X. Zhong, *Inorg. Chem.*, 2009, **48**, 9723–9731.
- 269 W. Zhang, H. Zhang, Y. Feng and X. Zhong, *ACS Nano*, 2012, **6**, 11066–11073.
- 270 P. Reiss, M. Protiere and L. Li, *Small*, 2009, **5**, 154–168.
- 271 R. G. Chaudhuri and S. Paria, *Chem. Rev.*, 2012, **112**, 2373–2433.
- 272 D. Punnoose, C. S. S. P. Kumar, H. W. Seo, M. Shiratani, A. E. Reddy, S. S. Rao, C. V. Thulasi-Varma, S.-K. Kim, S.-H. Chung and H.-J. Kim, *New J. Chem.*, 2016, **40**, 3423–3431.
- 273 J. Yang, J. Wang, K. Zhao, T. Izuishi, Y. Li, Q. Shen and X. Zhong, *J. Phys. Chem. C*, 2015, **119**, 28800–28808.
- 274 M. D. Regulacio and M.-Y. Han, *Acc. Chem. Res.*, 2010, **43**, 621–630.
- 275 R. E. Bailey and S. M. Nie, *J. Am. Chem. Soc.*, 2003, **125**, 7100–7106.
- 276 X. H. Zhong, Y. Y. Feng, W. Knoll and M. Y. Han, *J. Am. Chem. Soc.*, 2003, **125**, 13559–13563.
- 277 X. H. Zhong, M. Y. Han, Z. L. Dong, T. J. White and W. Knoll, *J. Am. Chem. Soc.*, 2003, **125**, 8589–8594.
- 278 A. Kumar, K.-T. Li, A. R. Madaria and C. Zhou, *Nano Res.*, 2011, **4**, 1181–1190.
- 279 M. A. Hossain, J. R. Jennings, N. Mathews and Q. Wang, *Phys. Chem. Chem. Phys.*, 2012, **14**, 7154–7161.
- 280 M. G. Panthani, V. Akhavan, B. Goodfellow, J. P. Schmidtke, L. Dunn, A. Dodabalapur, P. F. Barbara and B. A. Korgel, *J. Am. Chem. Soc.*, 2008, **130**, 16770–16777.
- 281 A. Chirila, P. Reinhard, F. Pianezzi, P. Bloesch, A. R. Uhl, C. Fella, L. Kranz, D. Keller, C. Gretener, H. Hagendorfer, D. Jaeger, R. Erni, S. Nishiwaki, S. Buecheler and A. N. Tiwari, *Nat. Mater.*, 2013, **12**, 1107–1111.
- 282 I. Repins, M. A. Contreras, B. Egaas, C. DeHart, J. Scharf, C. L. Perkins, B. To and R. Noufi, *Prog. Photovoltaics*, 2008, **16**, 235–239.
- 283 C.-C. Chang, J.-K. Chen, C.-P. Chen, C.-H. Yang and J.-Y. Chang, *ACS Appl. Mater. Interfaces*, 2013, **5**, 11296–11306.
- 284 J.-Y. Chang, J.-M. Lin, L.-F. Su and C.-F. Chang, *ACS Appl. Mater. Interfaces*, 2013, **5**, 8740–8752.
- 285 Y.-Q. Wang, Y.-C. Rui, Q.-H. Zhang, Y.-G. Li and H.-Z. Wang, *ACS Appl. Mater. Interfaces*, 2013, **5**, 11858–11864.
- 286 J.-Y. Chang, L.-F. Su, C.-H. Li, C.-C. Chang and J.-M. Lin, *Chem. Commun.*, 2012, **48**, 4848–4850.
- 287 T.-L. Li, Y.-L. Lee and H. Teng, *Energy Environ. Sci.*, 2012, **5**, 5315–5324.
- 288 K.-T. Kuo, D.-M. Liu, S.-Y. Chen and C.-C. Lin, *J. Mater. Chem.*, 2009, **19**, 6780–6788.
- 289 T.-L. Li, Y.-L. Lee and H. Teng, *J. Mater. Chem.*, 2011, **21**, 5089–5098.
- 290 G. Xu, S. Ji, C. Miao, G. Liu and C. Ye, *J. Mater. Chem.*, 2012, **22**, 4890–4896.
- 291 N. S. Makarov, H. McDaniel, N. Fuke, I. Robel and V. I. Klimov, *J. Phys. Chem. Lett.*, 2014, **5**, 111–118.
- 292 J. Yang, J.-Y. Kim, J. H. Yu, T.-Y. Ahn, H. Lee, T.-S. Choi, Y.-W. Kim, J. Joo, M. J. Ko and T. Hyeon, *Phys. Chem. Chem. Phys.*, 2013, **15**, 20517–20525.
- 293 S. Higashimoto, M. Murano, T. Arase, S. Mukai, M. Azuma and M. Takahashi, *Sol. Energy Mater. Sol. Cells*, 2017, **169**, 203–209.
- 294 D. Aldakov, A. Lefrancois and P. Reiss, *J. Mater. Chem. C*, 2013, **1**, 3756–3776.
- 295 M. G. Panthani, C. J. Stolle, D. K. Reid, D. J. Rhee, T. B. Harvey, V. A. Akhavan, Y. Yu and B. A. Korgel, *J. Phys. Chem. Lett.*, 2013, **4**, 2030–2034.
- 296 D. Mocatta, G. Cohen, J. Schattner, O. Millo, E. Rabani and U. Banin, *Science*, 2011, **332**, 77–81.
- 297 N. Pradhan, D. Goorskey, J. Thessing and X. G. Peng, *J. Am. Chem. Soc.*, 2005, **127**, 17586–17587.
- 298 N. Pradhan, D. M. Battaglia, Y. Liu and X. Peng, *Nano Lett.*, 2007, **7**, 312–317.
- 299 W. Zhang, Q. Lou, W. Ji, J. Zhao and X. Zhong, *Chem. Mater.*, 2014, **26**, 1204–1212.
- 300 W. Zhang, Y. Li, H. Zhang, X. Zhou and X. Zhong, *Inorg. Chem.*, 2011, **50**, 10432–10438.
- 301 W. Zhang, X. Zhou and X. Zhong, *Inorg. Chem.*, 2012, **51**, 3579–3587.
- 302 G. Rimal, A. K. Pimachev, A. J. Yost, U. Poudyal, S. Maloney, W. Wang, T. Chien, Y. Dahnovsky and J. Tang, *Appl. Phys. Lett.*, 2016, **109**, 103901.
- 303 M. P. A. Muthalif, Y.-S. Lee, C. D. Sunesh, H.-J. Kim and Y. Choe, *Appl. Surf. Sci.*, 2017, **396**, 582–589.
- 304 L. Yu, Z. Li, Y. Liu, F. Cheng and S. Sun, *Appl. Surf. Sci.*, 2014, **305**, 359–365.
- 305 C. V. V. M. Gopi, M. Venkata-Haritha, S.-K. Kim and H.-J. Kim, *Dalton Trans.*, 2015, **44**, 630–638.
- 306 Z. Li, L. Yu, Y. Liu and S. Sun, *Electrochim. Acta*, 2015, **153**, 200–209.
- 307 P. K. Santra and Y.-S. Chen, *Electrochim. Acta*, 2014, **146**, 654–658.
- 308 S.-K. Kim, C. V. V. M. Gopi, J.-C. Lee and H.-J. Kim, *J. Appl. Phys.*, 2015, **117**, 163104.
- 309 N. Firooz, H. Dehghani and M. Afroz, *J. Power Sources*, 2015, **278**, 98–103.
- 310 U. Poudyal, F. S. Maloney, K. Sapkota and W. Wang, *Nanotechnology*, 2017, **28**, 415401.
- 311 I. Mehmood, Y. Liu, K. Chen, A. H. Shah and W. Chen, *RSC Adv.*, 2017, **7**, 33106–33112.
- 312 J. Wang, Y. Li, Q. Shen, T. Izuishi, Z. Pan, K. Zhao and X. Zhong, *J. Mater. Chem. A*, 2016, **4**, 877–886.
- 313 M. A. Abbas, T.-Y. Kim, S. U. Lee, Y. S. Kang and J. H. Bang, *J. Am. Chem. Soc.*, 2016, **138**, 390–401.
- 314 Q. Tang, W. Zhu, B. He and P. Yang, *ACS Nano*, 2017, **11**, 1540–1547.
- 315 J. Briscoe, A. Marinovic, M. Sevilla, S. Dunn and M. Titirici, *Angew. Chem., Int. Ed.*, 2015, **54**, 4463–4468.
- 316 K.-H. Ye, Z. Wang, J. Gu, S. Xiao, Y. Yuan, Y. Zhu, Y. Zhang, W. Mai and S. Yang, *Energy Environ. Sci.*, 2017, **10**, 772–779.

- 317 P. Mirtchev, E. J. Henderson, N. Soheilnia, C. M. Yip and G. A. Ozin, *J. Mater. Chem.*, 2012, **22**, 1265–1269.
- 318 X. Yan, X. Cui, B. Li and L. S. Li, *Nano Lett.*, 2010, **10**, 1869–1873.
- 319 H. Wang, P. Sun, S. Cong, J. Wu, L. Gao, Y. Wang, X. Dai, Q. Yi and G. Zou, *Nanoscale Res. Lett.*, 2016, **11**, 27.
- 320 V. M. Blas-Ferrando, J. Ortiz, V. Gonzalez-Pedro, R. S. Sanchez, I. Mora-Sero, F. Fernandez-Lazaro and A. Sastre-Santos, *Adv. Funct. Mater.*, 2015, **25**, 3220–3226.
- 321 J.-G. Song, X. Song, T. Ling, X.-W. Du and S. Z. Qiao, *Ind. Eng. Chem. Res.*, 2012, **51**, 10074–10078.
- 322 S. Sarkar, A. Makhral, K. Lakshman, T. Bora, J. Dutta and S. K. Pal, *J. Phys. Chem.*, 2012, **116**, 14248–14256.
- 323 J. Chen, W. Lei and W. Q. Deng, *Nanoscale*, 2011, **3**, 674–677.
- 324 Y. Liu and J. Wang, *Thin Solid Films*, 2010, **518**, E54–E56.
- 325 H. Choi, R. Nicolaescu, S. Paek, J. Ko and P. V. Kamat, *ACS Nano*, 2011, **5**, 9238–9245.
- 326 S. Buhbut, S. Itzhakov, E. Tauber, M. Shalom, I. Hod, T. Geiger, Y. Garini, D. Oron and A. Zaban, *ACS Nano*, 2010, **4**, 1293–1298.
- 327 M. Shalom, J. Albero, Z. Tachan, E. Martinez-Ferrero, A. Zaban and E. Palomares, *J. Phys. Chem. Lett.*, 2010, **1**, 1134–1138.
- 328 J. Dana, P. Anand, S. Maiti, F. Azlan, Y. Jadhav, S. K. Haram and H. N. Ghosh, *J. Phys. Chem. C*, 2017, **122**, 13277–13284.
- 329 D. Van-Duong, P. Kim, S. Baek, L. L. Larina, K. Yong, R. Ryoo, S. H. Ko and H.-S. Choi, *Carbon*, 2016, **96**, 139–144.
- 330 G. Zhu, L. Pan, T. Xu and Z. Sun, *ACS Appl. Mater. Interfaces*, 2011, **3**, 3146–3151.
- 331 G. Zhu, L. Pan, T. Xu and Z. Sun, *ACS Appl. Mater. Interfaces*, 2011, **3**, 1472–1478.
- 332 G. Zhu, L. Pan, H. Sun, X. Liu, T. Lv, T. Lu, J. Yang and Z. Sun, *ChemPhysChem*, 2012, **13**, 769–773.
- 333 G. Hodes, J. Manassen and D. Cahen, *J. Electrochem. Soc.*, 1980, **127**, 544–549.
- 334 A. D. Savariraj, K. K. Viswanathan and K. Prabakar, *ACS Appl. Mater. Interfaces*, 2014, **6**, 19702–19709.
- 335 Y. Jiang, X. Zhang, Q.-Q. Ge, B.-B. Yu, Y.-G. Zou, W.-J. Jiang, J.-S. Hu, W.-G. Song and L.-J. Wan, *ACS Appl. Mater. Interfaces*, 2014, **6**, 15448–15455.
- 336 M. Ye, C. Chen, N. Zhang, X. Wen, W. Guo and C. Lin, *Adv. Energy Mater.*, 2014, **4**, 1301564.
- 337 X. Q. Chen, Z. Li, Y. Bai, Q. Sun, L. Z. Wang and S. X. Dou, *Chem. – Eur. J.*, 2015, **21**, 1055–1063.
- 338 S. S. Kalanur, S. Y. Chae and O. S. Joo, *Electrochim. Acta*, 2013, **103**, 91–95.
- 339 F. Xi, H. Liu, W. Li, L. Zhu, H. Geng, L. Quan and W. Liang, *Electrochim. Acta*, 2015, **178**, 329–335.
- 340 C. Shen, L. Sun, Z. Y. Koh and Q. Wang, *J. Mater. Chem. A*, 2014, **2**, 2807–2813.
- 341 M. Ye, X. Wen, N. Zhang, W. Guo, X. Liu and C. Lin, *J. Mater. Chem. A*, 2015, **3**, 9595–9600.
- 342 F. Wang, H. Dong, J. Pan, J. Li, Q. Li and D. Xu, *J. Phys. Chem. C*, 2014, **118**, 19589–19598.
- 343 W. Ke, G. Fang, H. Lei, P. Qin, H. Tao, W. Zeng, J. Wang and X. Zhao, *J. Power Sources*, 2014, **248**, 809–815.
- 344 Y. Wang, Q. Zhang, Y. Li and H. Wang, *J. Power Sources*, 2016, **318**, 128–135.
- 345 G. S. Selopal, I. Concina, R. Milan, M. M. Natile, G. Sberveglieri and A. Vomiero, *Nano Energy*, 2014, **6**, 200–210.
- 346 Y. Jiang, B.-B. Yu, J. Liu, Z.-H. Li, J.-K. Sun, X.-H. Zhong, J.-S. Hu, W.-G. Song and L.-J. Wan, *Nano Lett.*, 2015, **15**, 3088–3095.
- 347 Y. Jiang, X. Zhang, Q.-Q. Ge, B.-B. Yu, Y.-G. Zou, W.-J. Jiang, W.-G. Song, L.-J. Wan and J.-S. Hu, *Nano Lett.*, 2014, **14**, 365–372.
- 348 A. D. Savariraj, G. Rajendrakumar, S. Selvam, S. N. Karthick, B. Balamuralitharan, H.-J. Kim, K. K. Viswanathan, M. Vijayakumar and K. Prabakar, *RSC Adv.*, 2015, **5**, 100560–100567.
- 349 K. Zhao, H. Yu, H. Zhang and X. Zhong, *J. Phys. Chem. C*, 2014, **118**, 5683–5690.
- 350 H. Zhang, H. Bao and X. Zhong, *J. Mater. Chem. A*, 2015, **3**, 6557–6564.
- 351 M. Deng, S. Huang, Q. Zhang, D. Li, Y. Luo, Q. Shen, T. Toyoda and Q. Meng, *Chem. Lett.*, 2010, **39**, 1168–1170.
- 352 H. M. Choi, I. A. Ji and J. H. Bang, *ACS Appl. Mater. Interfaces*, 2014, **6**, 2335–2343.
- 353 F. Bo, C. Zhang, C. Wang, S. Xu, Z. Wang and Y. Cui, *J. Mater. Chem. A*, 2014, **2**, 14585–14592.
- 354 S. Wang, T. Shen, H. Bai, B. Li and J. Tian, *J. Mater. Chem. C*, 2016, **4**, 8020–8026.
- 355 M. Eskandari and V. Ahmadi, *Mater. Lett.*, 2015, **142**, 308–311.
- 356 Y. Bai, C. Han, X. Chen, H. Yu, X. Zong, Z. Li and L. Wang, *Nano Energy*, 2015, **13**, 609–619.
- 357 H. Zhang, C. Wang, W. Peng, C. Yang and X. Zhong, *Nano Energy*, 2016, **23**, 60–69.
- 358 B.-M. Kim, M.-K. Son, S.-K. Kim, N.-Y. Hong, S. Park, M.-S. Jeong, H. Seo, K. Prabakar and H.-J. Kim, *Electrochim. Acta*, 2014, **117**, 92–98.
- 359 C.-Y. Lin, C.-Y. Teng, T.-L. Li, Y.-L. Lee and H. Teng, *J. Mater. Chem. A*, 2013, **1**, 1155–1162.
- 360 C. V. Thulasi-Varma, S. S. Rao, K. D. Ikkurthi, S.-K. Kim, T.-S. Kang and H.-J. Kim, *J. Mater. Chem. C*, 2015, **3**, 10195–10206.
- 361 C. V. V. M. Gopi, J.-H. Bae, M. Venkata-Haritha, S.-K. Kim, Y.-S. Lee, G. Sarat and H.-J. Kim, *RSC Adv.*, 2015, **5**, 107522–107532.
- 362 Z. Tachan, M. Shalom, I. Hod, S. Ruehle, S. Tirosh and A. Zaban, *J. Phys. Chem. C*, 2011, **115**, 6162–6166.
- 363 K. Meng and K. R. Thampi, *ACS Appl. Mater. Interfaces*, 2014, **6**, 20768–20775.
- 364 C. Chen, M. Ye, N. Zhang, X. Wen, D. Zheng and C. Lin, *J. Mater. Chem. A*, 2015, **3**, 6311–6314.
- 365 M. S. Faber, K. Park, M. Caban-Acevedo, P. K. Santra and S. Jin, *J. Phys. Chem. Lett.*, 2013, **4**, 1843–1849.
- 366 Q. Luo, Y. Gu, J. Li, N. Wang and H. Lin, *J. Power Sources*, 2016, **312**, 93–100.

- 367 R. Seenu, C. V. V. M. Gopi, S. S. Rao, S.-K. Kim and H.-J. Kim, *Electrochim. Acta*, 2016, **204**, 255–262.
- 368 H. Chen, L. Zhu, H. Liu and W. Li, *J. Power Sources*, 2014, **245**, 406–410.
- 369 L. Quan, W. Li, L. Zhu, H. Geng, X. Chang and H. Liu, *J. Power Sources*, 2014, **272**, 546–553.
- 370 J. Xu, H. Xue, X. Yang, H. Wei, W. Li, Z. Li, W. Zhang and C.-S. Lee, *Small*, 2014, **10**, 4754–4759.
- 371 H.-J. Kim, D.-J. Kim, S. S. Rao, A. D. Savariraj, K. Soo-Kyoung, M.-K. Son, C. V. V. M. Gopi and K. Prabakar, *Electrochim. Acta*, 2014, **127**, 427–432.
- 372 C. V. V. M. Gopi, S. S. Rao, S.-K. Kim, D. Punnoose and H.-J. Kim, *J. Power Sources*, 2015, **275**, 547–556.
- 373 Y. Zhang, C. Shi, X. Dai, F. Liu, X. Fang and J. Zhu, *Electrochim. Acta*, 2014, **118**, 41–44.
- 374 D. Barpuzary, A. Banik, G. Gogoi and M. Qureshi, *J. Mater. Chem. A*, 2015, **3**, 14378–14388.
- 375 X. Dai, C. Shi, Y. Zhang, F. Liu, X. Fang and J. Zhu, *Mater. Lett.*, 2014, **116**, 251–253.
- 376 Y. Cao, Y. Xiao, J.-Y. Jung, H.-D. Um, S.-W. Jee, H. M. Choi, J. H. Bang and J.-H. Lee, *ACS Appl. Mater. Interfaces*, 2013, **5**, 479–484.
- 377 X. Zeng, W. Zhang, Y. Xie, D. Xiong, W. Chen, X. Xu, M. Wang and Y.-B. Cheng, *J. Power Sources*, 2013, **226**, 359–362.
- 378 X. Zeng, D. Xiong, W. Zhang, L. Ming, Z. Xu, Z. Huang, M. Wang, W. Chen and Y.-B. Cheng, *Nanoscale*, 2013, **5**, 6992–6998.
- 379 J. Xu, X. Yang, Q.-D. Yang, T.-L. Wong and C.-S. Lee, *J. Phys. Chem. C*, 2012, **116**, 19718–19723.
- 380 X. Zeng, W. Zhang, Y. Xie, D. Xiong, W. Chen, X. Xu, M. Wang and Y.-B. Cheng, *J. Power Sources*, 2013, **226**, 359–362.
- 381 A. Kay and M. Grätzel, *Sol. Energy Mater. Sol. Cells*, 1996, **44**, 99–117.
- 382 G. S. Paul, J. H. Kim, M.-S. Kim, K. Do, J. Ko and J.-S. Yu, *ACS Appl. Mater. Interfaces*, 2012, **4**, 375–381.
- 383 S.-Q. Fan, B. Fang, J. H. Kim, J.-J. Kim, J.-S. Yu and J. Ko, *Appl. Phys. Lett.*, 2010, **96**, 063501.
- 384 V.-D. Dao, Y. Choi, K. Yong, L. L. Larina and H.-S. Choi, *Carbon*, 2015, **84**, 383–389.
- 385 P. Sudhagar, E. Ramasamy, W.-H. Cho, J. Lee and Y. S. Kang, *Electrochem. Commun.*, 2011, **13**, 34–37.
- 386 J. Dong, S. Jia, J. Chen, B. Li, J. Zheng, J. Zhao, Z. Wang and Z. Zhu, *J. Mater. Chem.*, 2012, **22**, 9745–9750.
- 387 C. V. V. M. Gopi, M. Venkata-Haritha, S.-K. Kim and H.-J. Kim, *J. Power Sources*, 2016, **311**, 111–120.
- 388 Q. Zhang, S. Zhou, Q. Li and H. Li, *RSC Adv.*, 2015, **5**, 30617–30623.
- 389 A. Sahasrabudhe, S. Kapri and S. Bhattacharyya, *Carbon*, 2016, **107**, 395–404.
- 390 Q. Zhang, Y. Zhang, S. Huang, X. Huang, Y. Luo, Q. Meng and D. Li, *Electrochem. Commun.*, 2010, **12**, 327–330.
- 391 J. Yu, W. Wang, Z. Pan, J. Du, Z. Ren, W. Xue and X. Zhong, *J. Mater. Chem. A*, 2017, **5**, 14124–14133.
- 392 H. Zhang, C. Yang, Z. Du, D. Pan and X. Zhong, *J. Mater. Chem. A*, 2017, **5**, 1614–1622.
- 393 H.-J. Kim, T.-B. Yeo, S.-K. Kim, S. S. Rao, A. D. Savariraj, K. Prabakar and C. V. V. M. Gopi, *Eur. J. Inorg. Chem.*, 2014, 4281–4286.
- 394 D. Wu, Y. Wang, F. Wang, H. Wang, Y. An, Z. Gao, F. Xu and K. Jiang, *Carbon*, 2017, **123**, 756–766.
- 395 F. Liu, J. Zhu, Y. Li, J. Wei, M. Lv, Y. Xu, L. Zhou, L. Hu and S. Dai, *J. Power Sources*, 2015, **292**, 7–14.
- 396 D.-M. Li, L.-Y. Cheng, Y.-D. Zhang, Q.-X. Zhang, X.-M. Huang, Y.-H. Luo and Q.-B. Meng, *Sol. Energy Mater. Sol. Cells*, 2014, **120**, 454–461.
- 397 J. G. Radich, R. Dwyer and P. V. Kamat, *J. Phys. Chem. Lett.*, 2011, **2**, 2453–2460.
- 398 Y. Yang, L. Zhu, H. Sun, X. Huang, Y. Luo, D. Li and Q. Meng, *ACS Appl. Mater. Interfaces*, 2012, **4**, 6162–6168.
- 399 X. Zhang, X. Huang, Y. Yang, S. Wang, Y. Gong, Y. Luo, D. Li and Q. Meng, *ACS Appl. Mater. Interfaces*, 2013, **5**, 5954–5960.
- 400 D. Ghosh, G. Halder, A. Sahasrabudhe and S. Bhattacharyya, *Nanoscale*, 2016, **8**, 10632–10641.
- 401 P. Parand, M. Samadpour, A. Esfandiar and A. I. Zad, *ACS Photonics*, 2014, **1**, 323–330.
- 402 M. Eskandari, V. Ahmadi and R. Ghahary, *Electrochim. Acta*, 2015, **151**, 393–398.
- 403 L. Givalou, M. Antoniadou, D. Perganti, M. Giannouri, C.-S. Karagianni, A. G. Kontos and P. Falaras, *Electrochim. Acta*, 2016, **210**, 630–638.
- 404 M. Que, W. Guo, X. Zhang, X. Li, Q. Hua, L. Dong and C. Pan, *J. Mater. Chem. A*, 2014, **2**, 13661–13666.
- 405 J. H. Zeng, D. Chen, Y. F. Wang and B. B. Jin, *J. Mater. Chem. C*, 2015, **3**, 12140–12148.
- 406 L. Li, P. Zhu, S. Peng, M. Srinivasan, Q. Yan, A. S. Nair, B. Liu and S. Samakrishna, *J. Phys. Chem. C*, 2014, **118**, 16526–16535.
- 407 H.-J. Kim, S.-W. Kim, C. V. V. M. Gopi, S.-K. Kim, S. S. Rao and M.-S. Jeong, *J. Power Sources*, 2014, **268**, 163–170.
- 408 X. Song, M. Wang, J. Deng, Y. Ju, T. Xing, J. Ding, Z. Yang and J. Shao, *J. Power Sources*, 2014, **269**, 661–670.
- 409 S. S. Khalili and H. Dehghani, *RSC Adv.*, 2016, **6**, 10880–10886.
- 410 G. Yue, F. Tan, J. Wu, F. Li, J. Lin, M. Huang and W. Zhang, *RSC Adv.*, 2015, **5**, 42101–42108.
- 411 C. V. V. M. Gopi, M. Venkata-Haritha, S. Ravi, C. V. Thulasi-Varma, S.-K. Kim and H.-J. Kim, *J. Mater. Chem. C*, 2015, **3**, 12514–12528.
- 412 P. S. Tamboli, M. B. R. Prasad, V. S. Kadam, R. S. Vhatkar, Inamuddin, H. M. Pathan and S. S. Mahajan, *Sol. Energy Mater. Sol. Cells*, 2017, **161**, 96–101.
- 413 S. Licht, *Sol. Energy Mater. Sol. Cells*, 1995, **38**, 305–319.
- 414 Y.-L. Lee and C.-H. Chang, *J. Power Sources*, 2008, **185**, 584–588.
- 415 L. Li, X. Yang, J. Gao, H. Tian, J. Zhao, A. Hagfeldt and L. Sun, *J. Am. Chem. Soc.*, 2011, **133**, 8458–8460.
- 416 Z. Ning, C. Yuan, H. Tian, Y. Fu, L. Li, L. Sun and H. Ågren, *J. Mater. Chem.*, 2012, **22**, 6032–6037.
- 417 V. Jovanovski, V. Gonzalez-Pedro, S. Gimenez, E. Azaceta, G. Cabanero, H. Grande, R. Tena-Zaera, I. Mora-Sero and J. Bisquert, *J. Am. Chem. Soc.*, 2011, **133**, 20156–20159.

- 418 R. M. Evangelista, S. Makuta, S. Yonezu, J. Andrews and Y. Tachibana, *ACS Appl. Mater. Interfaces*, 2016, **8**, 13957–13965.
- 419 S. Y. Chae, Y. J. Hwang and O.-S. Joo, *RSC Adv.*, 2014, **4**, 26907–26911.
- 420 R. Dang, Y. Wang, J. Zeng, Z. Huang, Z. Fei and P. J. Dyson, *J. Mater. Chem. A*, 2017, **5**, 13526–13534.
- 421 C. Levy-Clement, R. Tena-Zaera, M. A. Ryan, A. Katty and G. Hodes, *Adv. Mater.*, 2005, **17**, 1512–1515.
- 422 J. P. Park, J. H. Heo, S. H. Im and S.-W. Kim, *J. Mater. Chem. A*, 2016, **4**, 785–790.
- 423 S. H. Im, C. S. Lim, J. A. Chang, Y. H. Lee, N. Maiti, H. J. Kim, M. K. Nazeeruddin, M. Grätzel and S. I. Seok, *Nano Lett.*, 2011, **11**, 4789–4793.
- 424 J. Du, X. Meng, K. Zhao, Y. Li and X. Zhong, *J. Mater. Chem. A*, 2015, **3**, 17091–17097.
- 425 H. Wei, G. Wang, J. Shi, H. Wu, Y. Luo, D. Li and Q. Meng, *J. Mater. Chem. A*, 2016, **4**, 14194–14203.
- 426 W. Feng, L. Zhao, J. Du, Y. Li and X. Zhong, *J. Mater. Chem. A*, 2016, **4**, 14849–14856.
- 427 Z. Yu, Q. Zhang, D. Qin, Y. Luo, D. Li, Q. Shen, T. Toyoda and Q. Meng, *Electrochim. Commun.*, 2010, **12**, 1776–1779.
- 428 S. Wang, Q.-X. Zhang, Y.-Z. Xu, D.-M. Li, Y.-H. Luo and Q.-B. Meng, *J. Power Sources*, 2013, **224**, 152–157.
- 429 H.-Y. Chen, L. Lin, X.-Y. Yu, K.-Q. Qiu, X.-Y. Lu, D.-B. Kuang and C.-Y. Su, *Electrochim. Acta*, 2013, **92**, 117–123.
- 430 J. Duan, Q. Tang, R. Li, B. He, L. Yu and P. Yang, *J. Power Sources*, 2015, **284**, 369–376.
- 431 Z. Huo, L. Tao, S. Wang, J. Wei, J. Zhu, W. Dong, F. Liu, S. Chen, B. Zhang and S. Dai, *J. Power Sources*, 2015, **284**, 582–587.
- 432 W. Feng, Y. Li, J. Du, W. Wang and X. Zhong, *J. Mater. Chem. A*, 2016, **4**, 1461–1468.
- 433 G. Hodes and D. Cahen, *Acc. Chem. Res.*, 2012, **45**, 705–713.
- 434 S. H. Im, H.-J. Kim, S. W. Kim, S.-W. Kim and S. I. Seok, *Energy Environ. Sci.*, 2011, **4**, 4181–4186.
- 435 D. C. Neo, N. Zhang, Y. Tazawa, H. Jiang, G. M. Hughes, C. R. Grovenor, H. E. Assender and A. A. Watt, *ACS Appl. Mater. Interfaces*, 2016, **8**, 12101–12108.
- 436 G. Laramona, C. Chone, A. Jacob, D. Sakakura, B. Delatouche, D. Pere, X. Cieren, M. Nagino and R. Bayon, *Chem. Mater.*, 2006, **18**, 1688–1696.
- 437 C.-F. Chi, P. Chen, Y.-L. Lee, I. P. Liu, S.-C. Chou, X.-L. Zhang and U. Bach, *J. Mater. Chem.*, 2011, **21**, 17534–17540.
- 438 J. Qian, Q. S. Liu, G. Li, K. J. Jiang, L. M. Yang and Y. Song, *Chem. Commun.*, 2011, **47**, 6461–6463.
- 439 G. Sfyri, S. Sfaelou, K. S. Andrikopoulos, N. Balis, G. A. Voyatzis and P. Lianos, *J. Phys. Chem. C*, 2014, **118**, 16547–16551.
- 440 Y. H. Lee, S. H. Im, J. A. Chang, J.-H. Lee and S. I. Seok, *Org. Electron.*, 2012, **13**, 975–979.
- 441 Y. Itzhaik, O. Niitsoo, M. Page and G. Hodes, *J. Phys. Chem. C*, 2009, **113**, 4254–4256.
- 442 J. A. Chang, J. H. Rhee, S. H. Im, Y. H. Lee, H. J. Kim, S. I. Seok, M. K. Nazeeruddin and M. Grätzel, *Nano Lett.*, 2010, **10**, 2609–2612.
- 443 S.-J. Moon, Y. Itzhaik, J.-H. Yum, S. M. Zakeeruddin, G. Hodes and M. Grätzel, *J. Phys. Chem. Lett.*, 2010, **1**, 1524–1527.
- 444 S. Nezu, G. Laramona, C. Chone, A. Jacob, B. Delatouche, D. Pere and C. Moisan, *J. Phys. Chem. C*, 2010, **114**, 6854–6859.
- 445 J. A. Chang, S. H. Im, Y. H. Lee, H. J. Kim, C. S. Lim, J. H. Heo and S. I. Seok, *Nano Lett.*, 2012, **12**, 1863–1867.
- 446 C. S. Lim, S. H. Im, J. A. Chang, Y. H. Lee, H. J. Kim and S. I. Seok, *Nanoscale*, 2012, **4**, 429–432.
- 447 C. S. Lim, S. H. Im, H. J. Kim, J. A. Chang, Y. H. Lee and S. I. Seok, *Phys. Chem. Chem. Phys.*, 2012, **14**, 3622–3626.
- 448 C.-S. Lim, S. H. Im, J. H. Rhee, Y. H. Lee, H.-J. Kim, N. Maiti, Y. Kang, J. A. Chang, M. K. Nazeeruddin, M. Grätzel and S. I. Seok, *J. Mater. Chem.*, 2012, **22**, 1107–1111.
- 449 P. P. Boix, Y. H. Lee, F. Fabregat-Santiago, S. H. Im, I. Mora-Sero, J. Bisquert and S. I. Seok, *ACS Nano*, 2012, **6**, 873–880.
- 450 Y. C. Choi, Y. H. Lee, S. H. Im, J. H. Noh, T. N. Mandal, W. S. Yang and S. I. Seok, *Adv. Energy Mater.*, 2014, **4**, 1301680.
- 451 G. M. Peng, X. Q. Xu, F. J. Mei, G. Xu, J. M. Wu, D. Gao, J. E. Ellis, Y. Zhao, Y. Xing and A. Star, *RSC Adv.*, 2014, **4**, 53335–53343.
- 452 Y. C. Choi and S. I. Seok, *Adv. Funct. Mater.*, 2015, **25**, 2892–2898.
- 453 Y. C. Choi, E. J. Yeom, T. K. Ahn and S. I. Seok, *Angew. Chem., Int. Ed.*, 2015, **54**, 4005–4009.
- 454 K. C. Godel, Y. C. Choi, B. Roose, A. Sadhanala, H. J. Snaith, S. I. Seok, U. Steiner and S. K. Pathak, *Chem. Commun.*, 2015, **51**, 8640–8643.
- 455 K. Tsujimoto, D.-C. Nguyen, S. Ito, H. Nishino, H. Matsuyoshi, A. Konno, G. R. A. Kumara and K. Tennakone, *J. Phys. Chem. C*, 2012, **116**, 13465–13471.
- 456 Y. C. Choi, T. N. Mandal, W. S. Yang, Y. H. Lee, S. H. Im, J. H. Noh and S. I. Seok, *Angew. Chem., Int. Ed.*, 2014, **53**, 1329–1333.
- 457 H.-Y. Wei, G.-S. Wang, H.-J. Wu, Y.-H. Luo, D.-M. Li and Q.-B. Meng, *Acta Phys.-Chim. Sin.*, 2016, **32**, 201–213.
- 458 K. E. Roelofs, T. P. Brennan, J. C. Dominguez, C. D. Bailie, G. Y. Margulis, E. T. Hoke, M. D. McGehee and S. F. Bent, *J. Phys. Chem. C*, 2013, **117**, 5584–5592.
- 459 Q. Shen, J. Kobayashi, L. J. Diguna and T. Toyoda, *J. Appl. Phys.*, 2008, **103**, 084304.
- 460 S. Yang, C. Huang, J. Zhai, Z. Wang and L. Jiang, *J. Mater. Chem.*, 2002, **12**, 1459–1464.
- 461 S.-H. Hsu, S.-F. Hung and S.-H. Chien, *J. Power Sources*, 2013, **233**, 236–243.
- 462 Y.-S. Lee, C. V. V. M. Gopi, A. E. Reddy, C. Nagaraju and H.-J. Kim, *New J. Chem.*, 2017, **41**, 1914–1917.
- 463 S. S. Rao, I. K. Durga, C. V. Tulasi-Varma, D. Punnoose, S.-K. Kim and H.-J. Kim, *Org. Electron.*, 2015, **26**, 200–207.
- 464 N. Guijarro, J. M. Campina, Q. Shen, T. Toyoda, T. Lana-Villarreal and R. Gomez, *Phys. Chem. Chem. Phys.*, 2011, **13**, 12024–12032.

- 465 Z. Peng, Y. Liu, Y. Zhao, K. Chen, Y. Cheng, V. Kovalev and W. Chen, *J. Alloys Compd.*, 2014, **587**, 613–617.
- 466 F. Huang, Q. Zhang, B. Xu, J. Hou, Y. Wang, R. C. Masse, S. Peng, J. Liu and G. Cao, *J. Mater. Chem. A*, 2016, **4**, 14773–14780.
- 467 F. Huang, J. Hou, H. Wang, H. Tang, Z. Liu, L. Zhang, Q. Zhang, S. Peng, J. Liu and G. Cao, *Nano Energy*, 2017, **32**, 433–440.
- 468 F. Huang, J. Hou, Q. Zhang, Y. Wang, R. C. Masse, S. Peng, H. Wang, J. Liu and G. Cao, *Nano Energy*, 2016, **26**, 114–122.
- 469 A. Subramanian, D. Punnoose, S. S. Rao, C. V. T. Varma, B. Naresh, V. Raman and H.-J. Kim, *New J. Chem.*, 2017, **41**, 5942–5949.
- 470 Z. Liu, M. Miyauchi, Y. Uemura, Y. Cui, K. Hara, Z. Zhao, K. Sunahara and A. Furube, *Appl. Phys. Lett.*, 2010, **96**, 233107.
- 471 M. Shalom, S. Dor, S. Ruhle, L. Grinis and A. Zaban, *J. Phys. Chem. C*, 2009, **113**, 3895–3898.
- 472 Z. Tachan, I. Hod, M. Shalom, L. Grinis and A. Zaban, *Phys. Chem. Chem. Phys.*, 2013, **15**, 3841–3845.
- 473 Z. Pan and X. Zhong, *J. Mater. Chem. A*, 2016, **4**, 18976–18982.
- 474 A. K. Chandiran, M. K. Nazeeruddin and M. Grätzel, *Adv. Funct. Mater.*, 2014, **24**, 1615–1623.
- 475 A. Kay and M. Grätzel, *Chem. Mater.*, 2002, **14**, 2930–2935.
- 476 E. Palomares, J. N. Clifford, S. A. Haque, T. Lutz and J. R. Durrant, *J. Am. Chem. Soc.*, 2003, **125**, 475–482.
- 477 J. Guo, C. She and T. Lian, *J. Phys. Chem. C*, 2007, **111**, 8979–8987.
- 478 T. Shen, L. Bian, B. Li, K. Zheng, T. Pullerits and J. Tian, *Appl. Phys. Lett.*, 2016, **108**, 213901.
- 479 S. Maiti, F. Azlan, P. Anand, Y. Jadhav, J. Dana, S. K. Haram and H. N. Ghosh, *Langmuir*, 2018, **34**, 50–57.
- 480 E. M. Barea, M. Shalom, S. Gimenez, I. Hod, I. Mora-Sero, A. Zaban and J. Bisquert, *J. Am. Chem. Soc.*, 2010, **132**, 6834–6839.
- 481 M. Solis de la Fuente, R. S. Sanchez, V. Gonzalez-Pedro, P. P. Boix, S. G. Mhaisalkar, M. E. Rincon, J. Bisquert and I. Mora-Sero, *J. Phys. Chem. Lett.*, 2013, **4**, 1519–1525.
- 482 A. N. Jumabekov, N. Cordes, T. D. Siegler, P. Docampo, A. Ivanova, K. Fominykh, D. D. Medina, L. M. Peter and T. Bein, *ACS Appl. Mater. Interfaces*, 2016, **8**, 4600–4607.
- 483 P. N. Kumar, A. Kolay, M. Deepa, S. M. Shivaprasad and A. K. Srivastava, *ACS Appl. Mater. Interfaces*, 2017, **9**, 25278–25290.
- 484 H. I. Wang, H. Lu, Y. Nagata, M. Bonn and E. Canovas, *ACS Nano*, 2017, **11**, 4760–4767.
- 485 X. Zhao, R. N. Ma, M. X. Yang, H. D. Yang, P. Jin, Z. Q. Li, Y. Z. Fan, A. Du and X. M. Cao, *J. Alloys Compd.*, 2017, **726**, 593–600.
- 486 P. Cheng and X. Zhan, *Chem. Soc. Rev.*, 2016, **45**, 2544–2582.
- 487 K. Domanski, E. A. Alharbi, A. Hagfeldt, M. Grätzel and W. Tress, *Nat. Energy*, 2018, **3**, 61–67.
- 488 M. Saliba, *Science*, 2018, **359**, 388–389.
- 489 N. Arora, M. I. Dar, A. Hinderhofer, N. Pellet, F. Schreiber, S. M. Zakeeruddin and M. Grätzel, *Science*, 2017, **358**, 768–771.
- 490 W. Chen, Y. Wu, Y. Yue, J. Liu, W. Zhang, X. Yang, H. Chen, E. Bi, I. Ashraful, M. Grätzel and L. Han, *Science*, 2015, **350**, 944–948.
- 491 H. Tan, A. Jain, O. Voznyy, X. Lan, F. P. G. de Arquer, J. Z. Fan, R. Quintero-Bermudez, M. Yuan, B. Zhang, Y. Zhao, F. Fan, P. Li, L. N. Quan, Y. Zhao, Z.-H. Lu, Z. Yang, S. Hoogland and E. H. Sargent, *Science*, 2017, **355**, 722–726.
- 492 C. V. V. M. Gopi, M. Venkata-Haritha, S.-K. Kim and H.-J. Kim, *Nanoscale*, 2015, **7**, 12552–12563.
- 493 S. Sfaelou, A. G. Kontos, L. Givalou, P. Falaras and P. Lianos, *Catal. Today*, 2014, **230**, 221–226.
- 494 Y. Chen, Q. Tao, W. Fu, H. Yang, X. Zhou, Y. Zhang, S. Su, P. Wang and M. Li, *Electrochim. Acta*, 2014, **118**, 176–181.
- 495 W. Guo, Z. Du, Q. Zhao, H. Zhang and X. Zhong, *J. Phys. Chem. C*, 2016, **120**, 16500–16506.
- 496 S. Wang, Q.-X. Zhang, Y.-Z. Xu, D.-M. Li, Y.-H. Luo and Q.-B. Meng, *J. Power Sources*, 2013, **224**, 152–157.
- 497 H. Kim, I. Hwang and K. Yong, *ACS Appl. Mater. Interfaces*, 2014, **6**, 11245–11253.
- 498 A. Fakharuddin, R. Jose, T. M. Brown, F. Fabregat-Santiago and J. Bisquert, *Energy Environ. Sci.*, 2014, **7**, 3952–3981.